VYSOKÉ UČENÍ TECHNICKÉ V BRNĚ

BRNO UNIVERSITY OF TECHNOLOGY

FAKULTA CHEMICKÁ
ÚSTAV CHEMIE MATERIÁLŮ

FACULTY OF CHEMISTRY
INSTITUTE OF MATERIALS SCIENCE

POKROČILÉ VRSTEVNATÉ KOMPOZITY PRO APLIKACE VE STOMATOLOGII

ADVANCED LAYERED COMPOSITES FOR DENTAL APPLICATIONS

DIZERTAČNÍ PRÁCE

DOCTORAL THESIS

AUTOR PRÁCE
AUTHOR

Ing. Zbyněk Šedivý

VEDOUCÍ PRÁCE
SUPERVISOR

prof. RNDr. Josef Jančář, CSc.

BRNO 2013

ABSTRAKT

Disertační práce se věnuje mechanické odezvě pokročilých vrstevnatých kompozitů pro stomatologické aplikace. Modelová kompozitní struktura je složena z vrstev s částicových a vlákny vyztužených kompozitů. Hlavní důraz byl kladen na zkoumání vlivu strukturálních charakteristik na mikro a mezo úrovni na deformační chování a porušení během statického tříbodového ohybu. Strukturální charakteristiky na mikro a mezo úrovni zahrnovaly orientaci vláken, objemový obsah vláken a částic, adhezi mezi vrstvami a skladbu vrstev. Je prezentován testovací protokol vhodný pro získání spolehlivých dat o vztahu mezi strukturou a vlastnostmi modelových vrstevnatých kompozitů, která jsou relevantní pro klinické aplikace těchto materiálů. Experimentálně zjištěné závislosti tuhosti a parametrů porušení na struktuře jsou podrobeny interpretaci s využitím existujících teoretických modelů. Data získaná z testů DMTA a ze statického tříbodového ohybu byla využita k analýze vlivu strukturálních charakteristik na tuhost a rozdělení napětí v průběhu statické deformace. Na základě těchto analýz jsou navržena základní pravidla pro klinické použití vrstevnatých kompozitů ve stomatologických aplikacích jako jsou minimálně invazivní můstky nebo stabilizační dlahy.

ABSTRACT

The PhD thesis deals with mechanical response of advanced layered composites for dental applications. Model composite superstructure is composed of fiber reinforced and particulate filled composite layers. The main concern was to investigate influence of microscale and mesoscale structural features on deformation behavior and ftracture during static three point bending test. The microscale and mesoscale structural features covered fiber orientation, fiber and particle volume fractions, interlayer adhesion and layering sequence. Testing protocol suitable to obtain reliable experimental data on structure-property relationship for model test specimen relevant for clinical applications is presented. An attempt is made to interpret experimentaly established structure-stiffness and structure-fracture relationships using existing models. Data gained out of static and DMTA three point bending were used to analyze an influence of structural features on stiffness and stress distribution. Based on these analyses, basic rules for clinical applications in dentistry such as minimally invasive bridges and stabilising devices (splints) of layered composites are proposed.

KLÍČOVÁ SLOVA

vrstevnaté kompozity, mechanická odezva, homogenizace, částicové kompozity, vláknové kompozity, minimálně invazivní stomatologie, test na tříbodový ohyb

KEYWORDS

layered composites, mechanical response, homogenisation, particle filled composites, fiber reinforced composites, minimally invasive dentistry, three-point bending test

PROHLÁŠENÍ

Prohlašuji, že jsem disertační práci vypracoval samostatně a že všechny použité literární zdroje jsem správně a úplně citoval. Disertační práce je z hlediska obsahu majetkem Fakulty chemické VUT v Brně a může být využita ke komerčním účelům jen se souhlasem vedoucího disertační práce a děkana FCH VUT.

Acknowledgement

I would like to thank my supervisor, prof. RNDr. Josef Jančář, CSc. for his support during my work on this thesis and to ing. Jaromír Wasserbauer for the SEM images.

Table of Contents

1 INTRODUCTION

Man has started to imitate the concept of composite materials existing in nature more than 7000 years ago in straw bricks. Continuous development of man-made composites accelerated dramatically when polymers became common in industrial use during several last decades. The most visible areas of expanded use of composites are building, aero-space, automotive, power and sport accessories industries.

The range of application of composites extends recently from the field of general engineering to bio-medical area such as implant medicine (artificial joins) and dentistry.

There are several highlight features of mechanical behavior of composites observable which were formulated in two basic principles:

(1) The strength of material in fibre form is many times greater that of the same material in the bulk. Also, the thinner the fiber, the greater the strength. (A. A. Griffith)

(2) When taken as a whole, a composite can withstand stresses that would fracture the weaker component, whereas the composite's stronger component can exhibit a greater percentage of its theoretical strength than when loaded singly. (G. Slayter)

The fast development of new composites and their applications is related to the progress in theoretical research which tries to formulate principles for prediction of properties of final composite based on the knowledge of the properties of constituents and their interactions. In order to validate theoretical hypothesis, the theoretical research should be accompanied with relevant experimental research. Focal point of current research in composites lies in multi-scale modeling of heterogenous media in general and correct preparation and interpretation of adequate experiments.These tasks require multi-disciplinary approach involving following sciences:

- thermo-mechanics: particularly theories of elasticity, visco-elasticity, and fracture mechanics,
- material science: particularly polymer science,
- computational methods for solving differential / partial differential equations (finite element method, boundary element method)
- application - relevant - sciences/arts: (dental morphology and anatomy e.g.).

Multi - disciplinarity of composite research generates terminology (semantic) problems: the same or similar phenomena are called differently in different sciences and vice - versa for completely different phenomena similar or same term is used in different sciences. This fact calls for clear definition of terms.

The presented work deals with layered composites used in dentistry. This type of composites provides new possibilities for clinical dentistry. It combines usually one or more layers of particle reinforced/filled composites with one or more layers of fiber/fabric reinforced composites. This concept offers exceptional esthetics important in dentistry along with high strength and stiffness and consequently it provides dentists clinically reliable, versatile and cost effective alternative to traditional dental metal alloys and ceramics.

The major topics of presented work are:

- to review the basic material and clinical aspects of layered composite,
- to review strategies for multi - scale modelling of layered composite,
- to investigate effects of microscale and mesoscale structural features of model layered composite superstructures on stiffness and stress distribution.

2 LITERATURE REVIEW

2.1 MATERIALS FOR DENTAL LAYERED COMPOSITES

2.1.1 Definitions

The term "layered composite" is not well define in current literature and clear definition is needed.

First we recapitulate some relevant facts and definitions: Common classification of composites takes in account two viewpoints:

(1) classification by the nature of constituents,

(2) classification by the form of discrete constituents:

- particle composites,
- fiber composites (long/continuous fibers, short aligned/random fibers, fabrics),
- structural (laminate, sandwich).

There are several alternatives of this general classification available in the literature (see [1], [2], [3], [4]).

Definition of a lamina:

"A lamina (also called a ply or layer) is a single flat layer of unidirectional fibers or woven fibers arranged in a matrix." [4]

Definition of laminate:

"A laminate is a stack of plies of composites. Each layer can be laid at various orientation and can be different material systems." [4]

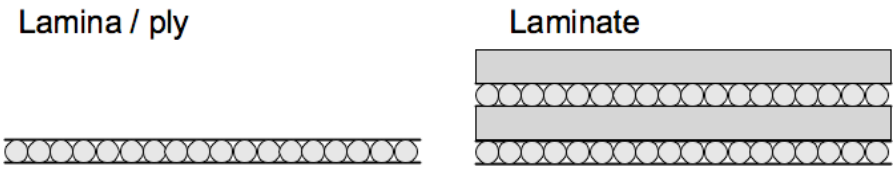

FIGURE 1: *Scheme of lamina and laminate*

Definition of prepreg:

"Prepregs are ready-made tape made of fibers in a polymer matrix." [4]

Definition of sandwich composite:

" The principle of sandwich construction consists in coating to a core (made of a light material or structure having good properties under compression on both sides) with two sheets or skins (having good properties under tension)." [3]

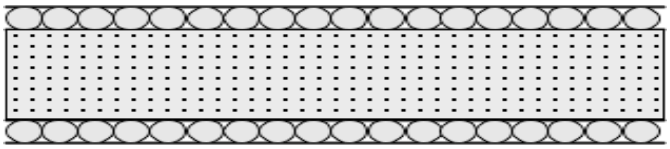

***FIGURE 2**: Scheme of sandwich composite*

Definition of the layered composites this work deals with:

Layered composite combines one or more layers of fiber-reinforced prepregs of the same or different types with one or more layers of PFC of one or more different types. Individual layers may be connected directly or through a thin layer of interphase consisting of resin (adhesive) with no or low volume of particles.

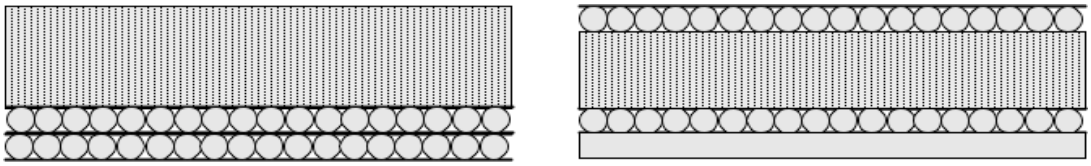

***FIGURE 3:** Schemes of several alternatives of layered composites*

2.1.2 Primary constituents of dental layered composites

2.1.2.1 Resins

In further text we concentrate on light-cured resins which represent the constituent of all materials in layers of layered composite:

- FRC layers
- PFC layers
- inter-layer interphase (adhesive).

A common composition of dental light-cured resins usually comprises:

- High viscosity monomer (bis-GMA)

Bis-GMA belongs to multifunctional methacrylates. As can be seen in Fig. 4 aromatic dimethacrylates contain in their central part two rings and two OH/NH group which provides the molecule rigidity causing extremely viscosity. This rigidity also reduces molecule's ability to rotate during polymerization and to participate efficiently in the polymerization process. [8]

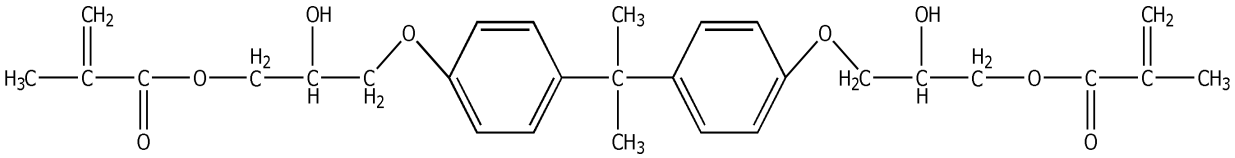

FIGURE 4: *Bis – GMA*

- Low viscosity monomer - (TEGDMA, UEDMA, HEMA)

Methacrylates with linear molecule (triethylene glycol dimethacrylate – TEGDMA – see Fig. 5, urethane dimethacrylate – UEDMA – see Fig.6, hydroxyethyl methacrylate – HEMA – see Fig. 7) are usually added to high viscosity monomer. Their linear flexible molecules without any rigid areas are able to reduce and control the viscosity of compound mixture of oligomers.

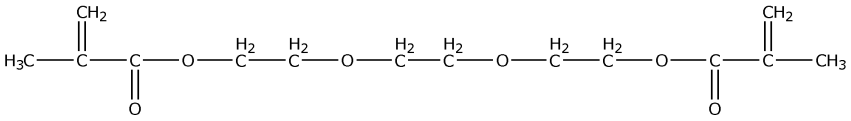

FIGURE 5: *Triethylene glycol dimethacrylate - TEGDMA*

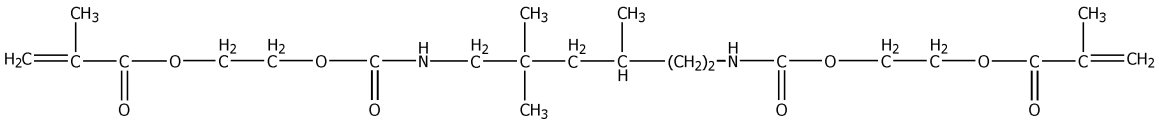

FIGURE 6: *Urethane dimethacrylate - UEDMA*

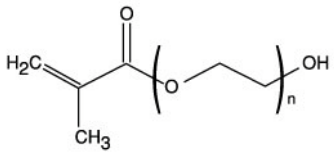

FIGURE 7: *Hydroxyethyl dimethacrylate - HEMA*

- Initiators

Initiator system of dental resins is of type II (bimolecular system) which means that two diffent photoinitiators contribute to initial free-radical generation.

1,2-Diketones, such as camphorquinone (CQ) are generally used in combination with amines as co-initiators (dimethyla,inoethyl-methacrylate DMAEMA). The α-amino-alkylradicals initiate the polymerization reaction, while the ketone radical mainly dimerizes or disproportionates. As the diketone is destroyed by photochemical reduction these co-initiatiors can undergo bleaching and allow the curing of thick layers, up to 20mm in dental restoring materials. [9]

a) Camphorquinone (CQ) b)dimethylaminoethyl-methacrylate (DMAEMA)

***FIGURE 8**: Photoinitiators*

- Polymerization, oxygen inhibition and polymerization shrinkage

Dental dimethacrylate resins undergo visible light induced free radical polymerization. The polymerization scheme consists of three phases: initiation, propagation and termination and two phenomena, oxygen inhibition and shrinkage should be taken in consideration when analyzing layered composites.

Initiation and oxygen inhibition:

If the resin is exposed to the air, oxygen inhibition occurs during initiation. The generated free-radicals react with a molecule of oxygen to form peroxy radicals, which are nonreactive towards the reactive group of the monomer. The free monomer layer - inhibited layer - will remain on the surface after curing as the free radicals are more reactive towards oxygen than the reactive groups of the monomer.

The measure of inhibition effect of oxygen is the degree of conversion (DC). For bis-GMA it changes from 20% on the surface to 80 % in the depth of 20 μm. The transition from inhibited to bulk regions was located at depth varying from 5μm (50 wt% of filler) to 15μm (30 wt% of filler). [40]

Inhibited layer still has the potential for polymerization if supplied with sufficient free radicals. It is thought that some polymer initiators will diffuse into the inhibited layer and induce a chemical reaction resulting in a bond of the cured lower layer to the newly-cured upper layer. [41]

The impact of inhibited layer to the bond strength of composites is an controversial issue. However recent studies have concluded that oxygen inhibited layer made no significant difference in bond strength. [38]

Propagation and polymerization shrinkage:

During polymerization of dimethacrylates monomers, the double bond in CH2═C~ opens reacting with available growing centre to prolongate the growing centre. These growth centres, initially generate discontinuous microgel regions, and as polymerization progresses they expand and encounter other regions of gelation. As gelation continues, the mobility of the propagating system decreases as the viscosity of the material increases and the gel-point is reached. [12]

When the groups of atoms of adjacent monomers react and create covalent bond they move closer and generates bulk contraction (shrinkage).

The majority of shrinkage takes place during the pre-gelation phase when the material behaves plastically and elastic modulus is low (see Figure 9). This part of shrinkage is manifested as shrinkage strain and it does not cause the shrinkage stress because it is eliminated by the viscous flow of polymer (plastic deformation).

During the post-gelation stage when the polymer solidifies, elastic modulus increases rapidly. The material present predominantly elastic behavior.

The shrinkage generated during this second stage cannot be manifested as a bulk contraction (strain) due to the gained rigidity and therefore it is manifested as a stress called polymerization shrinkage stress (see Figure 9). [35]

There are certain clinical consequences of oxygen inhibition and polymerization shrinkage. Shrinkage may cause failure in three different ways:

- Direct failure of weak tooth tissue,
- Failure of weak tooth tissue during the functional loading (mastication),
- Failure of tooth-restoration interface.

Factors contributing to polymerization shrinkage and respective stress comprise:

- monomer system,
- the concentration of diluent in the resin matrix (TEGDMA/BisGMA ratio e.g.),
- concentration of initiators and inhibitors,
- filler (contents, size and elastic modulus) in PFC,
- cavity geometry represented,
- hygroscopic expansion resulting from water sorption,
- light curing method,
- placement technique.

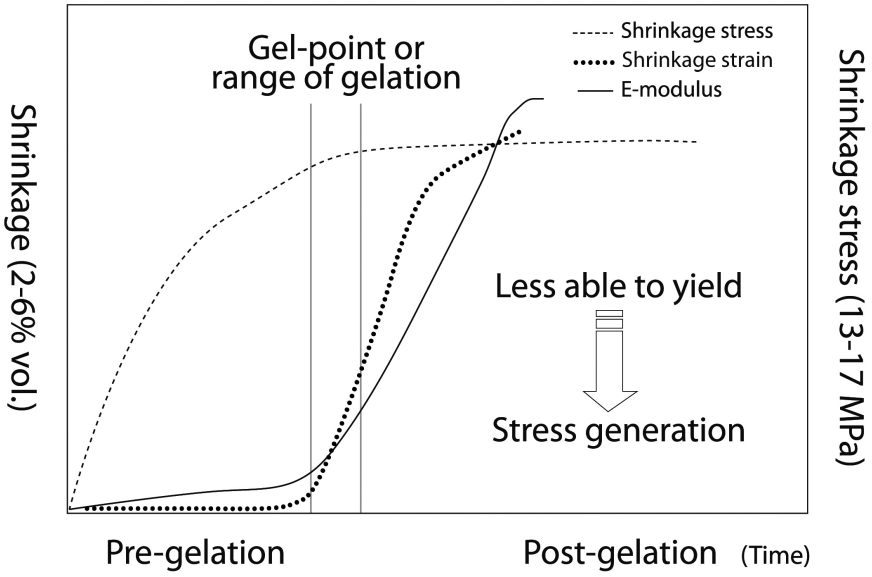

***FIGURE 9**: Relationship among the stages of polymerization and shrinkage and shrinkage stress [35]*

2.1.2.2 Fillers

Particle filled composites used in layer composites are either microhybrid composites or microfilled composites.

Microhybrid composites contain irregularly shaped glass (borosilicate glass, lithium or barium aluminum silicate, strontium or zinc glass) or fairly uniform diameter of quartz or zirconia particles. Typically, composites have a distribution of two or more sizes of fine particles plus microfine filler (5-15%). This distribution permits more efficient packing allowing to reach 60-70% filler by volume and 77-84% by volume.

Microfilled composites contain silica with a very high surface area and consequently only 25% by volume or 38% by weight can be added to the oligomer to keep the consistency of the paste sufficiently low for clinical applications. [6]

Radiopacity is essential to any type of restorative material. ISO norm [33] states that the minimum radiopacity of a restorative material should be equal or greater than that of the 2 mm-thick aluminum step wedge. In order to provide radiopacity fillers Barium (Ba), Srontium (Sr) or Lanthanum (La) are included into the glass fillers.

According to van Noort [7] the fillers offers potentially major benefits:

- reduction of polymerization shrinkage and coefficient of thermal expansion,
- reinforcing effect (improved strength and hardness),
- radiopacity,
- means of controlling esthetic features (color, translucency, fluorescence).

2.1.2.3 Fibers

Prevailing material for fibers in dental FRCs is glass. There are two types of glass fibers available in dental FRCs:

- E-glass - contains up to 1% $K_2O + Na_2O$. E-glass is based on the SiO_2-Al_2O_3-CaO-MgO system, which has good glass-forming ability. For relatively high content of calcium oxide (CaO), E-glass shows poor resistance to acid solutions. Hence, the composition of E-glass is modified by introducing boron oxide (B_2O_3) and decreasing the CaO content. However, amount of B_2O_3 in the glass fibers influences hydrolytic stability of the glass surface. It limits the use of E-glass fiber reinforced polymers in dental environment.
- S2-glass - high tensile-strength glass fibers are - with regard to their composition - more stable in aqueous environment. It does not contain alkali ions (K_2O and Na_2O) and there is no risk of hydrolytic stability loss. This makes S2-glass fibers exceptionally good for applications in dentistry.

Fibers are arranged in prepregs in two modes:

- unidirectional prepreg,
- multidirectional prepreg (woven, non-woven, braided).

TABLE 1: *Chemical composition of glass fibers used in dental FRCc [58]*

Chemical Component	**E-glass [%]**	**S2-glass [%]**
SiO_2	54,3	64,2
Al_2O_3	15,2	24,8
B_2O_3	8,0	trace
CaO	17,2	trace
MgO	4,7	10,3
Na_2O	0,6	0,3
Fe_2O_3	---	0,2

TABLE 2: *Selected mechanical and physical properties of glass fibers used in dental FRCs [58]*

Fiber property	**E-glass**	**S2-Glass**
Density [g/cm^3]	2,55 – 2,58	2,46 – 2,49
Tensile modulus [GPa]	69 - 72	86 - 90
Tensile strength (strand) [GPa]	500	665
Tensile strength (nominal design) [GPa]	270 - 390	530 – 620
Range of elongation [%]	4,5 – 5,0	5,4 – 5,8
Thermal expansion [10^{-6} cm/cm/°C]	5,4	1,62
Fiber diameter range [μm]	4 - 25	5 - 9

2.1.2.4 Surface treatment

The interaction between matrix and reinforcing / filling particles is the crucial issue in composites. The better adhesion is ensured, the better load distribution throughout the material and the better resistance to interfacial diffusion of water. Adhesion of lower moduli polymeric matrices to higher moduli inorganic fillers or reinforcements can be caused by several types of interactions: micro-mechanical interlocking mechanism, physical bonds (electro-static bonds, hydrogen bonds) or covalent bonds.

In order to allow good bond between matrix and reinforcing / filling particle functional organosilanes are used to mediate interfacial bonding between organic and inorganic phases.

Organosilanes, $(R_1R_2R_3)SiX_n$ (where n=1 to 3) have a hydrolytically active silicon based functional group. They can react with both inorganic and organic substrates as well as with themselves and other silanes.

R groups can be reactive with terminal functional groups capable of specific chemical reactions, e.g. a methacrylate group that will copolymerize with methacrylic monomers, respectively - see Fig 10. [18]

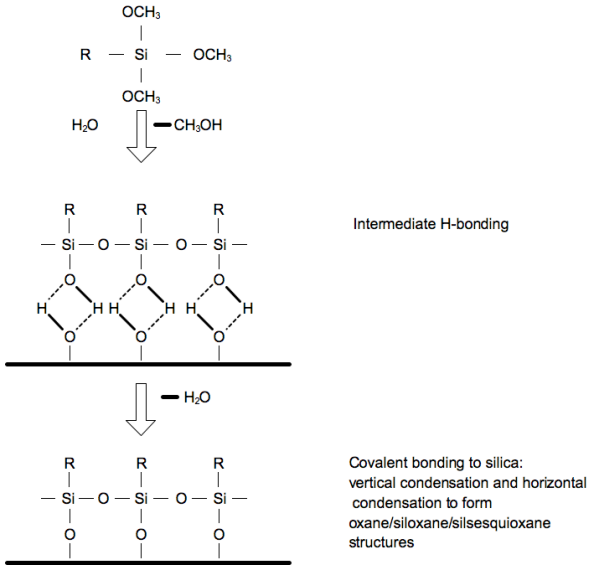

FIGURE 10: *Simplified reaction of organotrialkoxysilanes with silica surfaces [18]*

Typical coupling agent in methacrylic resin based dental composites is 3-methacryloxypropyltrimethoxysilane (MPTMS) - see Fig.11.

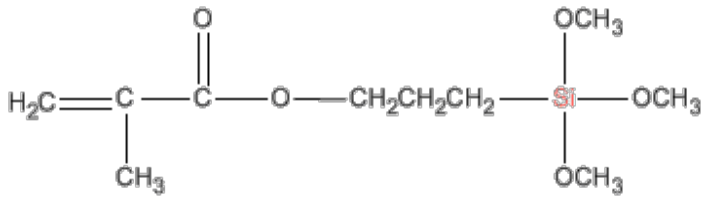

FIGURE 11: *3-methacryloxypropyltrimethoxysilane (MPTS)*

2.1.3 Materials in layers

2.1.3.1 Pre-impregnated fiber reinforced composites (FRCs) - prepregs

During the 1990's a number of dental fibre-reinforced resin systems have become available, either for the use in laboratory or in the dental surgery [7].

Several basic concept of using FRCs in dentistry can be identified:

- Cured pre-fabricated FRC posts for the retention of the crown in endodonticaly treated teeth.
- Cured FRC pins for the retention of the crown in endodonticaly treated teeth. This relatively new concept overcomes invasive post-ortho treatment as well as it preserves original biomechanics of the tooth and consequently prevents root fracture.
- Reinforcing tapes (dry reinforcing fabric). The final FRC is prepared chair-side in the dental surgery by wetting the tape with appropriate resin.
- Prepregs with uni-directional or multi-directional fibers combined with several dental PFCs and adhesives.

2.1.3.2. Restorative particle filled composites (PFCs)

The concept of the application of PFCs has developed since early 20th century. The development of composites in the 1960s resulted in higher mechanical properties, lower thermal coefficient and coefficient of expansion, lower dimensional change on setting, and higher resistance to wear, thereby improving clinical performance. Early composites were chemically activated, followed by photo-activated composites initiated with ultraviolet (UV) wavelengths. They were later replaced by composites activated in the visible wavelengths. Continued development of bonding agents for bonding composites to tooth structure has also improved the longevity of composite restorations. [6]

Dental PFCs consist typically of matrix, filler, internal interface coupling agent, initiator, accelerator, and pigments. Clinical function of dental PFCs depends also on an external coupling agent - bonding agent which is not an integral part of the PFC but which should be taken into consideration..

Classification of PFCs is not standardized and somewhat confusing because of mixture of several viewpoints. When clear classification criteria are adopted, classification of dental PFCs is derived as presented in Table 3 (material criteria) and Table 4 (procedure/application criteria).

Microfill hybrid and microfill flowable composites are the classes of the major interest in this work because they are combined with FRCs in layered composites.

2.1.3.3. Bonding agent

With regards to layered composites the following adhesive systems are taken in account:

- composite - adhesive - composite: intra - layer interphase, core - reinforced crown,
- enamel - adhesive - composite: splints, maryland bridge,
- dentine - adhesive - composite: inlay-, onlay-, crown- bridge.

Dentine bonding agents normally consist of three essential components[6] [7]:

- a conditioner (variety of acids that alter the surface appearance and characteristics of the dentine),
- a primer (adhesive providing a means of bonding hydrophobic composite to hydrophilic dentine),
- a sealer (mixture of Bis-GMA and HEMA based resin sealing the dentine surface via the primer and bonding to the composite resin).

The adhesive adheres to composite by the process of co-polymerization of residual double C=C bonds in the oxygen inhibition layer.

Some of bonding agents contain fillers and are regarded as particle filled composites from material point of view (cements, filled resins). This work focuses on bonding agents without fillers, which may usually form an interphase in layered composites.

TABLE 3: *Dental PFC – classification (materials used in layered composites are written bold italic)*

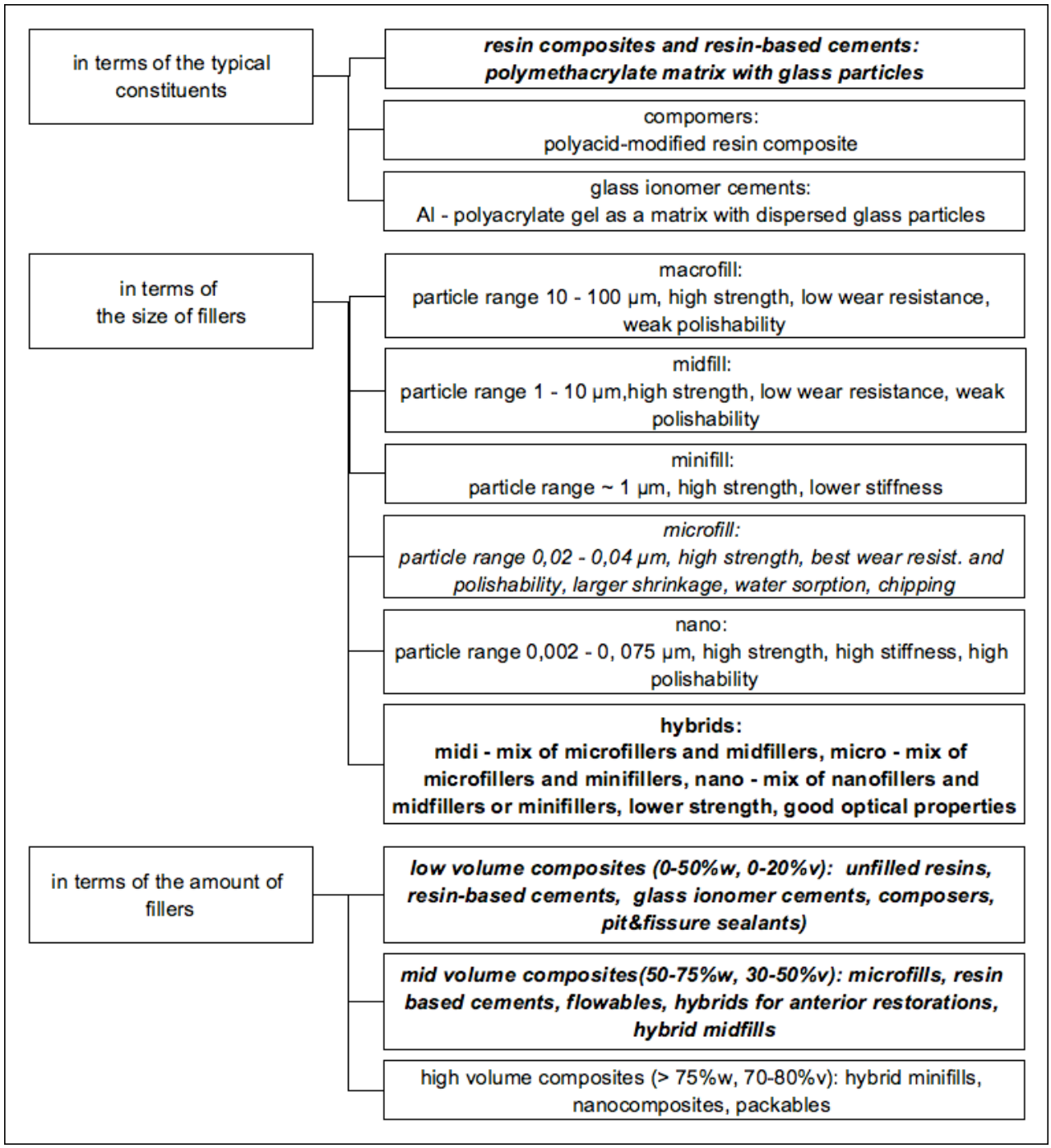

TABLE 4: *Dental PFCs – classification based on procedures (materials used in layered composites are written bold italic)*

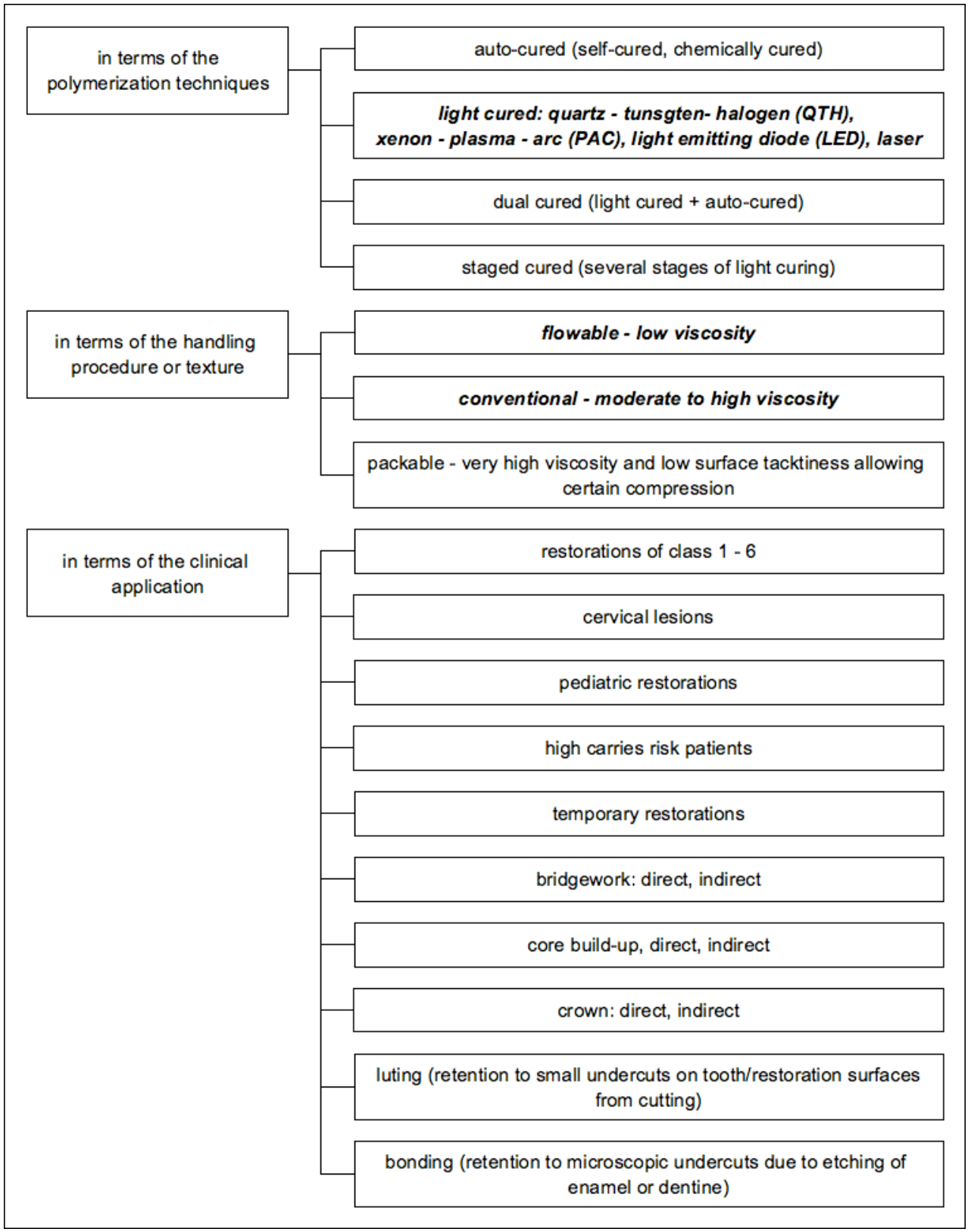

2.2 CLINICAL USE OF COMPOSITES IN DENTISTRY

2.2.1 Clinical use of dental composites – an overview

Clinical dentistry nowadays utilizes several types of structural materials: metal alloys, ceramics, polymer based adhesives, particle filled composites (PFC) and fiber reinforced composites (FRC). Clinical areas where composites are used are as follows:

- restorative dentistry - deals with restoration of damaged and removed tissue of dentin and enamel where the remaining tissue provides enough original function of the tooth (fillings),
- prosthodontics - deals with replacement of the whole tooth or its functional parts (crown),
- orthodontics and pediatric dentistry - deals with corrections of malocclusion,
- traumatology - deals with acute dental traumas,
- periodontics - deals with periodontal disease treatment.

FIGURE 12: *Structure of the tooth*

In restorative dentistry the dental materials are mainly used for filling-up of remaining tissues after removing the damaged tissue of enamel and dentin. For this reason, one of three options of material are used:

- amalgam,
- different types of PFC and relevant adhesives,
- ceramics and relevant adhesives.

It is supposed that the placed material restores the original tissue. In reality, the material usually restores the original geometry, esthetics and conditions in occlusion. Original biomechanics of tissue is often compromised with filling material. Clinical reliability of filling depends on the rate of recovery of all original functions of the tissues: geometry, integration (adhesion and biocompatibility), biomechanics.

Prosthodontics utilizes dental materials in two different situations:

- (i) replacement of the functional part of the tooth (usually crown),
- (ii) replacement of the whole tooth / several teeth / dentition.

When a functional part (crown) of the tooth is replaced - the attention should be focused on restoration of correct conditions in occlusion, on integration of the new functional part (adhesion, retention and its compliance with original biomechanics of the whole tooth) and esthetics. When the whole tooth is replaced - the attention should be focused on restoration of correct conditions in occlusion, on integration into remaining denture (appropriate deflection, adhesion, retention) and esthetics.

In orthodontics and pediatric dentistry the major problems deals with alignment of teeth in wrong position (malocclusion) and prevention of malocclusion. From this point of view one can divide orthodontic devices into two groups: active devices (applying external forces on denture arch in order to correct position of the teeth through remodeling of PDL) and passive devices (resisting undesirable movement of the teeth). When attention is paid to esthetics and clinical reliability of passive device (adhesion, physiological movement of the teeth, absence of patient collaboration), FRCs may be considered as the first choice.

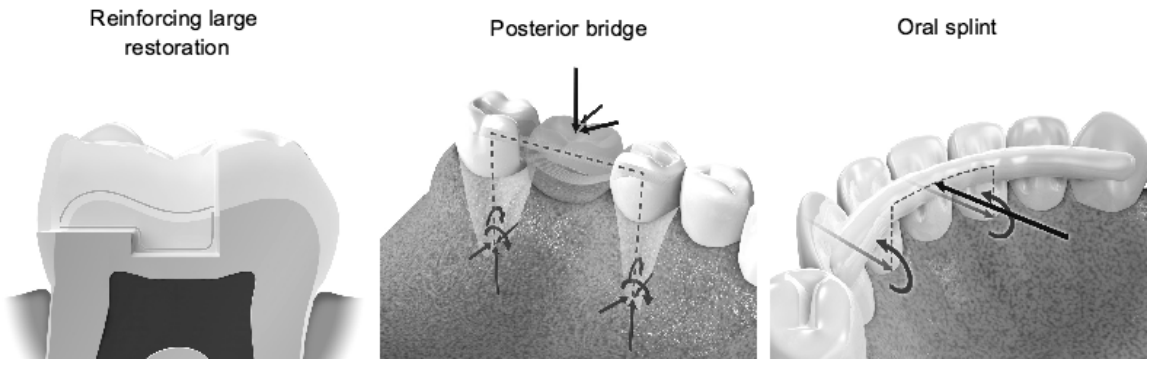

FIGURE 13: *Clinical applications of layered composites*

Devices for traumatology and periodontics (splints) resolve in the same problem: stabilization of mobile teeth. Compared to the other materials, layered composites offer the clinicians the opportunity:

- to be less invasive (save sound tissues) - due to high mechanical performance compared to the other options (e.g. PFC, metal),
- to mimick better the original biomechanics - due to the possibility to control mechanical properties,
- to provide highly esthetic clinical solutions - due to the optical properties of PFCs and high mechanical performance allowing to construct subtle devices.

2.2.2 Biomechanics of typical applications of layered composites

2.2.2.1 Biomechanics of splints

The main objective of splint is stabilize teeth in all three dimension. If splinting is to achieve any measure of success, the center of rotation of the abutment teeth must be located in the remaining supporting bone. In this way, the affected teeth are able to resist tooth movement.

Splint is a part of frame where abutment teeth serve as vertical beam and splint itself serves as horizontal beam which bears the forces from loosen teeth. Major loading forces are horizontal and perpendicular to dental arch. Stabilizing capacity of the splint is directly proportional to the stiffness of the splint and its adhesion to mobile and abutment teeth. However splint should allow physiological movement of the teeth.

2.2.2.2 Biomechanics of dental bridges

Primary roles of bridge framework are:

- to carry the pontic,
- to shift the load applied to pontic during mastication to abutment teeth.

The major portion of masticatory forces shifted by bridgework from pontic to abutment teeth acts verticaly. Therefore the bridgework is subjected to deflection. It creates compression in upper part of the structure and tension in lower part of the structure (it is opposite for cantilever bridge). This type of stress requires putting reinforcing prepreg in the bottom part of bridge framework. There are also peeks of shear stress in the inter-proximal area between abutment teeth and pontic. In order to minimize these peeks it is recommended to form a curvature of prepreg in this area.

2.2.2.3 Biomechanics of the strengthening of large restorations

The ultimate success on failure of a restored tooth dependends on clinical management such as material choice, cavity design, bonding techniques and others.

Clinical observations of fractured teeth show that most fractures are initiated in dentin at the internal line angles of the cavity base. Fatigue is considered to be the principal mechanism of tooth fracture as the clinical symptoms generally occur many years after the placement of the restoration. The pulpo-axial line angle in dentin at the base of the cavity is the site of a high stress concentration when a tooth is subjected to cyclic occlusal or thermal loading.

Critical area is dentino-enamel junction where brittle enamel changes into tough dentin. Mechanical analysis of dentino-enamel junction showed that it has extremely high value for work on fracture (W_f). This feature makes dentino-enamel junction effective crack deflector and blunter and zone capable of plastic deformation. FRC offer minimally invasive and effective way how to minimize risk of tooth fracture by mimicking this feature of intact tooth using a reinforcing net. The net is capable to spread eventually stress concentration into larger area when placed into the position where the largest stress concentrations are expected.

2.3 MECHANICAL PRELIMINARIES

2.3.1 Basic concepts

When a piece of material is loaded, several regimes of its response may occur depending on many factors such as the type of material, the size and geometry of the piece, magnitude of the loading and its time mode, temperature etc. The mechanical response is always related with the resistance against deformation.

Loading in the elastic regime generates reversible deformation contrary to loading in the plastic regime generating irreversible deformation and material behavior is dissipative. Visco-elastic behavior means time-dependent reversible deformation, material behavior is also dissipative. When the loading exceeds the strength of the piece of material, the piece disintegrates and fails.

Deformation in the point of the body is expressed by displacement which is a vector function:

$$u = \{ u(x), v(y), w(z) \} \quad (1)$$

Vector gradient of displacement provides 2nd rank tensor from which strain tensor **ε** is derived through the concept of engineering shear strain:

$$\varepsilon_{ij}=1/2(\partial u_i/dx_j + \partial u_j/dx_i) \qquad (2)$$

Stress tensor is derived by normalizing the load by cross-section and by eliminating the influence of mass and shape of resisting material through the concept of traction T:

$$T = \sigma\, n \qquad \text{(Cauchy's relation)} \qquad (3)$$

where: σ = stress (tensor)
n = normal vector to the surface $A \rightarrow 0$

The values of components of state of stress and strain depend on the orientation of coordinate system. In a particular coordinate system individual components reach their maximum value and others reach minimum value. Any stress state (stress tensor) has a coordinate system where the components of tensor are only on diagonal (off-diagonal components = 0). Any strain state (strain tensor) has a coordinate system where the components are only on diagonal (off-diagonal components = 0) – principal directions and respective principal stresses / strains.

Most of materials posses the same behavior in different directions - they demonstrate some type of symmetry.

Some specific symmetries of anisotropic materials relevant to composites are as follows:

- transversely isotropic material: its symmetry group includes all rotations about specified axis,
- orthotropic material: its symmetry group includes reflections with respect to each of three mutually orthogonal planes (various types of crystal symmetry are symmetry subgroups of full orthogonal group).

Mechanical constitutive equations define the relation between the traction caused by external loads and reflected in stress tensor and kinematic variables such as displacement represented by strain tensor or rate-of-deformation tensor with regards to the properties of specific material.

Constitutive equations should comply with following requirements:

- dimensional homogeneity
- independence of coordinate system (tensors)
- stress response is not affected by rigid body motion (invariance under translations and rotations of the frame of reference).

Constitutive equations describe the most important features of the material in specific situation. It is impossible to formulate the equations which would describe the behavior of specific material under all circumstances. The real equations describe behavior of idealized material (material model) under simplified circumstances as defined in special theories (elasticity, visco-elasticity etc.)

2.3.2 Strategy of the mechanical analysis

2.3.2.1 Problem formulation

The problem of the mechanics of deformable solids consists of seeking the displacement field u(M,t) and the stress field σ (M,t) at every point M of the body.

There is total amount of 15 unknown variables:

- three displacements: u, v, w
- six members of the strain tensor: ε_{xx}, ε_{yy}, ε_{zz}, $\varepsilon_{xy}=\varepsilon_{yx}$, $\varepsilon_{xz}=\varepsilon_{zx}$, $\varepsilon_{yz}=\varepsilon_{zy}$
- six members of the stress tensor: σ_{xx}, σ_{yy}, σ_{zz}, $\sigma_{xy}=\sigma_{yx}$, $\sigma_{xz}=\sigma_{zx}$, $\sigma_{yz}=\sigma_{zy}$

2.3.2.2 Available relations

For resolving the problem of the mechanics of deformable solids several relations are available:

(i) The fundamental equations (equilibrium equations) - three equations in total:

$$\partial\sigma_{ij} / \partial x_j + q_i = 0 \qquad (4)$$

where: q = body force

(ii) The strain - displacement equation (geometric equation) - six equations in total (2):

$$\varepsilon_{ij}=1/2(\partial u_i/dx_j + \partial u_j/dx_i)$$

(iii) The compatibility conditions relations satisfy the requirement that no gaps or overlaps are developed when the deformable body is deformed. They are obtained by integrating strain - displacement equations (2) and provide another six relations which ensure that the displacement field is unique:

$$(\partial^2\varepsilon_{ij}/\partial x_k\partial x_l) + (\partial^2\varepsilon_{kl}/\partial x_i\partial x_j) - (\partial^2\varepsilon_{ik}/\partial x_j\partial x_l) - (\partial^2\varepsilon_j l/\partial x_i\partial x_k) = 0 \quad (5)$$

(iv) Constitutional equations (behavior law) describe how the specific material behaves under certain mechanical regime, i.e. these equation relates stress and strain under certain circumstances as has discussed in preceding section an provide another six relations:

$$\sigma_{ij} = f(\varepsilon_{kl}) \tag{6}$$

(v) The boundary conditions are conditions at the boundary (Γ) of the deformable solid body (D). Boundary conditions are of two types (see Figure 14):

- geometrical conditions describe displacements (uΓ) given on the part of the boundary of the solid body (Γu):

$$(\Gamma_u) : u = u_\Gamma, v = v_\Gamma, w = w_\Gamma \tag{7}$$

- force conditions describe equilibrium between the external surface forces (fsΓ) given on the part of the boundary of the solid body (Γ_{fs}) and respective internal forces. If the external forces are given:

$$f_{s\Gamma} = \{f_{s\Gamma x}, f_{s\Gamma y}, f_{s\Gamma z}) \tag{8}$$

than the equilibrium on the surface part (Γ_{fs}) is:

$$(\Gamma_{fs}): \quad \begin{aligned} f_{s\Gamma x} &= \sigma_{xx}\alpha_x + \sigma_{xy}\alpha_y + \sigma_{xz}\alpha_z \\ f_{s\Gamma y} &= \sigma_{xy}\alpha_x + \sigma_{yy}\alpha_y + \sigma_{yz}\alpha_z \\ f_{s\Gamma z} &= \sigma_{xz}\alpha_x + \sigma_{yz}\alpha_y + \sigma_{zz}\alpha_z \end{aligned} \tag{9}$$

Boundary conditions provide another six relations and complete the set of equations available for mechanical analysis.

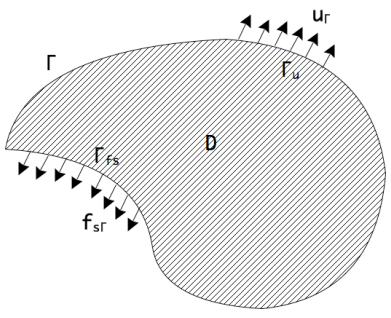

FIGURE 14: *Solid body subjected to external load*

2.3.2.3 Overview of strategies

There are several strategies available for mechanical analysis. They are classified according to several viewpoints:

In terms of the mathematic formulation

- differential formulation - seeking solution of the system of differential equations,
- variational formulation - seeking status where energy of the body reaches extreme value.

In terms of the choice of elastic functions (substituting variables in constitution equations one group is eliminated while other group is calculated first)

- deformation method - displacement (u, v, w) is calculated first,
- force method - stresses (σ_x, σ_y, σ_z, τ_{xy}, τ_{yz}, τ_{zx},) are calculated first,
- mixed method - some members of displacement and stress are calculated first.

According to the technique of calculation

- analytical - solution is a continuous function (mathematical analysis),
- numerical - discretization and seeking finite amount of parameters which approximate the function.

Thanks to computers, numerical variants of mechanical analysis became very widely used over the last decades. Among several numerical methods the methods of domain discretization and namely finite element method (FEM) are popular due to their versatility.

FEM is used with connection to specific software systems (ANSYS, ABAQUS etc.) which usually require following steps to set up the FEM calculation:

- The geometry of the solid. This is done by generating a finite element mesh for the solid. The mesh can usually be generated automatically from a CAD representation of the solid. Dimensionality and symmetries should be taken in account in order to reduce computing time.
- The properties of the material. This is done by specifying a constitutive law for the solid.
- The nature of the loading applied to the solid. This is done by specifying the boundary conditions for the problem.
- When the analysis involves contact between two or more solids, it is necessary to specify the surfaces that are likely to come into contact, and the properties (e.g. friction coefficient) of the contact.
- Specification of additional aspects relevant to the problem:
  - specification of linearity/non-linearity of the problem in the static analysis,
  - specification of the time period of the analysis, and of the size of the time step (or number of steps) for history dependent materials, etc.
- Specification of what are the output variables of the finite element analysis.

2.3.3 Elasticity

Constitutional equation of elastic behavior:

$$\sigma_{ij} = C_{ijkl}\,\varepsilon_{kl} \tag{10}$$

or

$$\varepsilon_{kl} = S_{klij}\,\sigma_{ij} \tag{11}$$

where: σ_{ij} = stress tensor
ε_{kl} = strain tensor
C_{ijkl} = stiffness tensor - fourth order tensor of material constants of resistence against deformation
S_{klij} = compliance tensor - fourth order tensor of material constants of compliance to deformation

Stiffness and compliance tensors are called elastic tensors and each of them has generally 9 x 9 = 81 members. This number can be reduced (based on the fact that stress and strain tensors have only 6 independent members) to 6 x 6 = 36 members

The number of elasticity tensor members ≠ 0 differs depending on the symmetry of material written as follows:

Stiffness tensor of an anisotropic materials - 36 members

$$C_{anisot} = \begin{bmatrix} C_{xxxx} & C_{xxyy} & C_{xxzz} & C_{xxyz} & C_{xxzx} & C_{xxxy} \\ C_{yyxx} & C_{yyyy} & C_{yyzz} & C_{yyyz} & C_{yyzx} & C_{yyxy} \\ C_{zzxx} & C_{zzyy} & C_{zzzz} & C_{zzyz} & C_{zzzx} & C_{zzxy} \\ C_{yzxx} & C_{yzyy} & C_{yzzz} & C_{yzyz} & C_{yzzx} & C_{yzxy} \\ C_{zxxx} & C_{zxyy} & C_{zxzz} & C_{zxyz} & C_{zxzx} & C_{zxxy} \\ C_{xyxx} & C_{xyyy} & C_{xyzz} & C_{xyyz} & C_{xyzx} & C_{xyxy} \end{bmatrix} \tag{12}$$

The physical meaning of individual members of elastic tensor depends on their position within the tensor:

- members with indices i=j ∨ k=l (upper left quadrant) determine how normal stresses influence elongations/contractions,
- members with indices i=j ∨ k≠l (lower left quadrant) determine how shear stresses influence elongations/contractions,
- members with indices i≠j ∨ k=l (upper right quadrant) determine how normal stresses influence distortions,
- members with indices i≠j ∨ k≠l (lower right quadrant) determine how shear stresses influence distortions.

Stiffness tensor of an orthotropic material (two planes of symmetry xy, xz) - 9 members:

$$C_{ortho} = \begin{bmatrix} C_{xxxx} & C_{xxyy} & C_{xxzz} & 0 & 0 & 0 \\ C_{yyxx} & C_{yyyy} & C_{yyzz} & 0 & 0 & 0 \\ C_{zzxx} & C_{zzyy} & C_{zzzz} & 0 & 0 & 0 \\ 0 & 0 & 0 & C_{yzyz} & 0 & 0 \\ 0 & 0 & 0 & 0 & C_{zxzx} & 0 \\ 0 & 0 & 0 & 0 & 0 & C_{xyxy} \end{bmatrix} \quad (13)$$

Stiffness tensor of an isotropic material (rotational symmetry) has 9 members. Because there are no privileged directions and the tensor must be invariant under every rotational transformation some members are related (dependent):

$$C_{xxxx} = C_{yyyy} = C_{zzzz} = E \quad (14)$$

$$C_{xxyy} = C_{xxzz} = C_{yyxx} = C_{yyzz} = C_{zzxx} = C_{zzyy} = B = -\mu E \quad (15)$$

$$C_{yzyz} = C_{zxzx} = C_{xyxy} = G \quad (16)$$

where: E = modulus of elasticity
μ = Poisson's constant
G = shear modulus of elasticity

$$G = E / 2(1+\mu) \quad (17)$$

Stifness tensor thus has only two independent elastic constants (E,μ) which should be derived from test for specific material:

$$C_{iso} = \begin{bmatrix} E & -\mu E & -\mu E & 0 & 0 & 0 \\ -\mu E & E & -\mu E & 0 & 0 & 0 \\ -\mu E & -\mu E & E & 0 & 0 & 0 \\ 0 & 0 & 0 & G & 0 & 0 \\ 0 & 0 & 0 & 0 & G & 0 \\ 0 & 0 & 0 & 0 & 0 & G \end{bmatrix} \quad (18)$$

2.3.4 Visco-elasticity

Materials display time- dependent mechanical behavior under certain conditions (temperature, strain rate). If the deformations in such behavior are reversible it is called visco-elasticity. Two phenomena are significant for visco-elasticity: creep (deformation progresess with constant load) and stress relaxation (stress decreases with constant strain) - see Figure 15.

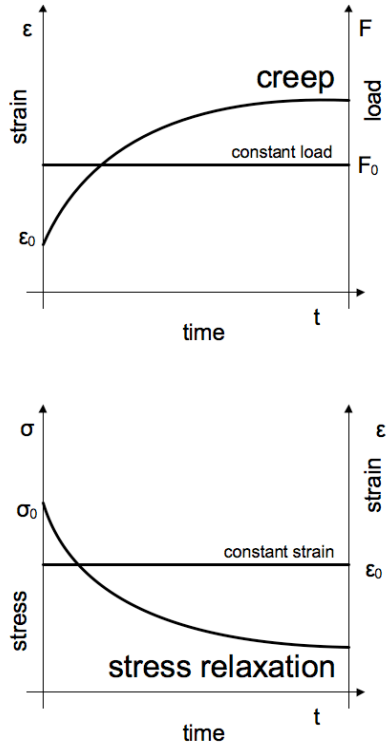

FIGURE 15: *Creep and stress relaxation*

Several formulations for constitutive equation of visco-elastic behavior were derived, among others the most general form given by hereditary integral:

$$\sigma_{ij}(t) = \int_{-\infty}^{t} R_{ijkl}(t-\tau)\frac{\partial \varepsilon_{kl}(\tau)}{d\tau}d\tau \qquad (19)$$

and its inverse relation

$$\varepsilon_{ij}(t) = \int_{-\infty}^{t} G_{ijkl}(t-\tau)\frac{\partial \sigma_{ij}(\tau)}{d\tau}d\tau \qquad (20)$$

where: R_{ijkl} = relaxation functions (4th order tensor)
G_{ijkl} = creep functions (4th order tensor)
τ = time inkrement
t = total time elapsed

2.3.5 Failure

Failure is the state when materials lose their strength under the action of external loads. There are several modes of failure (buckling, corrosion, wear etc.).

This text focuses on two of above mentioned failure modes: fracture and fatigue.

2.3.6.1. Fracture

Fracture disintegrates material due to the crack propagation. The resistance of material against the crack propagation and fracture is called toughness. Relation between the resistance of material against plastic deformation - strength (yield strength) and toughness (fracture toughness) determines the type of fracture:

- high yield strength and low fracture toughness leads = brittle fracture,
- low yield strength and high fracture toughness = ductile fracture.

Fracture mechanics deals with solids in which the presence of cracks is assumed and with relations between the crack length, material resistance to crack growth, and stress at which the crack propagates.

Several concepts of fracture mechanics comprises:

- Energy balance approach (Griffith, Irwin): When the crack propagates, it creates new surface. To create a surface costs energy called surface energy. This energy consist of elastic energy and energy needed for plastic deformation round the crack tip.
- Stress intensity approach: a remote stress concentrates around the crack. Local stress rises steeply as the crack tip is approached. New quantity was introduced by Owing in order to give the magnitude of the elastic stress field at the crack tip. This quantity is called stress intensity factor (K). Stress intensity factor depends on remote stress, length of the crack and local mode of crack surface displacement (Mode I – opening, Mode II – sliding, Mode III – tearing). The idea that the material can withstand the stresses on the crack tip up to a critical value of stress intensity factor K_c introduced the measure of material toughness, although this critical stress intensity factor depends on the local mode of crack surface displacement and other parameters. For material toughness standardized measure called "plane strain fracture toughness" (K_{Ic}) is used which is of course derived from critical stress intensity factor.

Two branches of fracture mechanics were formulated with respect to the material behavior at the crack tip:

- Linear-elastic fracture mechanics (LEFM): first assumes that the material is isotropic and linear elastic. Based on the assumption, the stress field near the crack tip is calculated using the theory of elasticity. In reality the stress around the crack tip exceeds the yield strength of material and plastic zone surrounds the crack tip. LEFM assumes that the plastic zone has the effect as if the crack was longer and with this assumption the theory of elasticity may be used. This is valid only when the inelastic deformation is small compared to the size of the crack, which is called small-scale yielding.
- Elastic-plastic fracture mechanics (EPFM): If large zones of plastic deformation develop before the crack grows, LEFM is not suitable for analyzing fracture. EPFM deals with this type of behavior and several concepts were developed of which two are of common acceptance:
  - concept focused on the strains in the crack tip region instead of stresses: crack opening displacement (COD) approach,
  - concept focusing on changes in potential energy during the crack growth: J-integral approach.

  COD approach is based on the idea, that in presence of plasticity a crack tip will blunt when it is loaded in tension and crack flank displacement at the tip of blunting crack, so called crack tip opening displacement (CTOD) may be used as a fracture parameter - see Figure 16 [23]. J-integral approach focuses on the idea that the contour integral that can be evaluated around any path enclosing the crack tip is considered as a fracture parameter equal to energy release rate for a crack in non-linear elastic material – see Figure 17. [23]

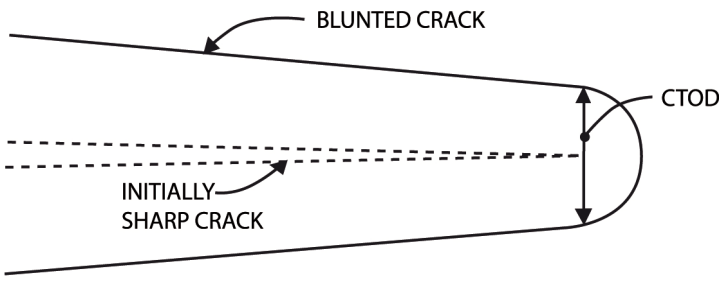

FIGURE 16: *Crack tip opening displacement [23]*

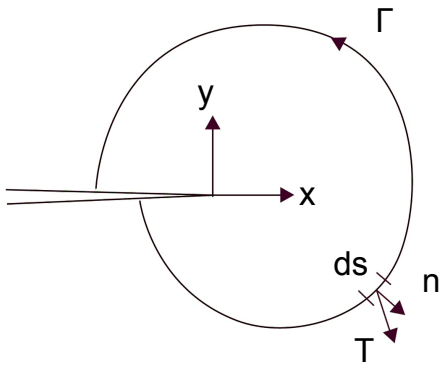

FIGURE 17: *J contour integral [23]*

2.3.6.2 Fatigue

Fatigue is a process in which damage accumulates due to the repetitive application of loads that may be well bellow the yield strength. Material characterization during failure provides S-N diagram where data are plotted as stress S versus the logarithm of the number of the cycles under assumption that loading in each cycle generates the same amplitude of stress - see Figure 18.

The S-N diagram unveils several important features of fatigue:

- fatigue is a probabilistic process,
- damage is cumulative, material do not recover when rested,
- the greater the applied stress, the shorter the life,
- two limits can be recognized: endurance (fatigue) limit - stress bellow which fatigue is not induced, fatigue strength - the stress level at which a component will survive certain number of loading cycles (typically 10^7).

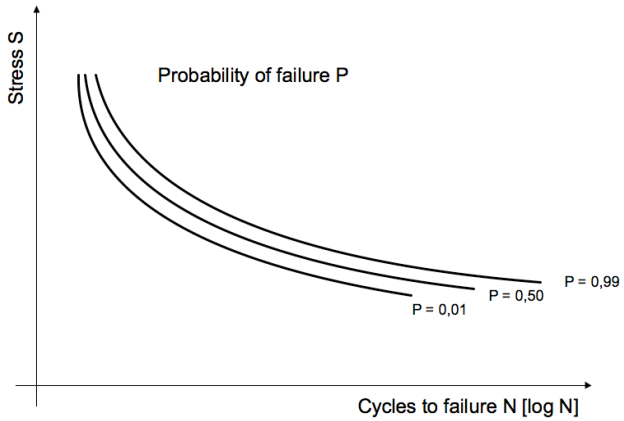

FIGURE 18*: S-N diagram: probability of failure*

2.4 MULTI-SCALE MODELING OF COMPOSITES

2.4.1 Basic concepts

Mechanical response of heterogenous materials, i.e. their mechanical properties, are highly influenced by geometrical arrangement of distinct phases. Composites - as heterogenous materials - have the capability to tailor their properties by varying their internal structure. The structure on finer scale influences the properties on coarser scale.

There are several different scales related to the structures:

- nano-scale (10^{-9}m - 10^{-8}m),
- meso-scale I (10^{-7}m),
- micro-scale (10^{-6}m - 10^{-4}m),
- meso-scale II(10^{-3}m),
- macro-scale: (10^{-2}m - 10^{0}m).

While geometry of a problem and boundary conditions are usually given on the macro-scale, the micro-structure of the material is defined on the micro - meso – scale. Direct numerical analysis of the material behavior which takes into account macroscopic boundary conditions and micro-geometries, would require very large computational resources. [24]

To overcome this problem two basic strategies are employed:

- multi-scale coupled modelling,
- multi-scale uncoupled modelling (homogenization and averaging of properties and microfields).

2.4.1.1. Multi-scale coupled modelling

The material behavior is modeled at the scale levels of both microstructures and the sample. [24]

2.4.1.2. Multi-scale uncoupled modelling

This approach solves the problem down-top on individual scales. Outputs from the lower scale are transferred in the appropriate way to the higher scale.

The basic assumption of multi-scale uncoupled modeling is that there exists relation between spatially variable properties of heterogenous material on micro scale and the effective macroscopic response of such material. A concept of homogenization (equivalent homogeneity) is used for determining the overall properties of the material.

The study of composite material behavior is therefore divided into two branches:

- micromechanics - wherein the constituent materials are studied on a microscopic scale with specific properties being assigned to each constituent; the interaction of the constituent materials is used to determine the properties of the composite,
- macromechanics - wherein the material is presumed homogeneous and the effects of the constituent materials are detected only as averaged apparent properties of the composite.

The concept of equivalent homogeneity states that effective material properties on macro-scale are determined by averages of field variables Ψ (stress, strain e.g.) when their space variation is statistically homogenous. The length of averaging δ must be of a dimension much larger than that of the inhomogeneity. The volume element which has a characteristic dimension identical with that of averaging dimension δ is called "representative volume element" - RVE and its volume is V.

The average field variables <Ψ> is than defined as:

$$\left\langle \Psi_{ij} \right\rangle = \frac{1}{V} \int_V \Psi \, dV \tag{21}$$

When the concept of equivalent homogeneity is applied on the elasticity the constitutional equation(10) is modified to:

$$\left\langle \sigma_{ij} \right\rangle = C^{eff}_{ijkl} \left\langle \varepsilon_{kl} \right\rangle \tag{22}$$

where: $\left\langle \sigma_{ij} \right\rangle$ = volume average stress

C^{eff}_{ijkl} = effective stiffness

$\left\langle \varepsilon_{kl} \right\rangle$ = volume average strain

Conditions of heterogeneity can occur either as a continuous variation of properties (e.g. biological gradient materials) or discontinuous changes of properties (e.g. interphase). In composites the latter case is involved. Within individual constituents of composite homogeneity and isotropy are assumed.

In order to determine the constitutive equations for the effective properties of a heterogenous material following tasks should be accomplished:

- Definition of the RVE which should be large enough to fulfill the concept of equivalent homogeneity and small enough to allow micromechanical analysis with available computational resources.
- Macro-micro transition (localization) which ensures that microscopic boundary conditions are derived from the conditions on macro-scale (geometry, strain, constitutive laws etc.).
- Micro-macro transition (homogenization) ensures that macroscopic properties of equivalent homogenous medium are evaluated.

With respect to the topic of present work it is practical to focus on the multi-scale uncoupled modeling with regard to micro-meso-macro-scales.

Several methods were developed in order to provide homogenization procedures appropriate to specific materials and conditions. These methods can be divided into following groups:

- analytical methods,
- numerical method (main stream averaging, unit cell method e.g.),
- semi-emiprical methods (Halphin Tsai method e.g.).

The analytical methods can be classified in terms of the theoretical principle used:

- based on effective medium theories (e.g. rule of mixture, Hashin-Shtrikman),
- based on equivalent inclusion theory (e.g. Eshelby, Mori Tanaka).

Overview of multi-scale modeling methods with respect to different types of composites is provided in [25], [26].

2.4.2 Rule of mixture

Assumptions of this method of homogenization are:

- heterogenous materials consists of constituent A with modulus E_A and volume content V_A, and constituent B with modulus E_B and volume content V_B,
- the strain is uniform throughout the material: $\varepsilon = \varepsilon_A = \varepsilon_B$ (Voigt), or
- the stress is uniform throughout the material: $\sigma = \sigma_A = \sigma_B$ (Reuss),
- both constituent display linear elastic behavior.

Under such assumptions rule of mixture determines the elastic tensors (e.g. stiffness) of heterogenous material by averaging stresses over all phases.

Rule of mixture - Voigt estimation of uniform strain - see Figure 19a:

$$E = E_A V_A + E_B V_B \tag{23}$$

Rule of mixture - Reuss estimation of uniform stress - see Figure 19b:

$$E = E_A E_B / (E_A V_A + E_B V_B) \tag{24}$$

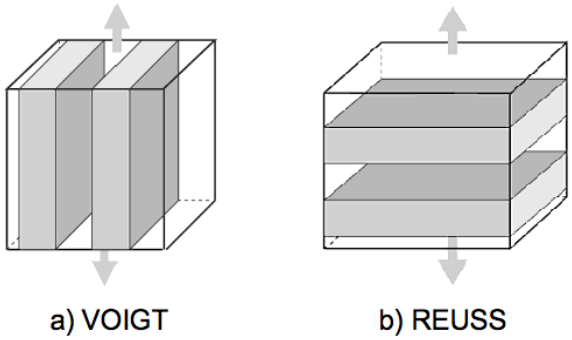

a) Materials in parallel connection - Voigt estimation of uniform strain,
b) Materials in series connection Reuss estimation of uniform stress

FIGURE 19: *Rule of mixture*

Reuss estimation gives the lower bounds of the elastic moduli for the composite, and Voigt estimation gives the upper bound:

$$E_A E_B / (E_A V_A + E_B V_B) \leq E \leq E_A V_A + E_B V_B \qquad (25)$$

Based on rule of mixture more advanced methods were derived by incorporating more micromechanical features and using variational principles (e.g. Hashin - Shtrikman model).

2.4.3 Hashin -Shtrikman model

Using variational principles, Hashin-Shtrikman established bounds on isotropic and homogeneneous multiphase materials of arbitrary phase geometry. This approach involves the application of the minimum complementary energy principles or minimum potential energy to set the lower and upper bounds for the elastic moduli. When the ratios between the different phase moduli are not too large, the bounds derived are close enough to provide a good estimate for the elastic moduli. [53]

2.4.4 Halpin - Tsai model

Halpin and Tsai showed that the property of a composite M could be expressed in terms of the corresponding property of the matrix M_m and the reinforcing phase M_p.

The rule of mixture in general form:

$$M / M_m = (1 + \xi\eta V_f) / (1 - \eta V_f) \quad (26)$$

$$\eta = [(M_f / M_m)-1] /[(M_f / M_m)+ \xi] \quad (27)$$

where:
- M = modulus of the composite under consideration (longitudinal, transversal)
- M_f = corresponding modulus of fibers
- M_m = corresponding modulus of matrix
- ξ = factor representing the measure of the reinforcement (based on experiments)
- η = coefficient given by (27)

ξ is a measure of second phase of the composite material and is dependent on the geometry of second phase, arrangement of particles, and the type of test (on the modulus considered).

2.5 MECHANICAL RESPONSE OF POLYMER MATRIX COMPOSITES

2.5.1 Particle filled composites

Elastic behavior of PFC is governed by the constitutional equations (10), (11) providing that the properties of composite are properly homogenized. When choosing the appropriate homogenization method, it is necessary to take into consideration the volume fraction of fillers, the size range and the interphase bonds. The model should comply with general rules for behavior of PFC provided by experimental investigation: increasing volume fraction of particles increases both Young's modulus and the fracture toughness, increasing particle size decreases Young's modulus and flexural strength, tensile strength is lower than tensile strength of pure polymer matrix. [31]

2.5.2 Unidirectional fiber reinforced composites (U-FRCs)

Elastic behavior of U-FRCs is governed by the constitutional equations (10), (11) provided that the properties of composite are properly homogenized. As discussed in the previous section several methods of homogenization are available. For U-FRCs loaded parallelry or perpendicularly to the fibers rule of mixture in appropriate form (Voigt, Reuss) is the correct choice. When FRC is subject to an arbitrary load, more sophisticated methods should be employed (Christensen) and the elements of elastic tensor should be calculated because couplings between normal and shear components can occur. The relevant relations are provided in the paragraph 2.6.1 which deals with mechanical analysis of a lamina because FRCs have ususally the form of a lamina.

There are several modes of failure of U-FRCs: fiber fracture, matrix fracture, debonding. These modes occurs in different loading situations in following variations when longitudinal tensile loading is applied:

- The main part of the load is born by the fibers and they tend to fail first. When the weakest fiber fails, the loading on remaining fibers increases which may cause the failure of other, especially, neighboring fibers.
- The cracks in the fibers cause higher stress concentration in the matrix, which can lead to the matrix cracking. However, if the fiber/matrix interface is weak, the crack extends and grows along the interface (debonding).
- If the matrix is brittle, the crack is formed initially in the matrix. If intact fibers are available behind the crack front and they are connecting the crack faces, the crack bridging mechanism is operative. In this case the load is shared by the bridging fibers and crack tip, and the stress intensity factor on the crack tip is reduced. [29]

Some of the tensile longitudinal failure mechanisms in unidirectional FRCs are shown in the Figure 20.

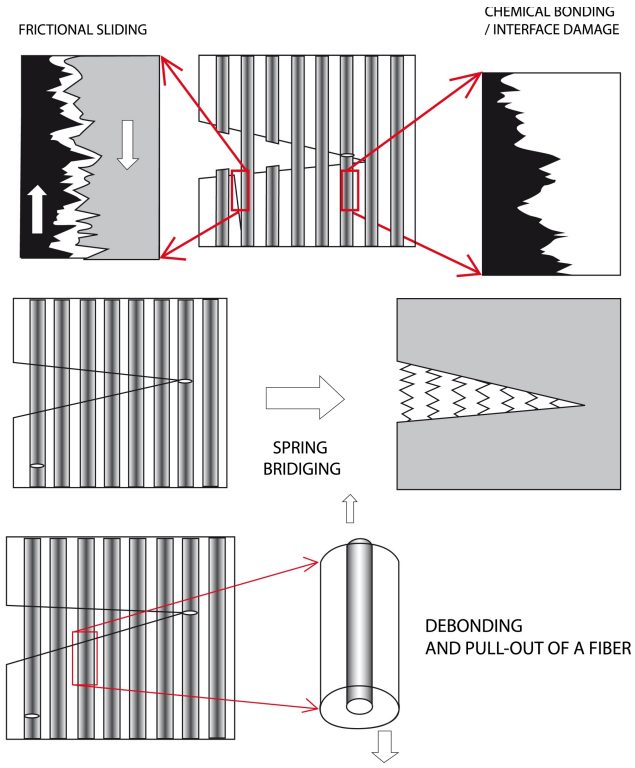

FIGURE 20: *Mechanisms of tensile failures in unidirectional FRCs [29]*

When transverse tensile loading is applied the fracture is produced by matrix fracture or debonding depending on the relation between fracture stress of matrix and interface.

When unidirectional FRC is subject to compressive loading fiber crushing, elastic and plastic micro-buckling of fibers and matrix failure due to the splitting or shear band formation take place.[32]

2.5.3 Multidirectional fiber reinforced composites (M-FRCs)

Elastic behavior and fracture modes of M-FRCs are analogous as of U-FRCs. Major difference is orientation averaging. Curved tow segments are divided into few grains in which the fiber orientation takes a spatially averaged value. Each grain is assigned the elastic properties of unidirectional composite.

For modeling multidirectional FRC numerical methods (unit cell) are dominant. For failure of M-FRCs following failure situations govern the developement of individual fracture modes:

- axial shear failure – is controlled by the properties of matrix,
- under compression M-FRCs fail by one of two mechnism: kink-band formation (a local shear instability in which a bundle of fibers rotates and ruptures, causing almost total loss of axial strength for the bundle) and delamination,
- failure under tension is caused mainly by rupture of fibers,
- delamination under through-tickness tension – typical for curved structures),
- shear delamination in bending close to free edges. [32]

2.5.4 Fatigue of composites

The fatigue models of composites can be classified in terms of fatigue criteria in three categories:

- Fatigue life models (extract information from the S-N curves and propose a fatigue failure criteria. These models do not take into account damage accumulation, but predict number of cycles at which fatigue failure occurs under fixed loading conditions.
- Phenomenological models to predict residual stiffness/strength
  - Residual stiffness models describe the degradation of the elastic properties during fatigue loading.
  - Residual strength models are of two types: sudden death model (useful for high level state of stress - residual strength degrades rapidly) and wearout model (useful for low level state of stress - residual strength degrades gradually).
- Progressive damage models introduce one or more properly chosen damage variables which describe the deterioration of the composite component. There are two classes of the models:
  - progressive damage models predicting damage growth (e.g. number of transverse matrix cracks per unit length, size of delaminated area),
  - progressive damage models predicting residual mechanical properties.

The detailed overview of particular fatigue models of structural composites is provided by [52].

2.6 LAYERED COMPOSITES: ANALYSIS OF MECHANICAL RESPONSE

The process of analyzing the mechanical behavior of a composite structure comprises three steps:

- analysis of the micromechanical behavior of a layer (lamina),
- modeling the local mechanical behavior of a composite (often laminate - macromechanical behavior of laminate),
- analysis of the composite structure.

2.6.1 Elastic response of a lamina

FRCs are usually orthotropic, i.e. having three mutually perpendicular planes of symmetry and often transversely isotropic which is special case of orthotropic symmetry where one axis of rotational symmetry is added.

Planar woven FRCs are typical orthogonal materials. Stiffness matrix of orthogonal material is given by (13).

Unidirectional FRCs included unidirectional woven FRCs are transversely isotropic materials. Assuming z is an axis of rotational symmetry (see Figure 21) this symmetry is reflected in the symmetry of the members of the stiffness matrix of transversely isotropic material as follows:

$$\begin{aligned} C_{xxzz} &= C_{xxyy} \\ C_{zzzz} &= C_{yyyy} \\ C_{zxzx} &= C_{xyxy} \\ C_{yzyz} &= (C_{yyyy} - C_{yyzz}) / 2 \end{aligned} \qquad (28)$$

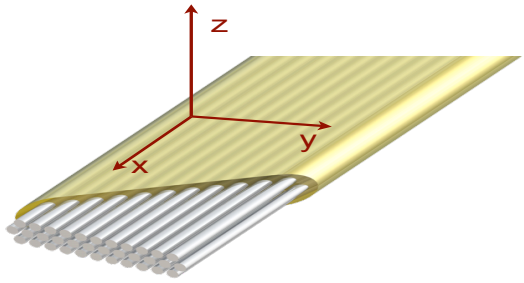

FIGURE 21: *Transversely isotropic FRC*

Providing that $C_{xxxx}=C_{11}$, $C_{xxyy}=C_{12}$, $C_{yyyy}=C_{22}$, $C_{yyzz}=C_{23}$, $C_{xyxy}=C_{66}$, the stiffness matrix of the transversely isotropic material is than:

$$C_{tran-iso} = \begin{bmatrix} C_{11} & C_{12} & C_{12} & 0 & 0 & 0 \\ C_{12} & C_{22} & C_{23} & 0 & 0 & 0 \\ C_{12} & C_{23} & C_{22} & 0 & 0 & 0 \\ 0 & 0 & 0 & (C_{22}-C_{23})/2 & 0 & 0 \\ 0 & 0 & 0 & 0 & C_{66} & 0 \\ 0 & 0 & 0 & 0 & 0 & C_{66} \end{bmatrix} \quad (29)$$

There are five independent elastic (engineering) constants as well as material constants (members of stiffness or compliance tensor) for transversely isotropic material. In practice following engineering constants are used: E_L, E_T, ν_{LT}, G_{LT} and $G_{TT'}$. These constants are defined in principal coordinate system called local system with the notation of directions L, T, T' or x, y, z or 1, 2, 3.

Several analytical methods are used for evaluating engineering constant. Rule of mixture and Hashin-Shtrikman method are the most widely used. Application of rule of mixture gives following equations for engineering constants:

$$E_L = E_f V_f + E_m (1 - V_f) \quad (30)$$
$$\nu_{LT} = \nu_f V_f + \nu_m (1- V_f) \quad (31)$$
$$E_T = E_m / (1 + V_f (E_m/E_f -1)) \quad (32)$$
$$G_{LT} = G_m / (1-V_f) \quad (33)$$

Cylinder model with three phases developed by Christensen and Lo [19] was used for deriving the equation for $G_{TT'}$:

$$G_{TT'} = G_m(1+(V_f/((G_m/(G_f-G_m)+((k_m+7/3G_m)/(2k_m+8/3G_m))(1-V_f) \quad (34)$$

where:
E_f = Young's modulus of fibers
E_m = Young's modulus of matrix
V_f = volume fraction of fibers
ν_f = Poisson ratio of fibers
ν_m = Poisson ratio of matrix
G_m = shear modulus of matrix
k_m = bulk modulus of matrix

As mentioned above elastic constants are expressed in the principal (local) directions where one axis is identical with the direction of the fibers/warp.

It is necessary to define elastic constants also for the situation where the direction of fibers/warp are different from the reference coordinate system (off-axis) and the difference is given by the angle θ between direction x and direction x' (reference coordinate system) supposing that direction of rotational symmetry z ≡ z'.

This system is called global system and it is given by (x', y', z ≡ 1', 2', 3). The stiffness / compliance tensors are transformed with respect to the change of reference system by:

$$C' = T_\sigma \, C \, T_\varepsilon^{-1} \tag{35}$$

$$S' = T_\varepsilon \, S \, T_\sigma^{-1} \tag{36}$$

where: C' = stiffness tensor in the reference system (x',y', z)
S' = compliance tensor in the reference system (x',y', z)
C = stiffness tensor in the principal system (x,y, z)
S = compliance tensor in the principal system (x,y, z)
T_σ = transformation matrix of stresses
T_ε = transformation matrix of strains

Based on the assumptions of CLT reviewed in section 2.6.3, strain and stress fields and constitutive equations are derived for a single lamina.

The strain tensor at point M (x,y,z):

$$\varepsilon(M) = \begin{bmatrix} \varepsilon_{xx} & \varepsilon_{xy} & 0 \\ \varepsilon_{xy} & \varepsilon_{yy} & 0 \\ 0 & 0 & 0 \end{bmatrix} \tag{37}$$

The strain field is the superposition of the strains in plane (midplane strains) ε^p and the flexural strains ε^f:

$$\varepsilon = \varepsilon^p + \varepsilon^f \tag{38}$$

In plane strain ε^p is a function of the displacements (u_0, v_0) of the points in the midplane:

$$\begin{aligned} \varepsilon^p_{xx} &= \partial u_0/\partial x \\ \varepsilon^p_{yy} &= \partial v_0/\partial y \\ \varepsilon^p_{xy} &= \partial u_0/\partial y + \partial v_0/\partial x \end{aligned} \tag{39}$$

The flexural (binding, twisting) strain ε^f is a function of the rotation of the deformed midplane and of the z coordinate of point M. It is expressed in general form by:

$$\varepsilon^f(M) = z(M)\, \kappa(x,y) \tag{40}$$

where: z(M) = z coordinate of point M
κ(x,y) = curvature matrix

The members of strain tensor at point M(x,y,z) can be expressed in displacements as follows:

$$\begin{aligned} \varepsilon_{xx} &= \varepsilon^{p}_{xx} + \varepsilon^{f}_{xx} = \partial u_0/\partial x + z\,(-\partial w_0/\partial x^2) \\ \varepsilon_{yy} &= \varepsilon^{p}_{yy} + \varepsilon^{f}_{yy} = \partial v_0/\partial y + z\,(-\partial w_0/\partial y^2) \\ \varepsilon_{xy} &= \varepsilon^{p}_{xy} + \varepsilon^{f}_{xy} = \partial u_0/\partial y + \partial v_0/\partial x + z\,(-2\partial^2 w_0/\partial x \partial y) \end{aligned} \quad (41)$$

The stress field at the point M (x,y,z) is given by stress tensor:

$$\sigma(M) = \begin{bmatrix} \sigma_{xx} & \sigma_{xy} & 0 \\ \sigma_{xy} & \sigma_{yy} & 0 \\ 0 & 0 & 0 \end{bmatrix} \quad (42)$$

The constitutive equations have the form:

$$\sigma(M) = Q\,\varepsilon(M) \quad (43)$$

$$\varepsilon(M) = \hat{S}\,\sigma(M) \quad (44)$$

where: Q = reduced stiffness matrix for plane stress state
$\hat{S}$ = reduced compliance matrix for plane stress state

When referred to the principal directions, Q is given by:

$$Q = \begin{bmatrix} Q_{xxxx} & Q_{xxyy} & 0 \\ Q_{xxyy} & Q_{yyyy} & 0 \\ 0 & 0 & Q_{xyxy} \end{bmatrix} \quad (45)$$

The reduced stiffness constants are functions of the engineering constants in the material directions. In case of plane state of stress only four engineering constants are required: E_L, E_T, ν_{LT}, G_{LT}, whether the materials are transverse isotropic (unidirectional FRC) or orthotropic (multidirectional FRC). These constants can be measured by tensile tests and in-plane shear test.

When referred to an arbitrary directions local and global stresses and strains are related as follows:

$$\sigma' = T^{-1}\sigma \quad (46)$$

$$\varepsilon' = T\varepsilon \quad (47)$$

where: T is transformation matrix.[3][4]

When considering dental layered composites, CLT can be used in particular analysis of single or multiple FRC layer.

2.6.2 Failure criteria for a lamina

In the case of composite materials, the end of elastic domain is generally associated with the development of failure. The theories of failure criteria are based mainly on the normal and shear strength of unidirectional lamina - stresses in the material (local) axes (contrary to principal normal stresses and maximum shear stresses in isotropic materials).

Following failure criteria have been establish with respect to the unidirectional lamina:

- maximum stress criterion,
- maximum strain criterion,
- energy (polynomial) criteria are based on extension of Von Mises criterion which is related to the strain energy stored in strained material to orthotropic materials. Several theories were developed within this framework:
    - Hill theory,
    - Tsai - Hill theory,
    - Hoffman's theory,
    - Tsai - Wu theory.

All above mentioned failure criteria can be complemented with the concept of strength ratio.

This ratio provides information about how much the load can be increased if the lamina is safe, or how much the load should be decreased if the lamina has failed. The strength ratio is defined as:

SR = Maximum load which can be applied / Load applied.

SR = 1 implies the failure load, SR > 1 implies the lamina is safe, SR < 1 implies the lamina is unsafe and stress needs to be reduced. [4][43]

2.6.3 Modelling the local mechanical behavior of a structural composite

Because of the fact that layered composites belong along with laminates, sandwiches to "structural" composites their mechanical behavior cannot be analyzed without respect to the appropriate structural model: beam, plate, shell etc. Accurate description of mechanical response of layered composite is possible if each layer is analyzed in proper structural model by the three dimensional theory of elasticity. A three dimensional solution of structural composite is complex and are available only for simple geometry and boundary conditions and hence solutions are not general.

The methods of analysis of specific models of structural composites has been developed since the early nineteen sixties mainly in the framework of beam and plate theories.

The suitability of particulate model or theory depends on the fact how they reflect phenomenological aspects of mechanical behavior of structural composites in specific situation under consideration. In dental layered composite the elastic properties are not constant along the thickness of the beam/shell. The stress and strain fields depend on the through thickness elastic properties. It becomes impossible to specify the stress/strain state through thickness by the state on any reference plane (mid-plane e.g.).

The characteristic-dimension-to-thickness ratio does not allow to use concepts for thin beams or plates and the Young's-to-shear modulus ratio is high. Therefore transverse normal and shear deformations are significant and should be taken in account.

In case that the join of the layers is rigid, then all the layers deform together. The layer interacts with regards to its elastic properties: the transfer of inter-laminar shear/normal stress from one layer to adjacent layer causes stress/strain mismatch depending on the difference of elastic constant of adjacent layers. The inter-laminar stresses increase near the free edges. The stresses affect the boundary region of the order of one laminate thickness. The inter-laminar strength is significantly smaller than the tensile strength of fibers, the integrity of thick beams/shells is often challenged with delaminations even when the inter-laminar stresses are much smaller than those in in-plane directions. Such delaminations reduce the bending stiffness. [49]

Following paragraph provides an overview of some theories which are commonly used for analyzing structural composites.

(i) ESL (structural member has the form of Equivalent Single Layer)

Beam theories

- EBT (Euler-Bernoulli Beam Theory): classical theory neglects transverse normal and shear deformation. The theory gives relatively accurate description of the response of thin, single-layered beams.
- TBT (Timoshenko Beam Theory): shear deformation theory, neglects transverse normal deformation.
- RBT (Reddy Beam Theory - Refined Equivalent Single Layer theories - RESL). Despite the improved capacity it is not a suitable representation of the displacement if the objective is to model the piecewise discontinuous strain distribution which occurs in multi-layered beams. [47]

(ii) Plate theories

- CLT (Classical Laminate Theory): classical theory neglects transverse normal and shear deformation. The theory gives relatively accurate description of the response of thin plates. CLT is based on Kirchoff's plate hypothesis which has following assumptions:
  - displacements at every point M with coordinates (x,y,z) of a plate is expressed in the form of polynomials in z limited to one degree (first order theory),
  - the transverse shear is neglected and consequently the deformation of the normal to the middle plane (Oxy) is then a straight line normal to the deformed middle plane - see Figure B, C,
  - the plate is a thin plate, i.e. the thickness to characteristic dimension of the middle surface ratio is lower than 1/20.

  CLT extends further the assumptions of Kirchoff's plate:
  - the plate is allways subject of plane stress state
  - each lamina is orthotropic,
  - each lamina is homogenous,
  - each lamina is elastic,
  - no slip occurs between the lamina interfaces.

- FSDT (First-order Shear Deformation Theory): shear deformation theory, neglects transverse normal deformation. It is based on Mindlin-Reissner plate theory which was developed for laminates by Whitney and Pagano [49]. This theory predicts constant transverse shear stress through the thickness of plate. A shear correction factor is adopted in similar way as in TBT.

- HSDT (Higher-order Shear Deformation Theory - Refined Equivalent Single Layer theories - RESL)

(iii) LWT (Layer-Wise Theories):

In general layer-wise theories presume that the laminate deformation and stress fields depend significantly on the behavior of the individual layers. In these theories each composite layer is treated as a separate three dimensional solid. The displacement field for each layer (n) is a function of the displacements of adjacent layer. The layer-wise representation of the kinematics yields zig-zag-like displacement through the beam/plate thickness. The major drawback of these theories, however, is that the number of kinematic variables is dependent on the number of the layers in the beam or plate. [50]

(iv) GLWT (General Layer-Wise Theories

- ZZT (Zig-Zag Theory): These theories assume a zig-zag pattern for the in-plane displacements and enforce continuity of the transverse shear stresses across the entire laminated beam/plate thickness. ZZT run into a theoretical difficulties when the shear stress does not correspond to the total shear force required by equilibrium. [50]
- RZZT (Refined Zig-Zag Theory): free the theory of the shortcomings of ZZT. The key attributes of RZZT are:
    - the proposed zig-zag function vanishes at the top and bottom surfaces of the beam and does not require full shear-stress continuity accross the laminated beam depth,
    - all boundary conditions can be modeled adequately. [50]

3 GOALS OF THE WORK

The main aim of this work is to investigate effects of micro-scale and meso-scale structural features of model layered composite superstructures composed of fiber reinforced and particulate filled composite layers on macro-mechanical deformation behavior and fracture during three-point bending test.

Both unidirectional and multidirectional prepregs were examined. Specifically, fiber orientation, fiber and particle volume fractions, interlayer adhesion and layering sequence are the micro- and meso-scale structural variables. Another goal of this work is to develop a suitable testing protocol allowing to obtain reliable experimental data on structure-property relationships for model test specimens relevant for clinical applications of layered composites as load bearing substructures in prosthetic dentistry. Furthermore, an attempt is made to interpret experimentally established structure-rigidity and structure-fracture relationships using existing models. Data gained out of static and DMTA three-point bending were used to analyze influence of structural features on stiffness and stress distribution.

4 EXPERIMENTAL

4.1 MATERIALS

There were following materials selected for the preparation of the model test specimens:

(This is not full description, commercial names are used, however, detailed composition must be briefly described –type of resin, filler loading, manufacturer´s declared properties)

- BOSTON CB, manufacturer Arkona - Laboratorium Farmakologii Stomatologicznej, Lublin, Poland - crown and bridge composites (high-viscous light curing particle filled composited with silica particles and methacrylate based resin),
- BOSTON FLOW, manufacturer Arkona - Laboratorium Farmakologii Stomatologicznej,, Lublin, Poland - flowable composites (low-viscous light curing particle filled composited with silica particles and methacrylate based resin),
- light curing methacrylate based resin (50% BIS-GMA, 50% TEGMA),
- DENTAPREG PFU, manufacturer ADM a.s. Brno, Czech Republic, unidirectional prepregs (S and E glass fibers, methacrylate based resin),
- DENTAPREG SFM, manufacturer ADM a.s. Brno, Czech Republic, multidirectional prepregs (E glass fibers, methacrylate based resin).

TABLE 5: *Characteristics of FRC strips*

Type of FRC	Material of the fibers	Number of the fibers	Diameter of the fibers [μm]	TEX
PFU	S-2 glass	8.400	9	1320
SFM	E glass	7840	5	400

TABLE 6*: Characteristics of PFC used*

Type of PFC	Type of material	Content of inorganic particles [wt. %]	Standard deviation [%]
Boston CB	Crown & Bridge	76.18	0.83
Boston FLOW	Flowable	65.98	0.79

4.2 METHODS

4.2.1 Structural Analysis

In order to characterize materials used in mechanical analysis several techniques of structural analysis will were employed:

4.2.1.1 Thermogravimetric analysis - TGA

TGA measures the change of the weight of the specimen (amount or/rate) as a function of temperature or time under controlled atmosphere and heating rate. TGA was carried out in order to determinate fibre / particle volume fraction in respective composites. The thermogravimetric analyser TGA 6 (Perkin Elmer, Waltham, MA, USA) was used.

The measurements were performed on specimens of ca 20 mg of weight in controlled nitrogen atmosphere. The specimen were placed in an open platinum pan and heated from 20°C (equilibrated for 1 min.) up to 650°C. The heating rate was 20°C/min. and the air cool time was 9 min. Five signals were monitored during measurement: Time[min], Temperature [°C], Weight [mg], Balance Purge Flow [mL/min.] and Sample Purge Flow [mL[min]. The data presented in this thesis represent an average of five measurements. Standard deviations from 2 % to 3 % were obtained.

4.2.1.2 Differential scanning calorimetry - DSC

The principle of DCS is to measure the difference in the amount of heat (energy) needed to increase the temperature of the sample and the reference. Based on this difference endothermic and exothermic transitions as a function of temperature are analyzed.

DSC was carried out in order to determine degree of conversion (DC) in cured matrices of particle filled composites as well as unidirectional prepreg, which were used in the layout of layered composites examined in mechanical tests. The differential scanning calorimeter DSC 2920 (TA Instrument, New Castle, DE, USA) combined with the photo calorimeter was used.

The measurements were performed on specimen of ca 10 mg of weight, in controlled nitrogen atmosphere. The specimens were placed in an open aluminum pan. The reference was an empty pan. Three signals were monitored during the test: Time [min], Temperature [°C] and Heat Flow [mW]. Due to the fact that light curing composites were tested, photo-calorimetry was used instead of conventional calorimetry. The specimens were irradiated by a 200W high pressure mercury arc lamp for the time period of 10 minutes.

The purge flow of nitrogen was 70 ml/min and the test temperature was 34°C. The data presented in this thesis represent the average of five measurements. Standard deviation of 5 % was obtained.

4.2.1.3 Scanning electron microscopy - SEM

SEM observations were carried out in order to provide morphological analysis of microstructural features which are of relevance to interpretation of micromechanical processes which influence macromechanical behavior of the specimens. Scanning electron microscope EVO LS 10 (Carl Zeiss Microscopy GmbH, Jena, Germany) was used.

The observations were performed under following parameters:

- magnification: 50x, 200x, 1000x, 5000x, 30000x,
- field of view: 6 mm,
- size of the chamber: 310 mm (diameter), 220 mm (height),
- image framestore: 3072 x 2304 pixel,
- signal acquisition by integrating and averaging,
- acceleration voltage: 0,2 – 30 kV.

4.2.1.4 High speed camera monitoring

To record the visual effects elucidating mechanisms causing fracture under three-point static bending, high speed digital camera monitoring was used. The recording speed was 100 pictures/sec which is the double compared to the sampling rate of testing machine for three-point static bending. High speed camera i-Speed 3 (Olympus, Tokyo, Japan) was used.

The observations were performed under the following parameters:

- resolution 800 x 600,
- lens 50mm, F 1.4 plus tele-convertor 2x,
- tungsten illumination Olympus ILP2 – 75W Ultra high performance.

4.2.2 Mechanical Analysis

4.2.2.1 Dynamical mechanical thermal analysis - DMTA

Dynamical mechanical thermal analysis measures the temperature dependence of the elastic response of the specimen under applied cyclic deformation and under controlled temperature conditions at defined heating rate. The deformation was applied sinusoidally. The response to the deformation can was monitored as a function of temperature.

DMTA was carried out in order to evaluate visco-elasticity of respective materials by determining storage modulus, loss modulus, and loss tangent. The DMTA analyser DMA 2980 (TA Instruments, New Castle, DE, USA) was used.

The measurement were performed on specimens of the beams of 20 mm x 20 mm x 50 mm. The beam was deformed in the three-point bending, the span of the support was 40 mm. The testing procedure consisted of the following steps:

- Step 1) Conditioning - transducer
- Step 2) Conditioning - sample: temperature 35°C, Soak time 10 s
- Step 3) Set initial value: axial force 0.5 N, sensitivity 0.01 N
- Step 4) Oscillation sinusoidal, temperature ramp: start temperature 35°C, end temperature 120°C, ramp rate 3°C/min., soak time after ramp 1 s, sampling rate 10 pts/s, strain 0,0015 %, frequency 1 Hz

4.2.2.2 Static three point bending test

Static three point bending tests was conducted in order to obtain comparative data of flexural properties of layered composites. The bending moment, applied stress, stiffness in flexure and the full stress-strain behavior of the beam were obtained. The geometry of the test was relevant for clinical applications (width of the specimen) and ensured that shear during bending could be omitted (aspect ratio of the specimen equal 30).

A rectangular specimen was simply supported close to its ends and centrally loaded. The measurements were performed on specimen of beams of 20 mm (width) x 20 mm (depth) x 70 mm (length) where span of the support was 60 mm. Diameter of the loading thorn was 6 mm, diameter of supports was 3mm.

The test temperature was 21°C, the crosshead speed was 50 mm / min and sampling rate was 50 pts/s. Universal Testing Machine Zwick Z010 (Zwick GmbH, Ulm, Germany) was used.

The test arrangement is illustrated schematically in Fig.22.

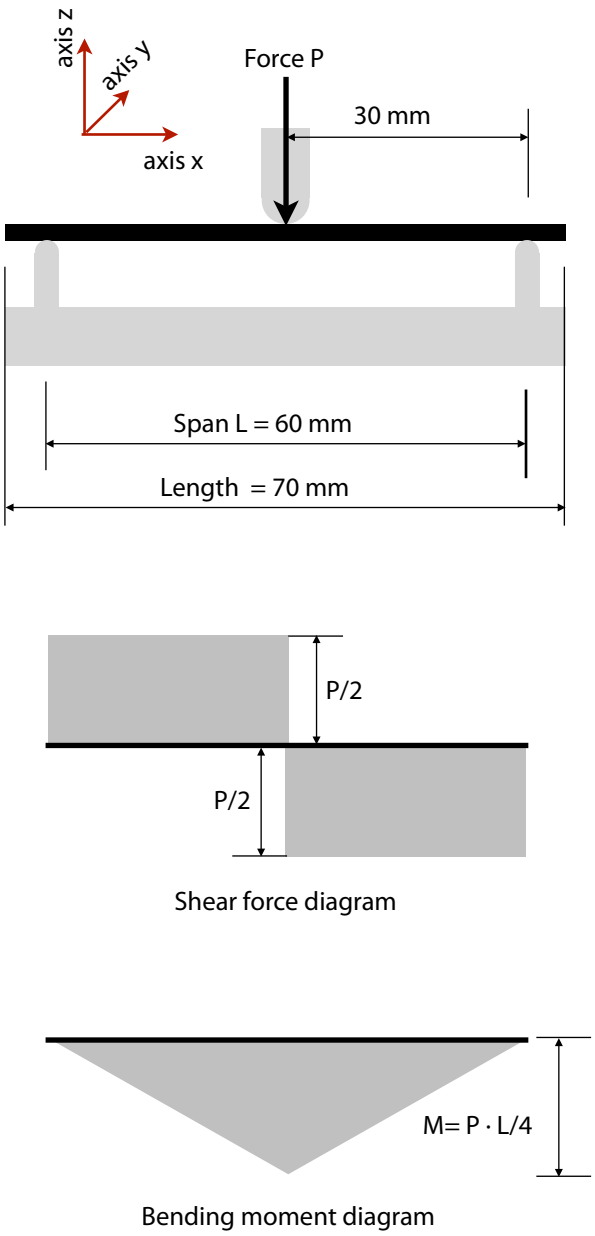

***FIGURE 22**: Three point flexure test together with shear force and bending moment diagrams*

The coordinate x is associated with the longitudinal direction of the specimen, and the y and z are taken along its width and depth, respectively.

The flexural response of the specimen was obtained by recording the load applied and the resulting displacement at the center of the specimen assuming that the beam theory applies and strains can be calculated (axis x laying in neutral surface does not experience any change in length, all cross sections remain plane and perpendicular to the axis x, any deformation of the cross section within its own plane is neglected).

The maximum normal stress (compression, tension) under such conditions is given by equation:

$$|\sigma_C| = |\sigma_T| = \frac{3 \bullet P \bullet L}{b \bullet h^2} \tag{48}$$

where:
P = load [N]
L = span of the specimen [mm]
b = width of the specimen [mm]
h = depth of the specimen [mm]

The stiffness B of the beam is given by equation for mid span delection D_{max} which can be obtained integrating the moment-curvature equation of the beam:

$$D_{\max} = \frac{P \bullet L^3}{48 \bullet B} \Rightarrow B = \frac{P \bullet L^3}{48 \bullet D_{\max}} \quad D_{\max} = \frac{P \bullet L^3}{48 \bullet B} \Rightarrow B = \frac{P \bullet L^3}{48 \bullet D_{\max}} \tag{49}$$

where:
$D_{\max}$ = maximal deflection [mm]
P = load [N]
L = span of the specimen [mm]

Based on stiffness and the moment of inertia of the cross section the modulus of elasticity E of the material of the beam is given by equation (50):

$$E = \frac{B}{I} \tag{50}$$

where:
I = momoment of inertia of the cross section [mm^4]

4.2.2.3 Finite element analysis

Finite element analysis was used as a complementary tool in this work. We utilized the calculation protocol proposed by Jan Pěnčík [68] for ANSYS software package for fiber reinforced structures. The mesh of the model is created with four-nodal 2D "PLANE 42" elements. The loading is applied step-wise and is transferred to the structure using contact elements "CONTA 172" and "TARGE 169". Combination of bi-linear stress-strain diagrams (BISO) was used to model material response together with modulus of elasticity E_{fmax}, strength in tension σ_{Tmax} and strength in compression σ_{Cmax}. The chosen model includes influence of large displacements, and rotation of the finite elements.

4.3 SPECIMEN PREPARATION

4.3.1 Specimen schedule

All specimens were prepared on the base of the form which was required for static three point test: a beam 20 mm (depth) x 20 mm (width) x 70 mm (length).

Several types of beam layout were prepared according to the schedule in the TABLE 7.

***TABLE** 7: Specimen schedule*

Type of the specimen	Particulate composite (PFC)	Fiber reinforced composite (FRC)	Interlayer
Components (mono-layered beams)			
F	Low viscous PFC (FLOW)	None	None
C	High viscous PFC (CB)	None	None
P	None	Unidirectional strip PFU	None
S	None	Multidirectional strip SFM	None
Combinations (bi-layered beams)			
F1P	Low viscous PFC (FLOW)	Unidirectional strip PFU x 1	Direct contact
C1P	High viscous PFC (CB)	Unidirectional strip PFU x 1	Direct contact
C1PI	High viscous PFC (CB)	Unidirectional strip PFU x 1	BisGMA-TEGMA
C2P	High viscous PFC (CB)	Unidirectional strip PFU x 2	Direct contact
C3P	High viscous PFC (CB)	Unidirectional strip PFU x 3	Direct contact
C4P	High viscous PFC (CB)	Unidirectional strip PFU x 4	Direct contact
C1S	High viscous PFC (CB)	Multidirectional strip SFM x 1	Direct contact
C2S	High viscous PFC (CB)	Multidirectional strip SFM x 2	Direct contact

4.3.2 Specimen for thermogravimetric analysis

For TGA specimen of mono-layer beams only were tested. Pieces of the beams of about 2 mm of length were separated (cut by rotating cutter) from the long beams prepared according to the specimen schedule. The weight of the specimen for TGA was ca 20 mg.

4.3.3 Specimen for differential scanning calorimetry

Specimens of mono-layer beams only were investigated exclusively for differential scanning calorimetry. Pieces of the beams of about 1 mm of length were separated (cut by rotating cutter) from the long beams prepared according to the specimen schedule. The weight of the specimen for differential scanning calorimetry was ca. 10 mg.

4.3.4 Specimen for scanning electron microscopy

For SEM investigation several specimens which were subject to the three point bending and which displayed typical structural features (cracks in PFC, fracture of fibres) were selected. In case that the size of the specimen exceeded the dimensions of the SEM chamber the specimen was cut. The surface of the selected specimen was coated with Au before placing into the SEM chamber.

4.3.5 Specimen for dynamical mechanical thermal analysis

Dynamical mechanical thermal analysis was applied on all types of the beams according to the specimen schedule. The original form of the beams was cut to the length of 50 mm by rotating cutter.

4.3.6 Static three point bending test

The procedure of preparation of the specimens for static three point test encompassed the following steps:

- Preparation of the transparent rubber mold with 9 grooves of the size of the specimen (20 mm x 20 mm x 70mm).
- Trimming the appropriate FRC strips to the length of 70 mm and protecting the trimmed pieces against the light (not applied for mono-layer PFC specimen).
- Placing the appropriate number of trimmed FRC strips into individual grooves (not applied for mono-layer PFC specimen).
- Covering the groove with PFC.
- Adjusting the mold for polymerization - inserting it between two rectangular pieces of a flat clear glass.

- Light polymerization of the set of specimen in the rubber mold for 4 minutes period twice (first period mold on the top, second period mold on the bottom) (more detailed description of the process).
- Removing the specimens from the mold, adjusting the final shape and marking them.
- The specimens for static three point bending test were defaults for all other testing methods.

4.3.7 Specimen for high speed camera monitoring

High speed camera monitor was applied on the specimen under static three point test. No special adjustment of the specimen was required in the process of high speed monitoring.

5 RESULTS AND DISCUSSION

5.1 STRUCTURAL ANALYSIS OF LAYERED COMPOSITES AND THEIR COMPONENTS

5.1.1 Thermogravimetric analysis

TGA was carried out to estimate the content of inorganic material (silica filler in PFC, S-glass fibers in PFU and E-glass fibers in SFM) in respective components of layered composites.

Two patterns were identified in output data.

The first one refers to PFC materials where smooth weight loss identifies that only one type of resin was present in the composite – see Fig. 23.

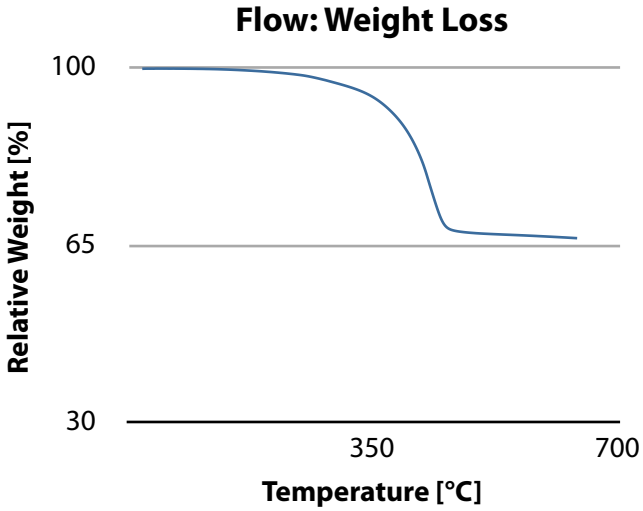

***FIGURE 23**: TGA-gramm of low viscous particulate filled composite (F)*

The second pattern refers to FRC materials. The stepwise shape of the curve indicates that the resulting network of matrix is composed of two different copolymers. Based on the manufacturer's data there are to monomers used in the matrix: 1,12-dodecandioldimethacrylate and dimethacrylate under manufacturer's code V377. When undergoing polymerization two types of domains in which the relative composition of monomers differs are created - see Fig. 24.

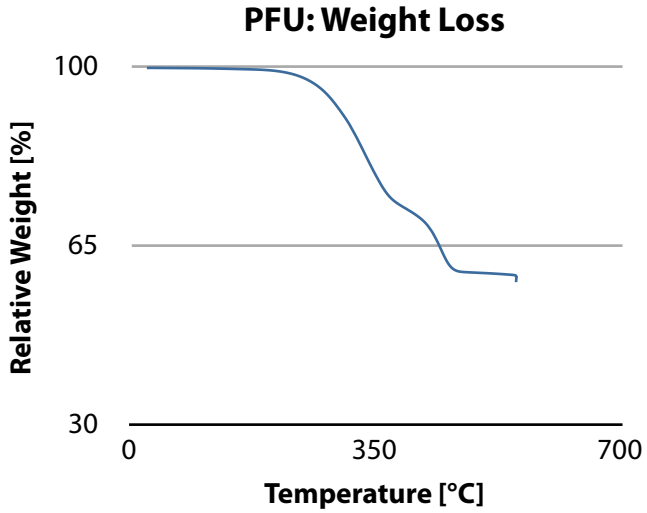

***FIGURE 24**: TGA-gramm of unidirectional fiber reinforced composite (P)*

The results obtained from the TGA measurements are in accordance with the manufacturer's data – see Figure 25 and Table 8.

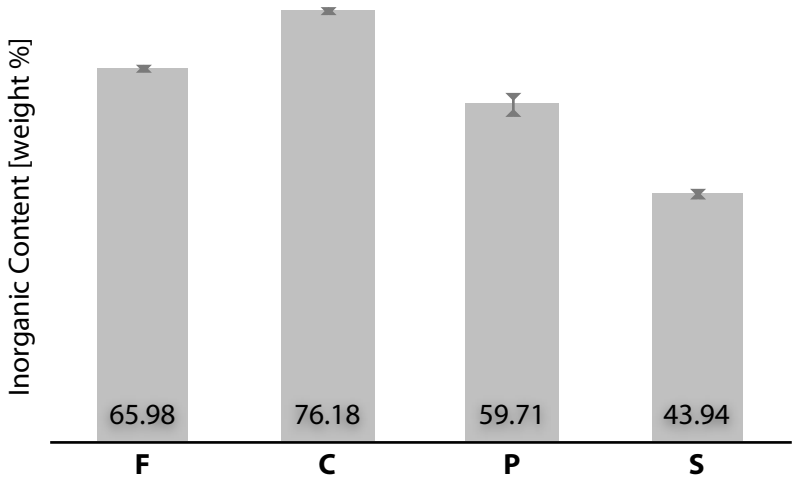

***FIGURE 25**: Content of inorganic material in components of layered composites*

TABLE 8: Content of inorganic material in components of layered composites

Type of specimen	Content of inorganic material [wt %]	Standard deviation [%]
F	65.98	0.79
C	76.18	0.83
P	59.71	2.30
S	43.94	1.10

5.1.2 Differential scanning calorimetry

Specimens of components of layered composites (low and high viscous particulate filled composites – F,C and unidirectional fiber reinforced composite - P) were investigate by mean of differential scanning photo-calorimetry. Output data testified that there were no transitions present during irradiation. Based on this fact it can be considered that all specimens were fully cured during preparation – see Fig.26.

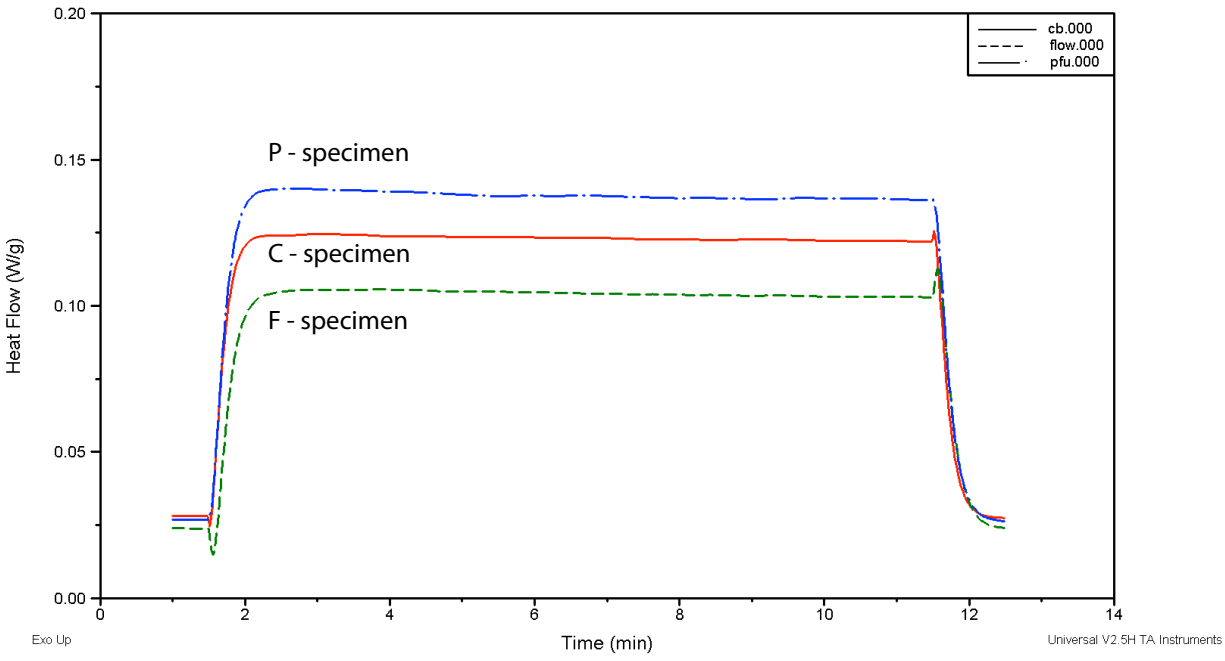

FIG. 26: Heat flow of cured components of layered composites

5.1.3 Scanning electron microscopy

Scanning electron microscopy was used in order to analyse visual features of deformed specimens after being subject to the static three-point bending test. Following types of beam specimens were analysed:

- F – specimen
- C – specimen
- P – specimen
- S – specimen
- C1P – specimen
- C1S - specimen

Significant visual features are shown in the following series of SEM pictures in different magnification. For clear orientation red rectangle is placed in the field displayed in the following SEM picture in larger magnification.

Beams of particulate composite of type F and C failed during static three point test in the brittle fracture manner. The fracture surfaces were smooth and in a larger magnification silica filler particles embedded in the resin became visible. There are no major differences between the micro-structure of F and C beams as their components are very similar. On the C specimen fracture surface defects of internal pores are visible. Their diameters vary around 10 μm and they are typical for nanofill and microhybrid composites. These flaws are originated during the manufacturing process [53].

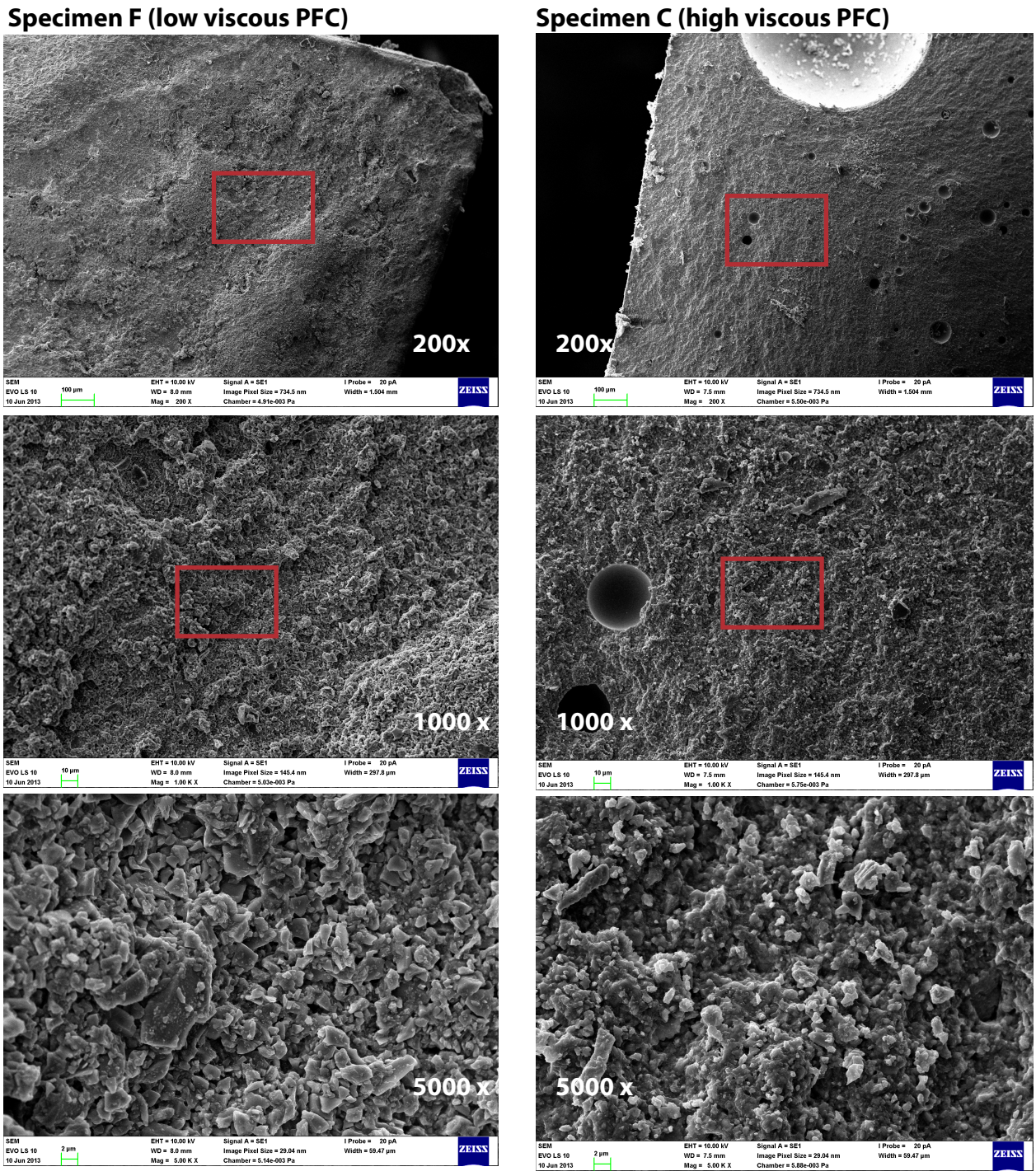

***FIGURE 27**: SEM of fractured particulate filled composites F and C*

P composite displays non-uniform dispersion distribution of fibres across the cross section of a single pre-impregnated strip. Consequently resin rich domains in the PFU strip specimen are founded. When deformed in three-point bending, the failure of the specimen is caused by several types of events:

- The fibers break due to growing tension in a range where they are not surrounded by the matrix. In the range where they are embedded in the matrix, the matrix bridges the fractured part and transmits the load to other part of the fibre or to adjacent fibres. This event reduces tension strength [67].
- The fibers loss their stability (microbuckling) due to growing compression in a range where they are not surrounded by the matrix. In the range where they are embedded in the matrix, the matrix bridges the buckled part and transmits the load to other part of the fibre or to adjacent fibres. This event reduces strength in compression [65].
- The matrix cracking due to raising tensile stresses. This event reduces stiffness of the beam. It also increases areas where fibers are not embedded in the matrix.
- Fibre de-bonding (pull-out) occurs when bonding strength is exceeded due to local stress concentration [60]. The consequence is reduced stiffness of the beam.

All types of events develop gradually and in parallel in the areas of local micro-structural geometry discontinuities resulting in local stress concentration. As these micro-events propagate more individual fibres or bunches of fibres detach from the resin matrix the loss of stiffness becomes evident and finaly the beam losses its strength due to the buckling of fibres in compressed part of the cross-section of the beam. Growth of the stress in the part of the cross-section, which is still able to carry the load leads to the progress in detachment of the fibres and the matrix and finally the beam fails due to the disintegration of its micro-structure.

When considering failure of S beam it is necessary to take in account the structure of the lamina. Uncured multi-directional lamina has well defined outer geometry due to mechanical bond of braided yarns. This structural feature leads to different behavior of the multi-directional lamina within the layred composite compared to uni-directional lamina. Outer geometry of uncured uni-directional lamina changes when the strip is built in a layered composite. Individual fibers disperse across boundaries of the layers and make the transition between layers gradual. Gradual transition sustains larger shear load between layers compared to a steep transition. In steep transition between layers smaller area than in gradual transition resists the load. It is in accordance with experimental results published in [54].

The failure of the S beam is controlled by delamination of individual laminae due to the inter-layer shear stress which exceeds the adhesion between the layers.

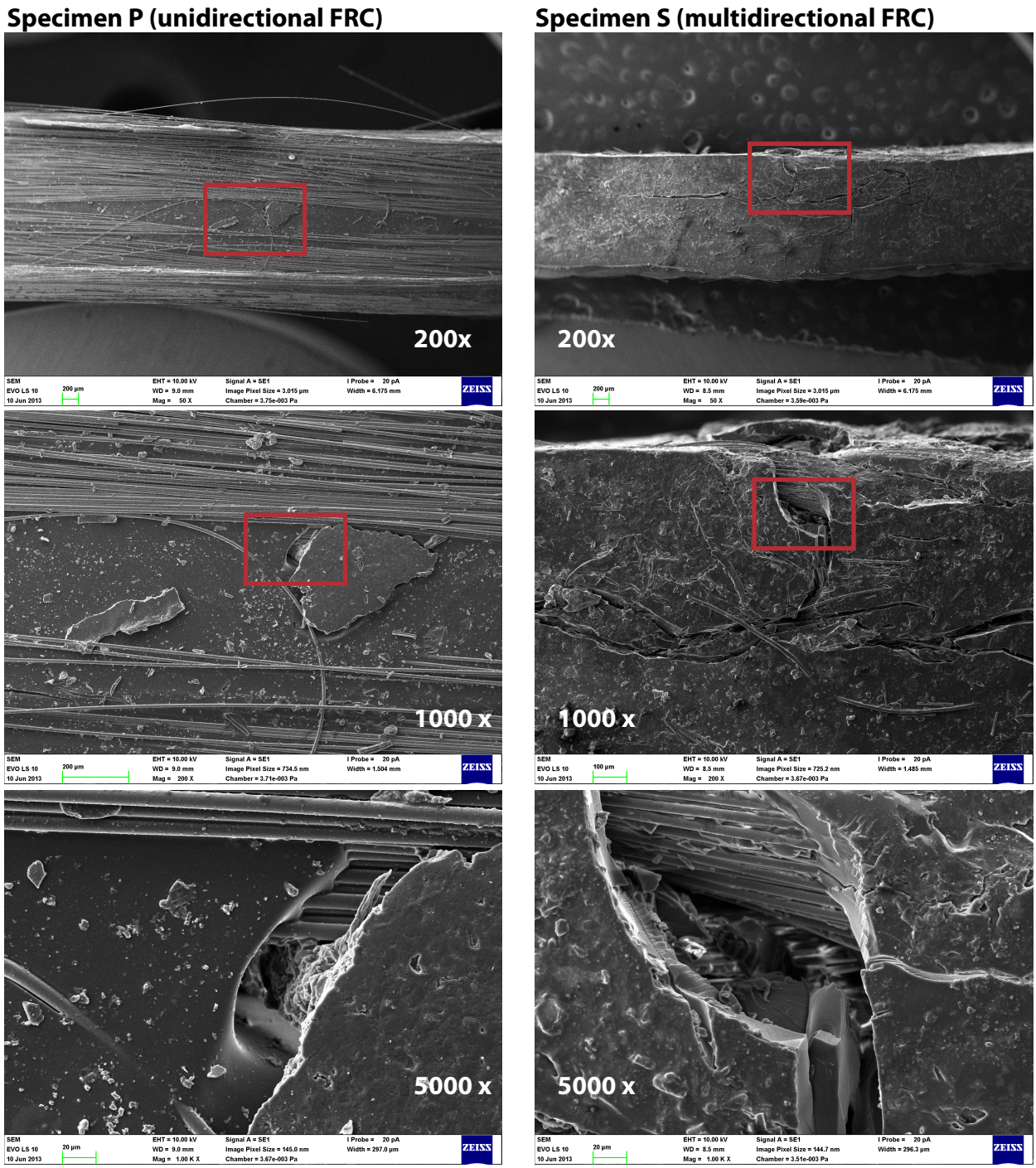

***FIGURE 28**: SEM of fractured fibre reinforced composites P and S*

Layered beam C2P based on the combination of two uni-directional FRC layers (P) and high viscous particulate filled composite (C) exhibits fracture surfaces in the PFC layer.

Fibres in the lower layer preclude cracks propagation from the PFC layer. The normal stress parallel to longitudinal axis of the beam caused by bending in FRC layer leads gradually to debonding of individual fibres followed by tensile rupture.

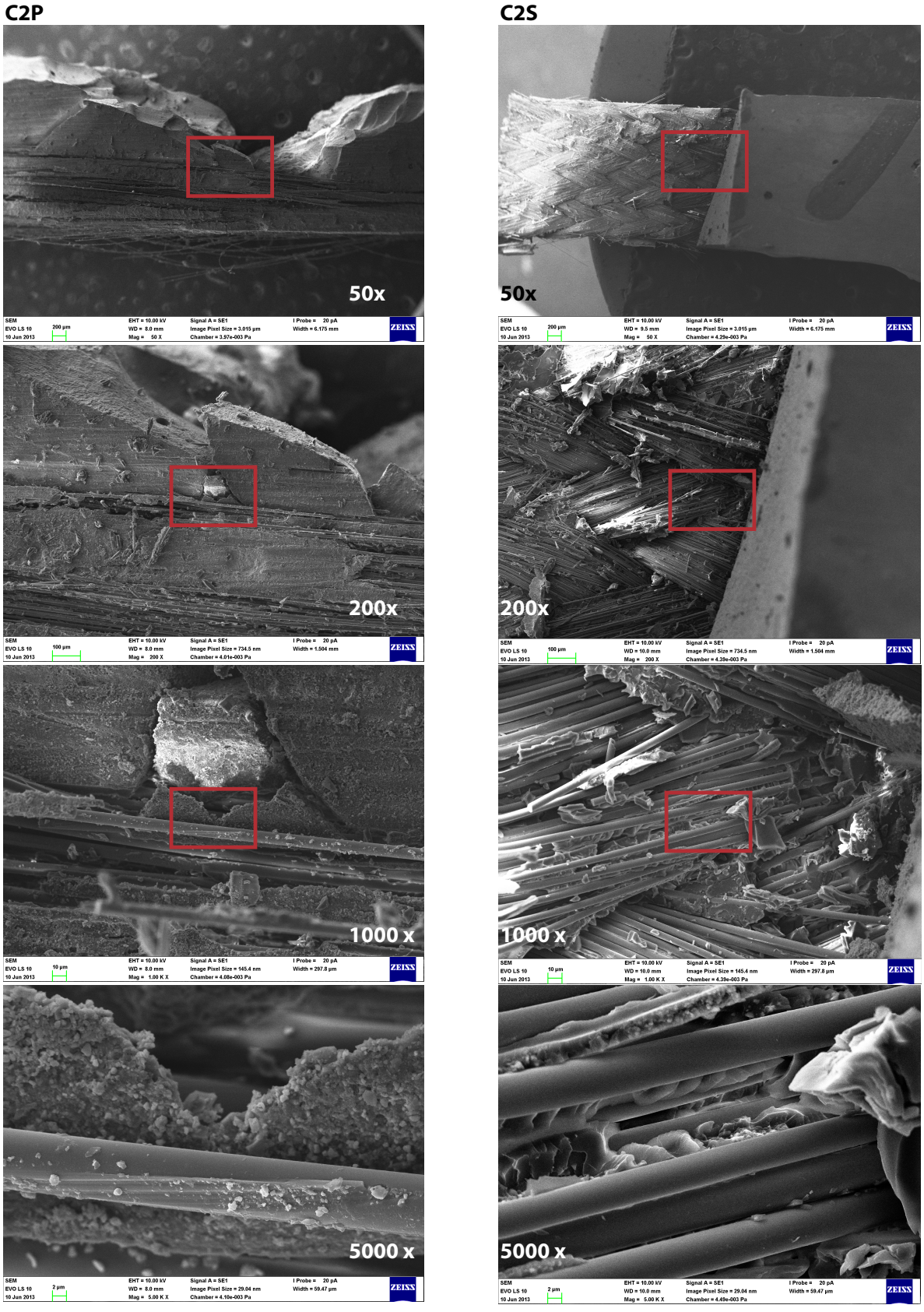

***FIGURE 29**: SEM of fractured fibre reinforced composites P and S*

Layered beam C2S combining layers made of two multidirectional FRC strips (S) and high viscous particulate filled composite (C) displays failure brittle fracture of PFC followed by de-bonding of the FRC layer adjacent to CB layer and finally delamination of individual laminae in the FRC layer.

It is apparent that the microstructure of all types of specimens exhibits large number of different inhomogeneities such as voids, fiber misalignment, imperfections in fibre-matrix interface caused by fabrication process. These microstructural features cause an appreciable scatter in parameters of mechanical response given by mechanical tests and theoretical calculations.

Output of finite elements analysis depicts the distribution of normal stress in the stage of initiation of FRC and PFC layers delamination – see Figure 30.

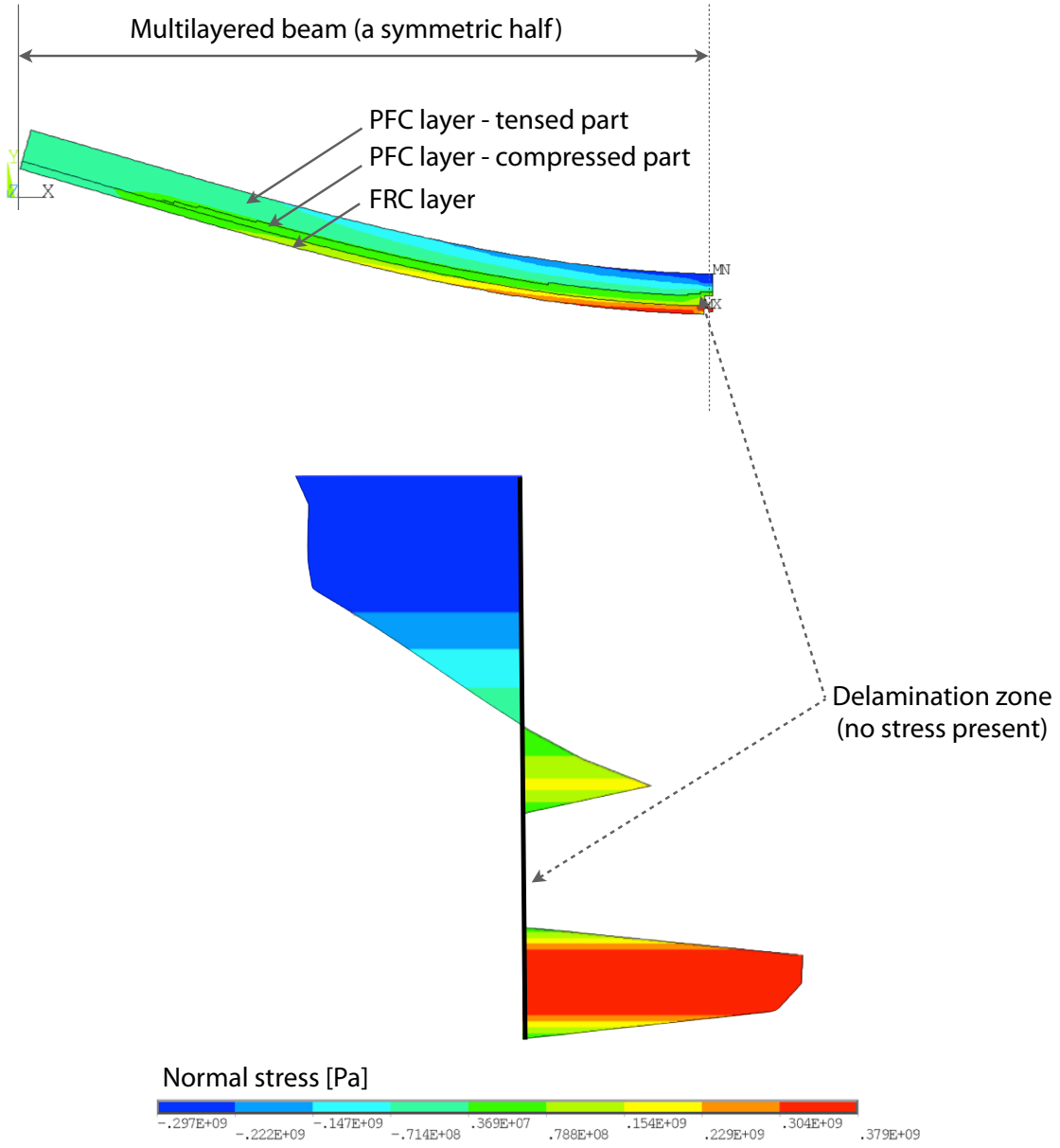

***FIGURE 30**: FEM analysis of normal stress distribution during initiation of delamination of the layers in bi-material beam*

5.1.4 High speed camera monitoring

High speed camera recorded static three-point test of selected type of specimen in order to visualize deformation events in the specimen and relate them to the characteristic points of load - deflection curve.

Figure 31 shows different modi of the failure of the specimen P (a) and the specimen C4P (b).

P beam failed due to the separation of the fibres from the matrix in the compressed part of the cross section followed by buckling.

C4P beam failed due to separation fibres from the matrix in the tensed part of the cross section followed by gradually rupturing the individual fibres in tension. The loading-deformation action through the whole test is documented by series of snapshots depicted in Fig. 32.

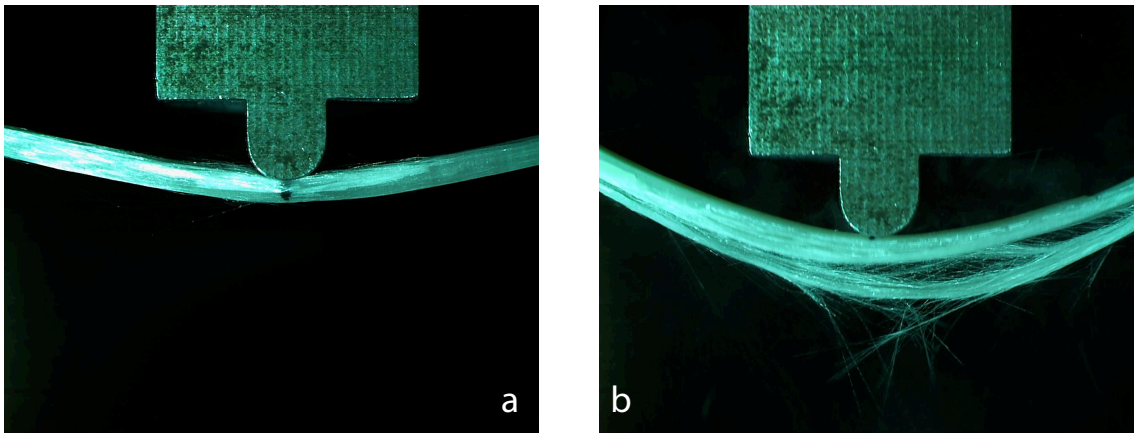

***FIGURE 31**: Modi of failure of the specimens P (a) and C4P (b)*

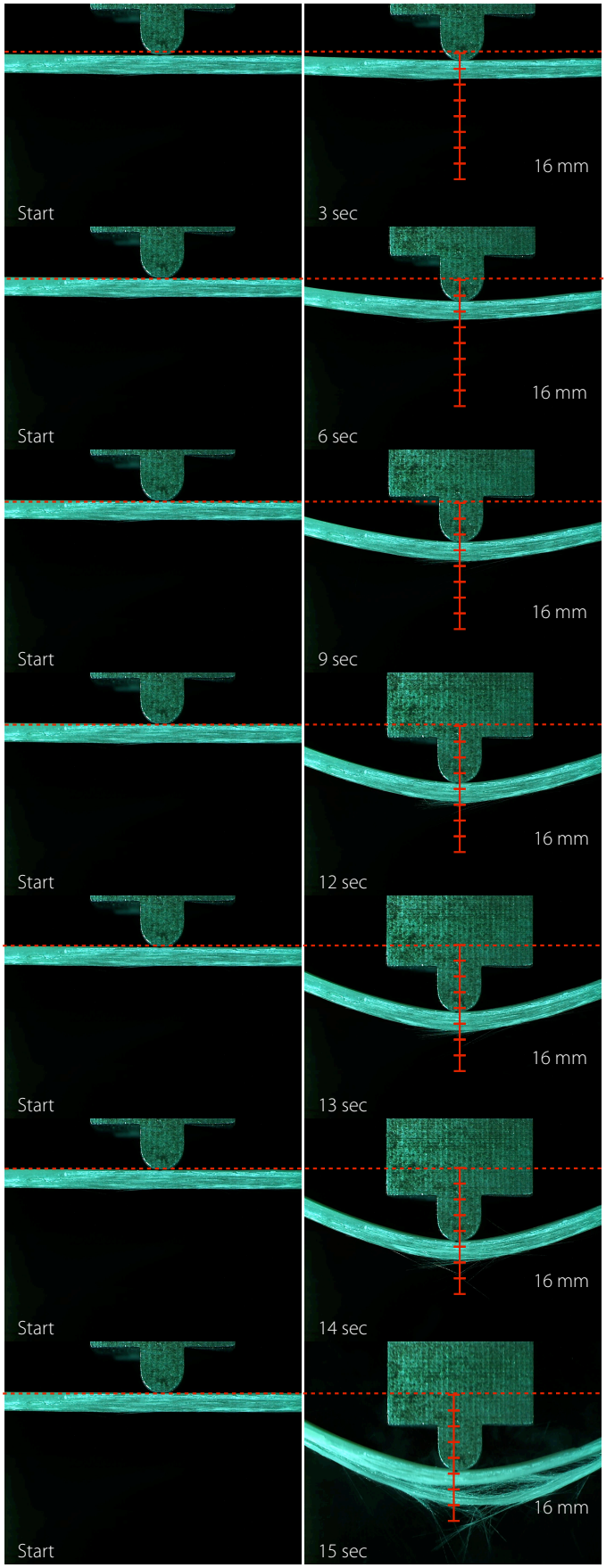

***FIGURE 32**: The sequence of three-point test of C4P beam*

5.2 MECHANICAL ANALYSIS

5.2.1 DMTA tests

All types of investigated beams were subjected to DMTA test. The test was used to study the visco-elastic response as well as to establish a storage moduli of the beams as well.

The measure of overall stiffness of visco-elastic beam is a complex modulus of elasticity of the specimen E_{DMTA} which is consisting of the storage modulus E_{ST} and the loss modulus E''. Phase shift δ between deformation is generated by the testing machine and specimen response is calculated as a ration between E“ and E_{ST}. Storage modulus E_{ST} is a measure of the ability of the specimen to store energy (i.e. elasticity of the specimen). Loss modulus E'' represents the ability of the specimen to dissipate energy (i.e. viscosity). Phase angle δ is a measure of material damping (tan δ). If the phase angle δ=0° the specimen displays purely elastic response, if δ=90° the specimen displays purely viscous response. The relation between parameters measured by DMTA and the complex modulus E_{DMTA} is given by vector decomposition of the complex modulus E_{DMTA} – see Fig.33.

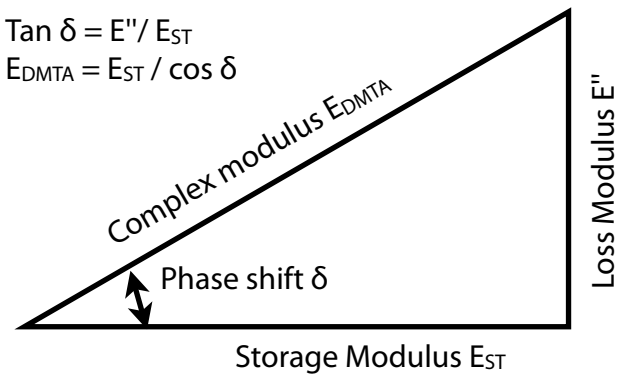

***FIGURE 33**: Relation between storage modulus and loss modulus*

All types of beams investigated exhibited relatively large ability to store energy from the deformation (quotient of E_{ST} > 99.5% of E_{DMTA}) i.e. prevailing mode of the response was elasticity - see Fig.34.

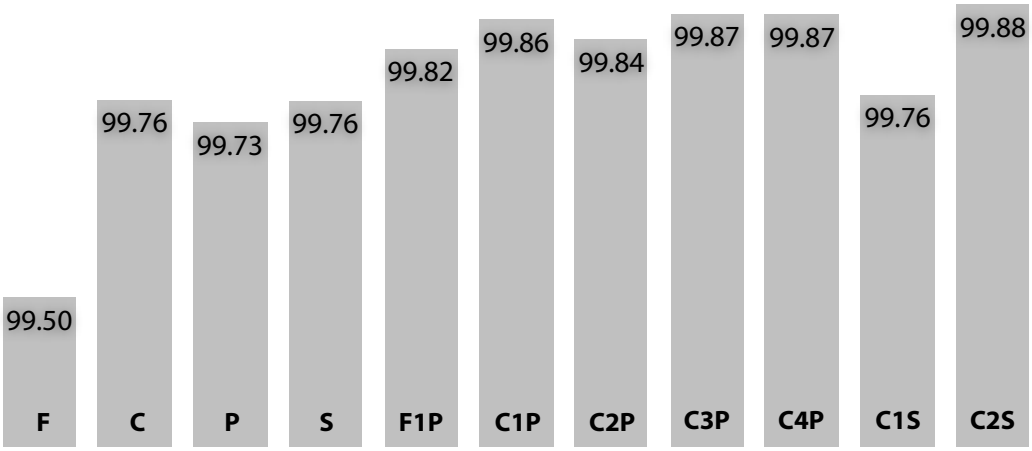

***FIGURE 34**: Quotient of E_{ST} [% of E_{DMTA}]*

Figure 35 shows the diagram for DMTA – three point bending in specimen P. Table 9 presents values of the storage modulus E_{ST}, phase angle δ, complex modulus E_{DMTA} obtained during DMTA. The portion of E_{ST} on E_{DMTA} is calculated as well.

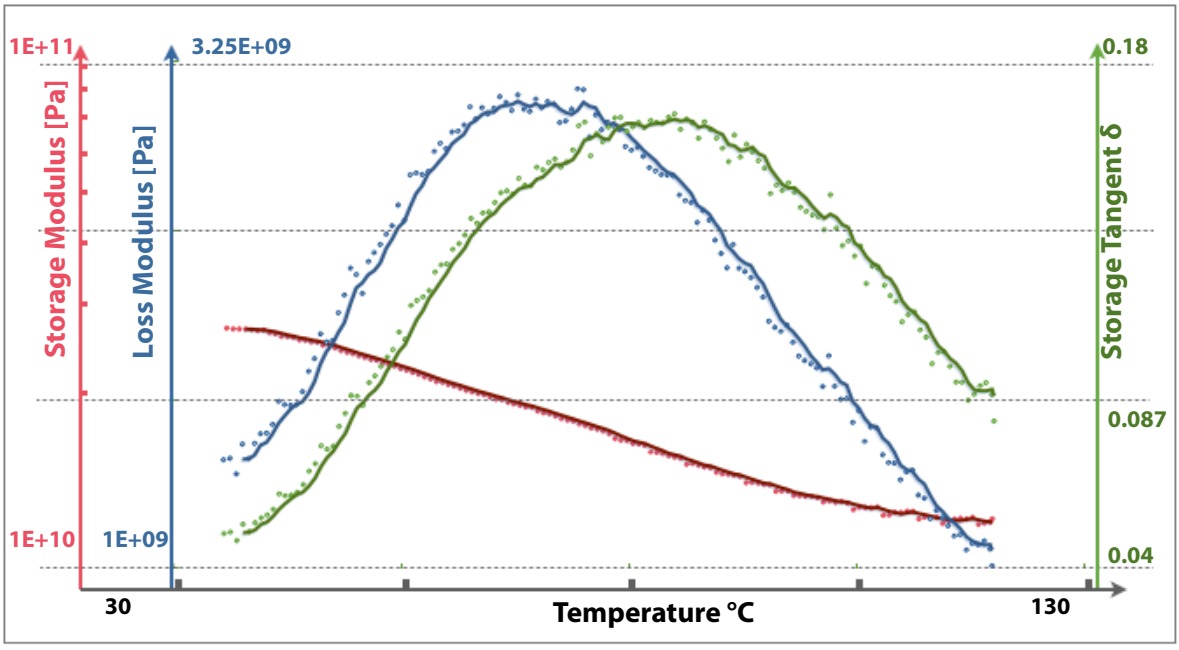

***FIGURE 35**: DMTA – Three poin bending, specimen P*

***TABLE 9**: DMTA test values – An overview*

Type of the specimen	AVG E_{ST} [MPa]	STD E_{ST} [MPa]	AVG δ	STD δ	E_{DMTA}	$100\frac{E_{ST}}{E_{DMTA}}[\%]$
F	7974	322	0.100	0.008	8015	99.50
C	11938	141	0.070	0.005	11967	99.76
P	21315	7780	0.074	0.026	21373	99.73
S	19064	3234	0.070	0.011	19111	99.76
F1P	6592	5419	0.059	0.005	6604	99.82
C1P	13550	243	0.052	0.004	13568	99.86
C2P	13890	363	0.057	0.004	13912	99.84
C3P	16802	870	0.051	0.004	16824	99.87
C4P	16684	1337	0.051	0.004	16705	99.87
C1S	12353	23	0.069	0.001	12382	99.76
C2S	16682	2126	0.049	0.009	16702	99.88

5.2.2 Patterns of mechanical response on static three-point bending

Individual types of specimens exhibit different response to three-point bending which is represented by load-deflection diagram. Several characteristic values were derived from the data obtained during tests such as stiffness, modulus of elasticity and characteristic stresses in the cross-section of the specimen. The procedures of deriving these values depended on the type of response to three point bending.

Two forms of load-deflection diagrams were observed:

- 1 - Smooth curve of the relation demonstrates continuous deformation without sharp changes within internal structure of the specimen. A single peak of the load – deflection curve is followed by a catastrophic reduction in load (stress) in one or more steps. The respective SEM images indicates the failure mode of this type of specimen.
- 2 - The complex curve with multiple local extremes (peaks) demonstrate multi-steps changes within internal structure. Multiple peaks are indicative of subcritical cracking [57] and they are accompanied by stress redistribution which leads to the next peak on the curve. Output of finite element analysis of the specimen F1P illustrates how the normal stress is redistributed during deformation when subcritical cracks propagate – see Figure 36 a,b.

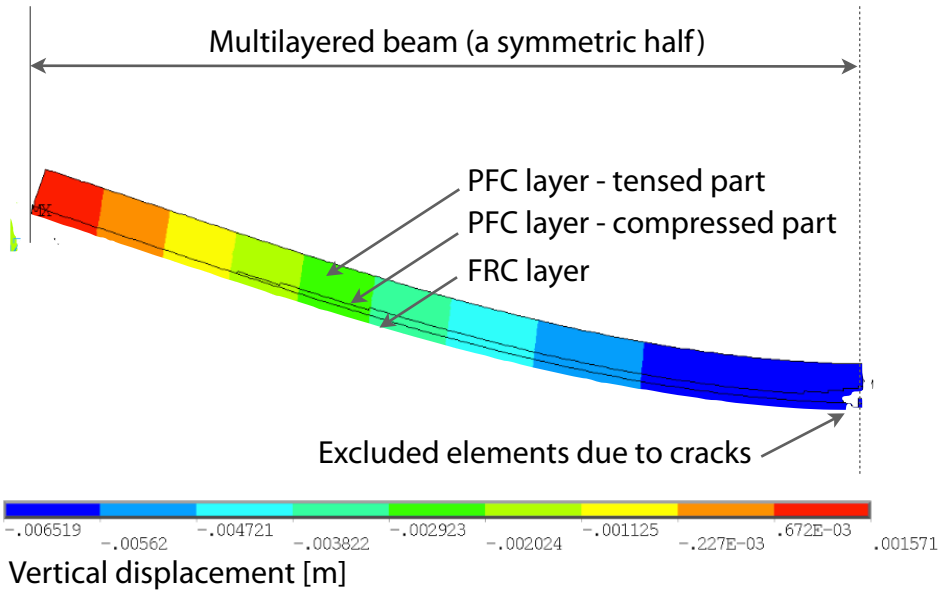

***FIGURE 36a**: FEA of vertical displacements in specimen F1P during subcritical cracks propagation*

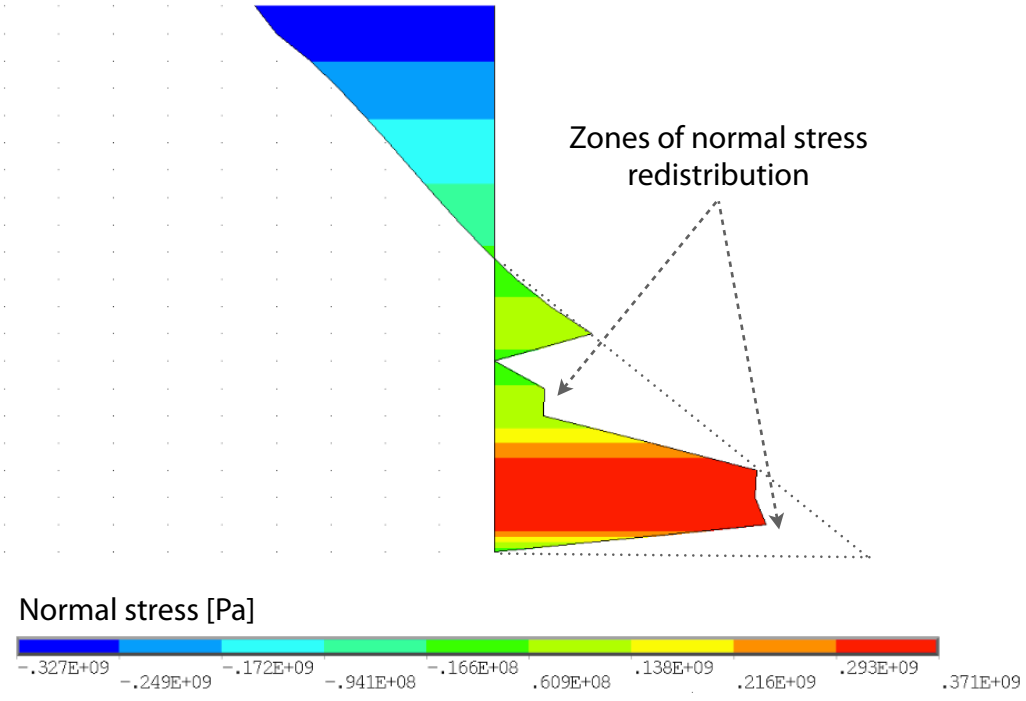

***FIGURE 36b**: FEA of normal stress distribution in specimen F1P during subcritical cracks propagation*

Only a part of the range of data was included in the stiffness analysis in specimens with complex load-deflection curve. This range begins at the start of the curve and ends when the first peak occurs. When deriving characteristic (maximum) stresses, the range of the curve where maximum load occurs is taken into consideration.

5.2.3 Testing protocol

Three-point bending test is widely accepted in the composite material industry. Several protocols for testing fibre reinforced composites are recommended in different standards (ASTM D 790M-99, BS 2782 method 1005, ISO-14125 etc.). All published standards for testing FRC's in flexure focus on FRC laminates. The data obtained from bending test need to be treated with caution due to some limitiations such as:

- The maximum fiber stress may not always occur at the outermost layer in a composite laminate at the outermost layer.
- In the three point bending mode, both normal stress parallel to longitudinal axis of the beam σ_{xx} and shear transversal stress τ_{xz} are present throughout the beam span. The shear deflection can be quite significant, since the E/G ratio for composites is often quite large. The shear deflection can be reduced employing a high aspect ratio for the beam.
- Bending moments create both bending and twisting curvatures. Twisting curvature causes the opposite ends of a flexural specimen to lift off its support [55].

The standard protocols deal with these limitations by defining strict applicability limits, testing conditions (specially dimensions of the specimen, nose radii, loading rate etc.) and relevant calculation of flexural modulus and strength of the specimen.

It was proved during our work that the standard testing protocol for composite laminates are not suitable for analyzing layered composites. There are several reasons of this fact:

- Layered composites of our interest do not comply with the applicability limits of standards (exceeding strain limits at failure e.g. – refer to [56]).
- Geometry of layered composites leads to more complex load – deflection relation (see Figures 37 a – l) than in laminates and calculations proposed in standards for calculating strength and stresses are therefore not applicable.

- Standards focus on flexure modulus as a measure of tendency for a material to bend and do not focus on modulus of elasticity as a measure of the resistance of a material against the deformation.
- Testing specimens of layered composites exhibited steep growth of the resistance against deformation at the start of loading followed by stable range of the resistance. This behavior excluded to derive modulus of elasticity from the values at the very beginning of the test.
- Due to the fact that during bending the values of load and deflection were recorded it was not possible to derive modulus of elasticity from the slope of the load – deformation curve.

Based on this findings testing protocol suitable for layered composites for dental applications was proposed and followed during three-point tests.

Experimental data were processed in the following manner:

- Raw data from testing machine were adjusted in order to eliminate major part of instability of the specimen position at the beginning of the test.
- The original Load - Deformation curve were substituted with an interpolation polynomial function and respective values of load and deformation were calculated.
- Based on the type of load-deformation curve the initial range for calculating stiffness was selected.
- Elastic moduli for each pair of interpolated value of load and deformation were calculated. The governing formula is:

$$E = \frac{P \bullet L^3}{48 \bullet D \bullet I} \tag{51}$$

where:
P = load [N]
L = span of the beam [mm]
D = deflection [mm]
I = b * d^3 /12 = moment of inertia [mm^4]

- The maximum value of modulus for each specimen was identified (E_{fmax}) and the value of modulus at the point of maximal deflection as well (ED_{max})
- Relative stiffness for each pair of interpolated value of load and deformation were calculated according to the formula (52).

$$S_{rel} = \frac{E_{f\max}}{E_{D\max}} \tag{52}$$

where:
E_{fmax} = maximum modulus of elasticity
E_{Dmax}= modulus of elasticity at maximum deflection

Relative stiffness – deflection curve provides information about non-linearity of elastic deformation which reflects a complicated geometry with irregularities in fibres orientation and micro-defects of several origin (polymerisation shrinkage e.g.) inclusions and other irregularities.

There are two patterns of relative stiffness - deformation curve observed:

- 1- Steep growth of the stiffness until maximum stiffness is reached and then slower decrease of the stiffness until maximum deformation is reached.
- 2- Steep growth of the stiffness until maximum stiffness is reached and then little decrease followed by constant part until maximum deformation is reached.

It is assumed that the steep growth at the beginning of the loading relates to the gaining of positional stability of the specimen on the supports and the decrease of stiffness relates to propagation of micro-defects.

Figures 36 a – l bring an overview of typical patterns of mechanical response for individual types of the specimen.

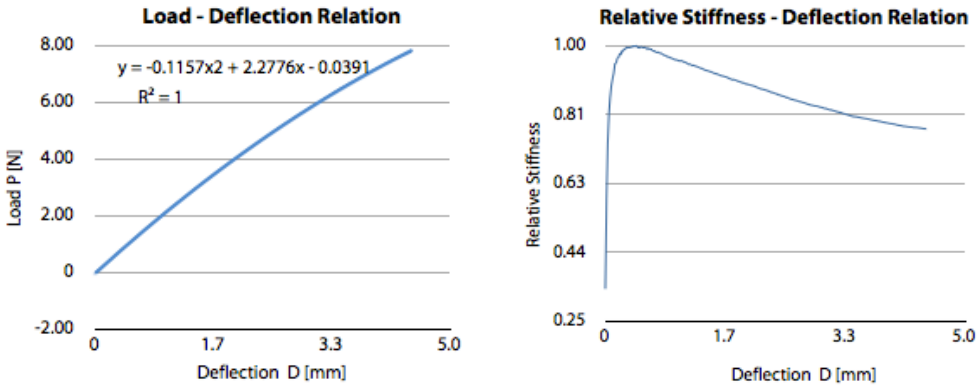

***FIGURE 37-a**: Three point bending – specimen F*

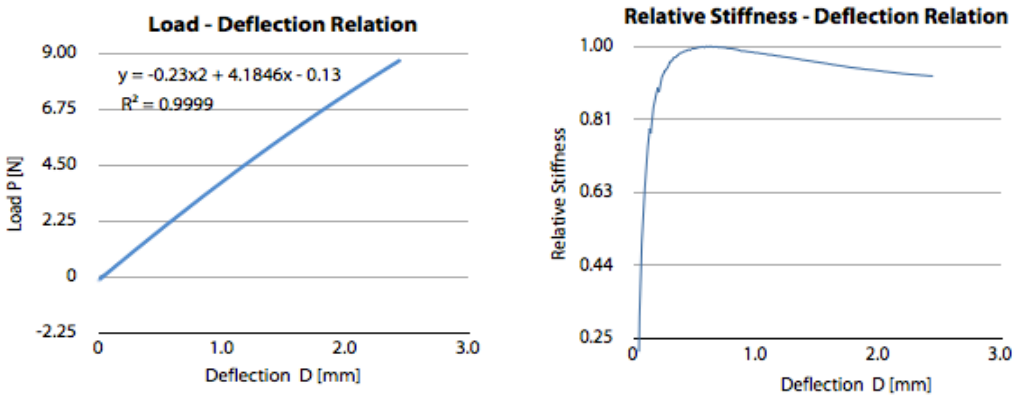

***FIGURE 37-b**: Three point bending – specimen C*

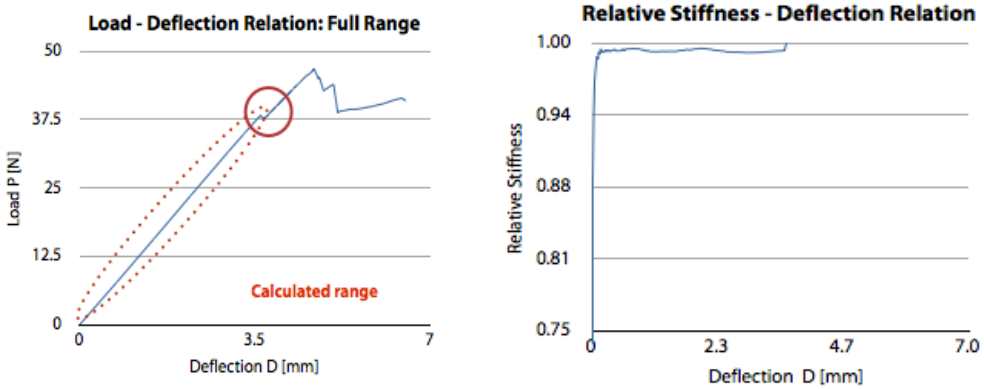

***FIGURE 37-c**: Three point bending – specimen P*

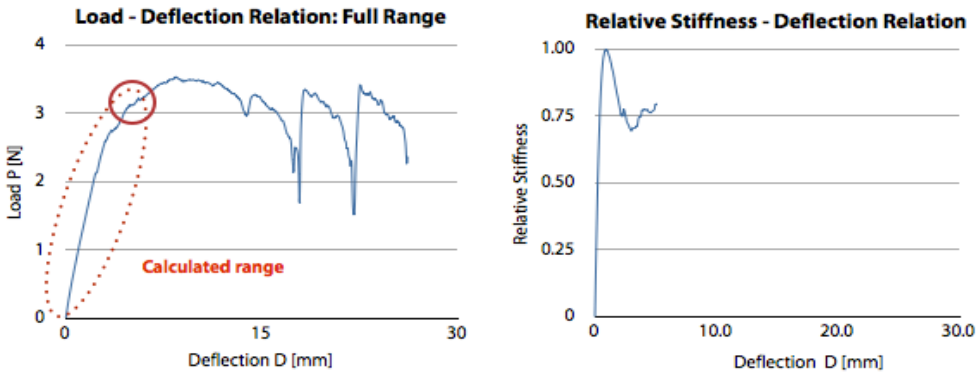

***FIGURE 37-d**: Three point bending – specimen S*

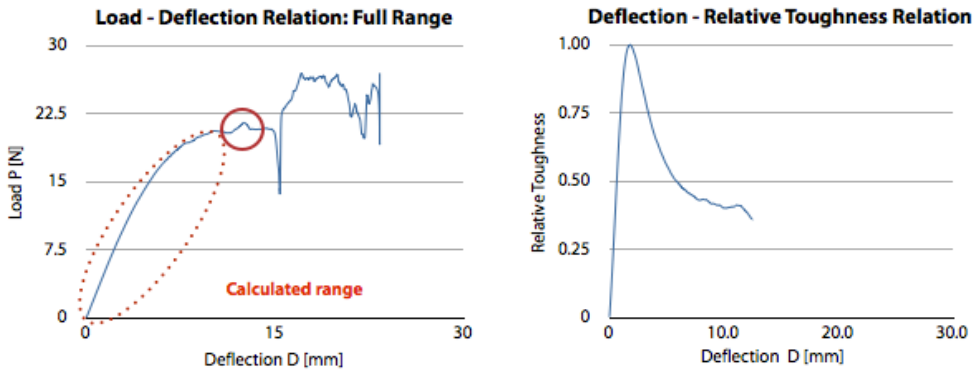

***FIGURE 37-e**: Three point bending – specimen F1P*

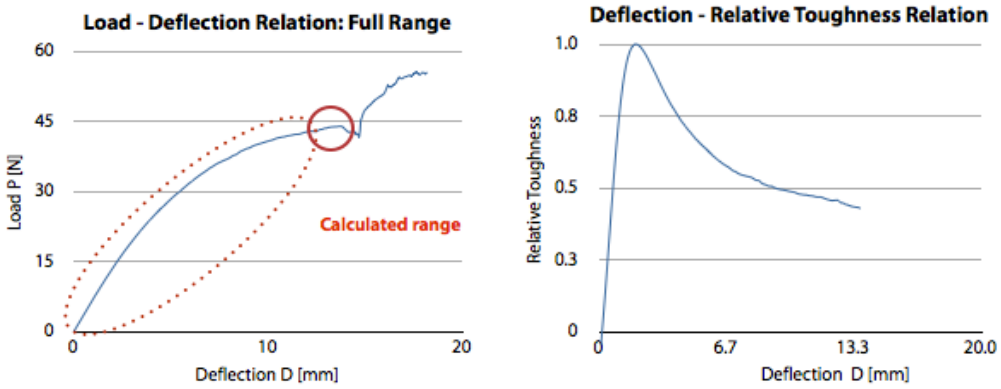

***FIGURE 37-f**: Three point bending – specimen C1P*

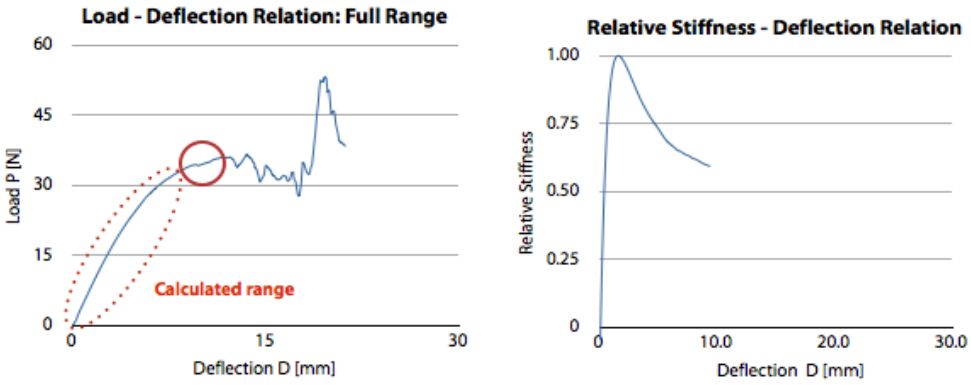

***FIGURE 37-g**: Three point bending – specimen C1PI*

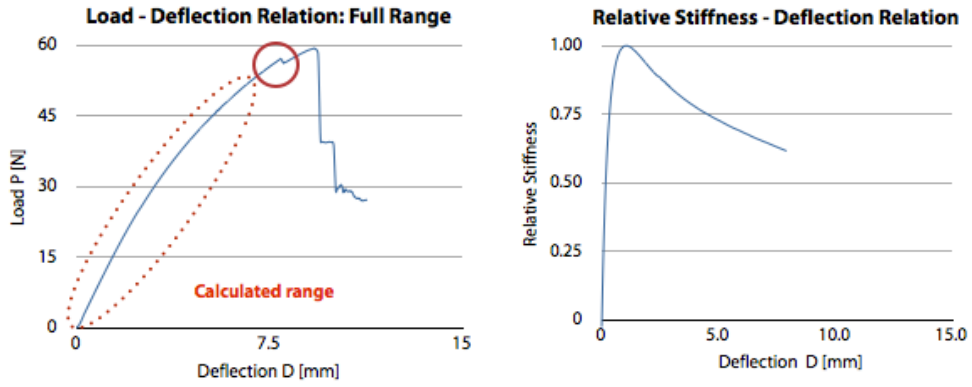

***FIGURE 37-h**: Three point bending – specimen C2P*

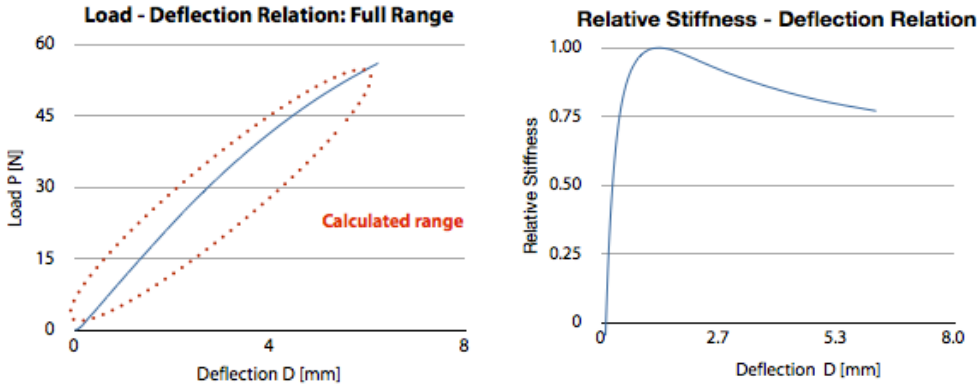

***FIGURE 37-i**: Three point bending – specimen C3P*

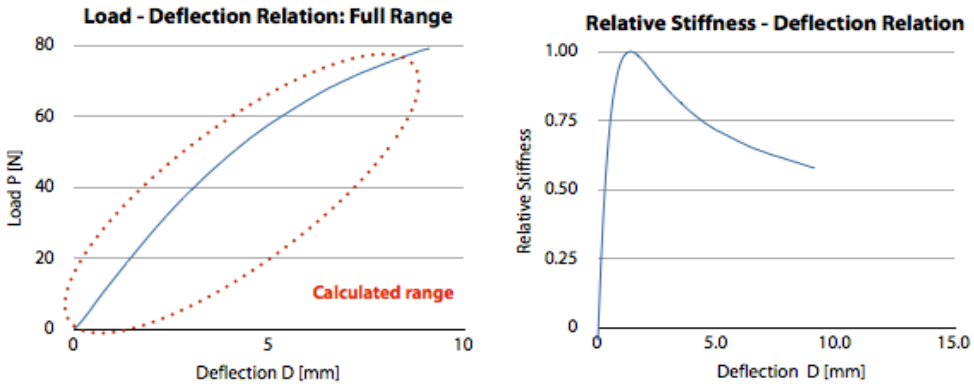

***FIGURE 37-j**: Three point bending – specimen C3P*

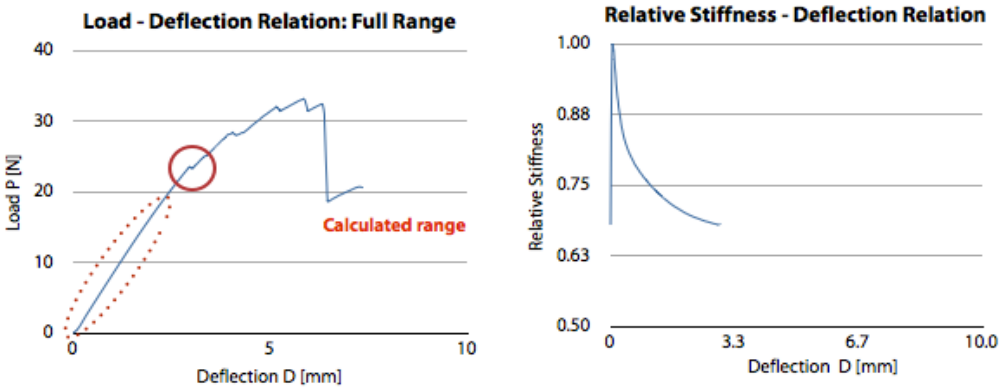

***FIGURE 37-k**: Three point bending – specimen C1S*

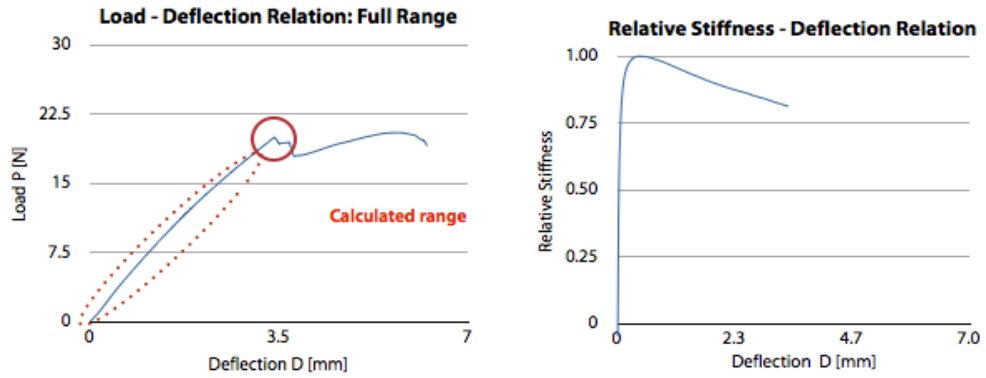

***FIGURE 37-l**: Three point bending – specimen C2S*

In order to interperet experimental results of three point bending test in the proper way it is necessary to remark that the stiffness obtained from the presented test protocol does not have direct relation to the Young modulus of elasticity in general. Bending test generates material response different in its nature to the unidirectional stress caused during a tensile test.

Flexural load causes simultaneously both tensile and compressive normal stresses in a structural element along the thickness of the specimen as well as transverse shear stress. The role of the transverse shear during the failure of the specimen depends on the aspect ratio of the specimen. It is apparent that deformation response of material to bending is more complex than to unidirectional loading in tension or compression. So the stiffness of the specimen in bending reflects more complex processes of resistance of the material to deformation especially when the tensile and compressive moduli differ.

5.2.4 Stiffness in the initial range of deformation

5.2.3.1. Influence of filler content of PFC on stiffness

When considering filler content of particulate filled composite in a layered beam it influences the resistance of the beam against deformation. Layered beam of the same sequence of layers but with higher filler content of PFC layer displays higher stiffness compared with that with lower filler content of PFC – see Table 10 and Figure 38.

A filler content influences the stiffness in accordance with the principle of equivalent homogeneity. Both theories (effective medium theory and equivalent inclusion theory) lead to the same qualitative output: the higher content of the component with the higher value of certain parameter brings the higher effective value of the respective parameter of the final composite. Silica filler has higher modulus of elasticity than the resin and in accordance with the principle of equivalent homogeneity the higher content of silica filler brings higher stiffness to the final composite. This feature of the micorstructure PFC layer is demonstrated at macroscale in the higher stiffness of the layered composite.

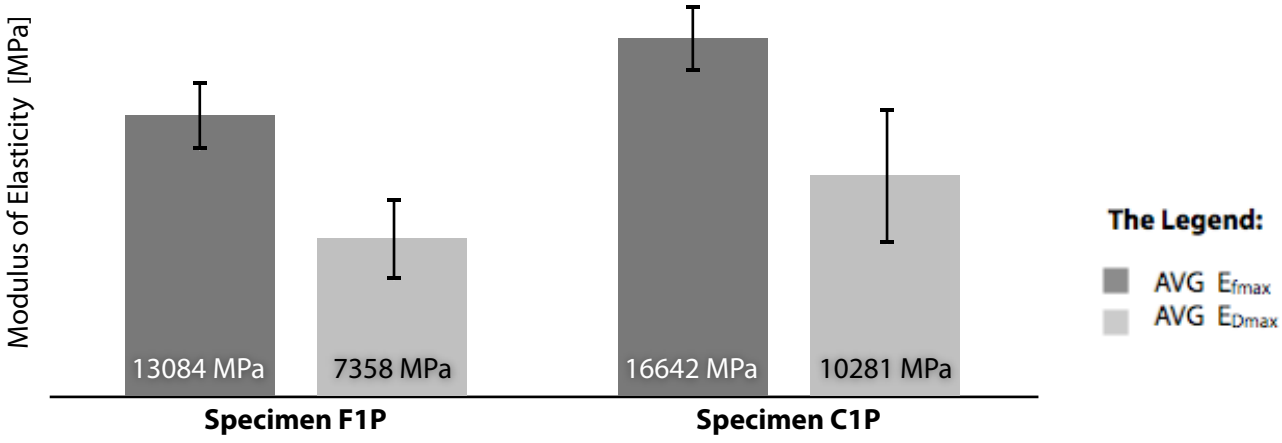

***FIGURE 38**: Influence of filler content of PFC on stiffness*

***TABLE 10**: Influence of filler of PFC on stiffness*

Type of the specimen	Filler content of PFC [wt.%]	STD of the filler content of PFC [wt.%]	AVG E_{fmax} [MPa]	STD E_{fmax} [MPa]	AVG E_{Dmax} [MPa]	STD E_{Dmax} [MPa]
F1P	65.98	0.79	13084	1658	7358	1953
C1P	76.18	0.83	16642	1564	10281	3207

5.2.3.2. Influence of the reinforcement on stiffness

Analysis of the influence of the reinforcement on stiffness is based on the concept of multi-scale modeling in this work. The properties on micro-scale are homogenized and used as an input on meso-scale.

In a layered composite FRC, a layer can be seen as a reinforcing part of the superstructure. The microscale elastic properties of FRC lamina are well mathematically described and bending tests provided relevant data, which can be considered as effective properties of FRC as well. The assumptions of homogenization are fulfilled: the space variation of material properties in FRC is statistically homogenous because the length of averaging is larger than that of inhomogeneity.

For unidirectional FRC the length of inhomogeneity is given by the diameter of single fiber (5 μm) and the density of fibers (1 fiber/10^{-4} mm^2) and is equal to 0.01 mm in all directions while the shortest length of averaging is 0.3 mm (minimal thickness of the PFU strip). This complies with the rule that the length of averaging should be more than 10 times larger than the length of inhomogeneity.

For multidirectional FRC the length of inhomogeneity is given by geometrical model of the fabric. The minimal grain in which the tow segments were divided based on SEM image analysis is 0.04 mm^2. The length of the inhomogeneity is therefore 0.2 mm. Considering the minimal thickness of SFM strip (0.2 mm) homogenization is acceptable in the plane xy parallel to the borders of the layers.

Due to the homogenization of FRC layer it is possible to treat FRC as a homogenous layer with effective elastic properties given obtained by calculations or by experiment.

In this work we use experimental data obtained from three-point tests. In this respect, the measure of the reinforcement is the volume content of FRC layer in the specimen measured by the portion of FRC layer on the cross section area of the beam. We call this parameter later in the text a rate of the reinforcement and it is related to specific type of FRC .

As seen in Table 11 and Figure 39 this parameter – the rate of the reinforcement – strongly influences the stiffness of the layered beam. Higher portion of FRC layer on the cross section area (rate of the reinforcement) brings higher stiffness of the beam.

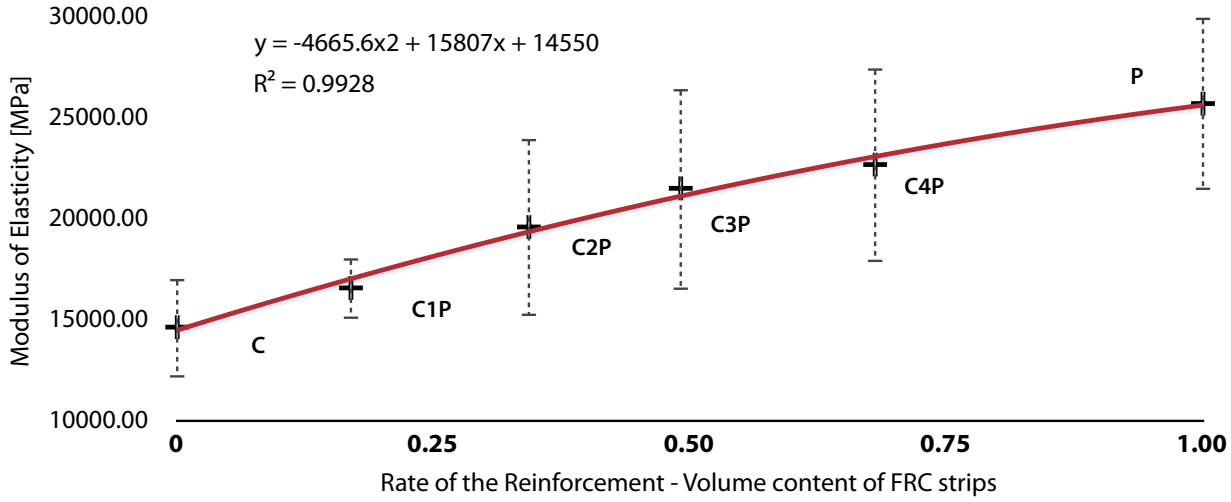

***FIGURE 39**: Influence of the rate of the reinforcement on stiffness*

***TABLE 11**: Influence of the rate of the reinforcement on stiffness*

Type of the specimen	AVG Volume content of FRC strip V_{VFRC}	AVG E_{fmax} [MPa]	STD E_{fmax} [MPa]	AVG E_{Dmax} [MPa]	STD E_{Dmax} [MPa]
C	0.00	14700	2526	12744	1753
C1P	0.17	16642	1564	10281	3207
C2P	0.34	19658	4435	12867	2347
C3P	0.49	21572	5058	15762	3278
C4P	0.68	22748	4858	14364	2519
P	1.00	25767	4308	24830	3632

5.2.3.3. Influence of the interlayer on stiffness

There was no impact of different interlayer designs (resin interlayer between FRC and PFC layers or no interlayer) observed in our test – see Figure 40 and Table 12. It indicates that adhesion between layers does not necessarily influence the resistence of the beam against deformation which is in good agreement with the fact that the resin used for interlayer has lower modulus of elasticity than other constituents (2408 MPa ± 176). There was neither negative influence observed because the thickness of the interlayer was ~ 0.01 mm (based on SEM image analysis) and the volume content of the resin in the beam could be neglected.

However, this result should be considered in the context of a fiber architecture of FRC. When the longitudinal shear strength between the layers controls the overall mode of failure than the presence of interlayer may positively contribute to the stiffness of the beam.

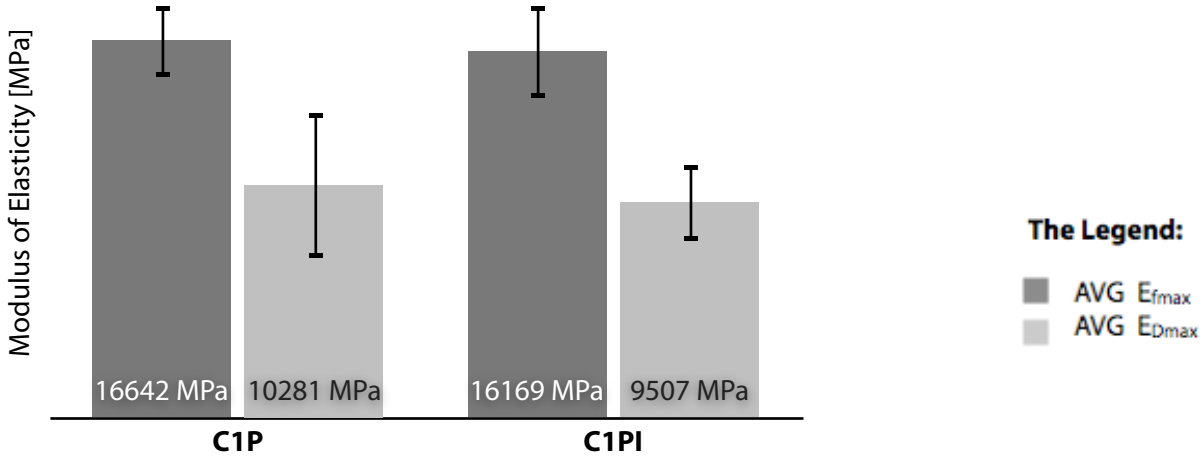

***FIGURE 40**: Influence of the interlayer on stiffness*

***TABLE 12**: Influence of the interlayer on stiffness*

Type of the specimen	AVG E_{fmax} [MPa]	STD E_{fmax} [MPa]	AVG E_{Dmax} [MPa]	STD E_{Dmax} [MPa]
C1P	16642	1564	10281	3207
C1PI	16169	2038	9507	1655

5.2.3.4. Influence of different architecture of FRC on stiffness

Fiber architecture of FRC is an important structural parameter on meso-scale. The real impact of the FRC architecture may be evaluated in case the beams of the same volume content (rate of reinforcement) of different FRC are compared. In this case FRC layer is considered as a homogenous reinforcing part of the layer composite based on the same assumptions as when discussing the influence of the reinforcement on stiffness in paragraph 5.2.3.2. It is apparent that the same volume content of unidirectional strip in a layered beam brings larger stiffness compared to the same content of fibers in the multidirectional strip due to the more effective orientation of fibres in the strip – see Figure 41 and Table 13. This is in agreement with expectations because the effective modulus of homogenized unidirectional strip is higher than that of multidirectional strip (see the values of modulus at volume content = 1.0 at Figure 41). It also explains the tendency of convergence of the values of modulus when the volume content of FRC reinforcement decreases.

From multi-scale modeling point of view the architecture – layout of fibers (micro-scale feature) – influences the effective stiffness of FRC lamina (meso-scale feature) according to the well known rules of lamina. On the macro-scale of the layered beam the architecture of fibers is reflected indirectly as one of the factors contributing to the effective stiffness of the FRC layer.

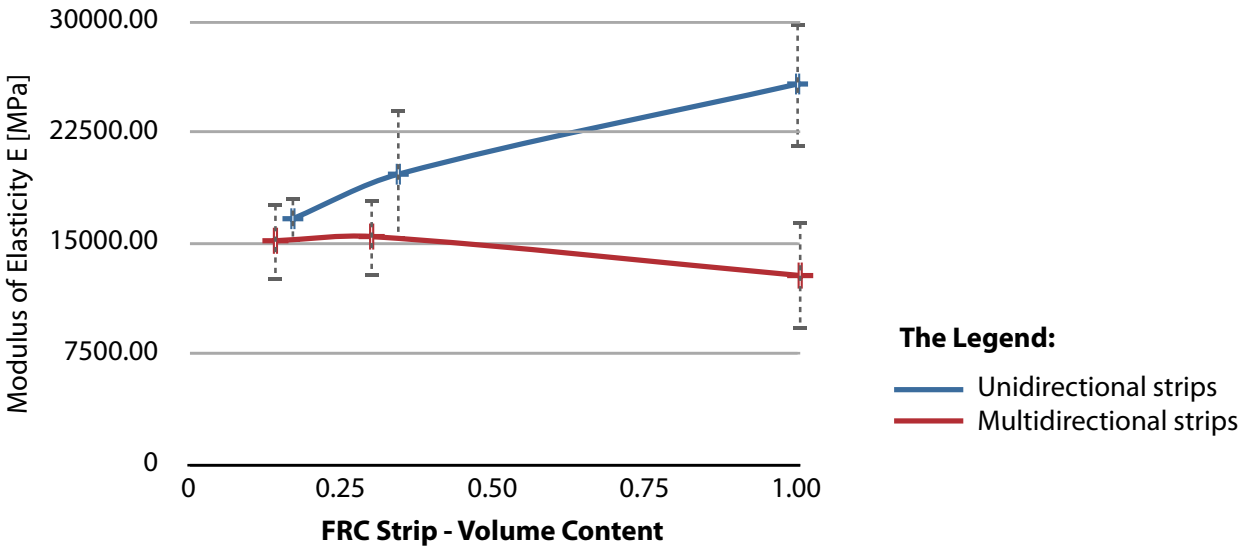

***FIGURE 41**: Influence of FRC architecture on stiffness*

***TABLE 13**: Influence of FRC architecture on stiffness*

Type of the specimen	AVG Volume Content of FRC strips V_{VFRC}	AVG E_{fmax} [MPa]
C1P	0.17	16642 ± 1564
C2P	0.34	19658 ± 4435
P	1	25767 ± 4308
C1S	0.14	15149 ± 2716
C2S	0.30	15434 ± 2725
S	1	12791 ± 3712

5.2.5 Correlation between experimental data and selected analytical model

The analytical model is based on the Rule of mixture for homogenization of the material in the beam. In a layered composites firm bond between individual layers and uniform strain is expected and consequently the Voigt version of the Rule of mixture was used.

The modulus of elasticity for this model was calculated in accordance with the following equation:

$$E_{ROM} = E_{FRC} \bullet V_{VFRC} + E_{PFC} \bullet V_{VPFC} \tag{53}$$

where
E_{FRC} = modulus of elasticity of FRC strip [MPa]
V_{VFRC} = volume content of FRC strip in the beam
E_{PFC} = modulus of elasticity of PFC [MPa]
V_{VPFC} = volume content of PFC in the beam

Outputs of the analytical estimation of the effective modulus by the Rule of mixture were compared with experimental data obtained from static three-point tests and DMTA of three point bending as well. Graph in Figure 42 shows the compliance of the values gained in both types of experiments (DMTA and static three point bending) and analytical model, Table 14 provides an overview of respective data.

Based on this comparison it can be stated that Rule of mixture is a robust analytical method to estimate effective resistance to deformation of the layered composites of our interest.

The difference between E_{fmax} and ED_{max} indicates the extension of micro-defects which propagate during the loading and influence the resistance of the specimen to flexure and non-linear elasticity of layered composites as well.

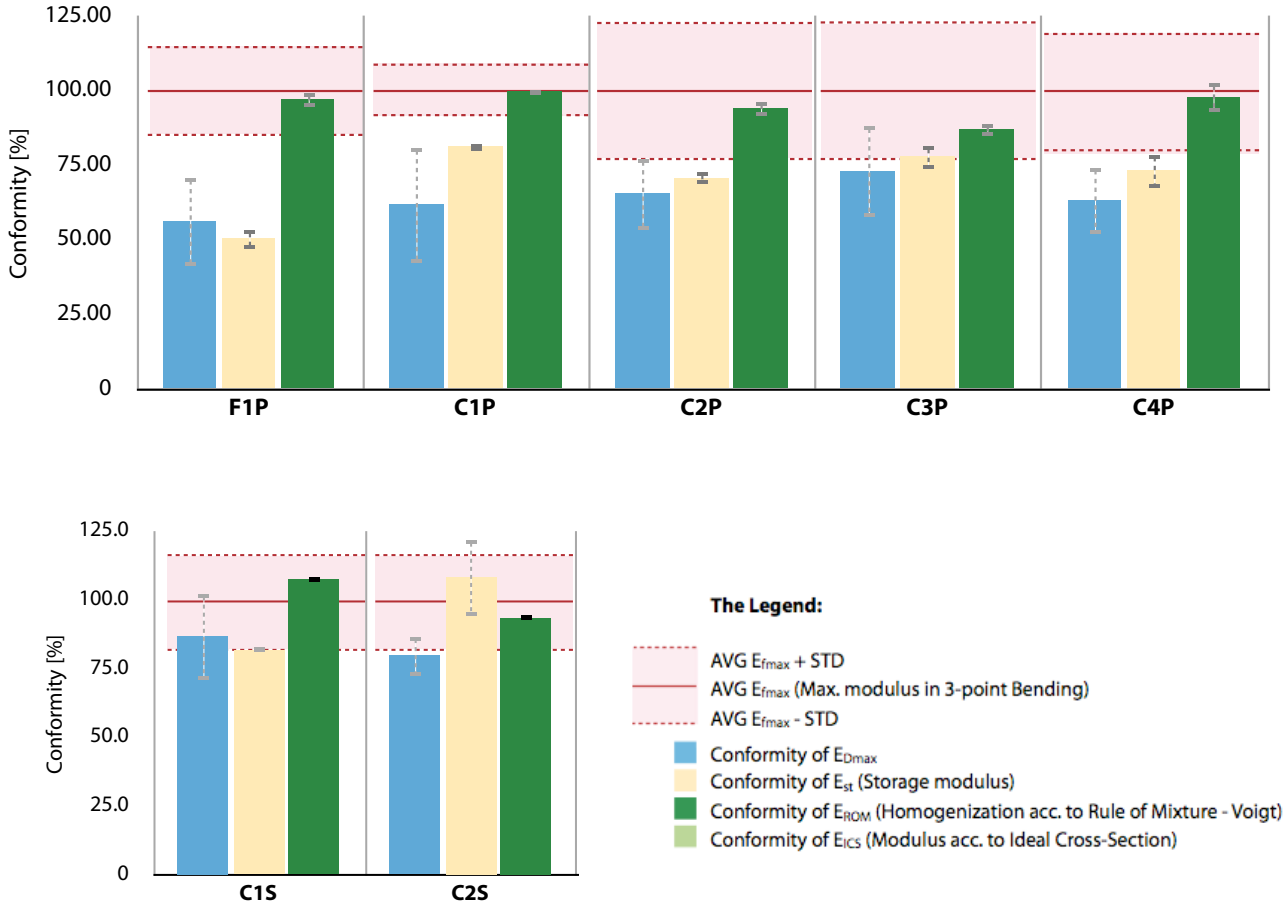

***FIGURE 42**: Comparison of different stiffness moduli*

***TABLE 14**: Comparison of different stiffness moduli*

Type of the specimen	E_{fmax} [MPa]	E_{Dmax} [MPa]	E_{ST} [MPa]	E_{ROM} [MPa]
F1P	13084 ± 1658	7358 ± 1953	6592 ± 419	12695 ± 327
C1P	16642 ± 1564	10281 ± 3207	13550 ± 243	16574 ± 117
C2P	19658 ± 4435	12867 ± 2347	13890 ± 363	18494 ± 485
C3P	21572 ±5058	15762 ± 3278	16802 ± 870	18774 ± 463
C4P	22748 ± 4858	14364 ± 2519	16684 ± 1337	22230 ± 1106
C1S	15149 ± 2716	13146 ± 2372	12353 ± 23	16251 ± 137
C2S	15434 ± 2725	12311 ± 1117	16682 ± 2126	14416 ± 23

5.2.6 Maximum stresses and stress distribution

For the stress analysis, the point where maximum load was reached on the load - deformation curve was chosen. The calculation protocol for the maximum stress varied based on the type of the beam (mono-layer and bi-layer). Due to the high aspect ratio of specimen (L/D>20), the transversal stress could be neglected. The governing relation for estimation of a normal stress is the flexure formula:

$$\sigma_{flex} = \left(\frac{M}{I}\right) \bullet c \tag{54}$$

where
σ_{flex} = maximum normal stress at the point on cross section [MPa]
M = internal moment from load P [Nmm]
I = moment of inertia of the cross section
c = perpendicular distance from the neutral axis to the point where σ_{flex} acts [mm]

Since the flexure formula was developed for homogenous materials, it is necessary for bi-material beams to transform the beam's cross section as it is made of a single material. This is often referred to as an "ideal cross section".

The principle of converting bi-material cross section in an ideal cross section is to reduce the part made of material with lower modulus of elasticity using a transformation factor:

$$n = \frac{E_1}{E_2} \tag{55}$$

where
$E_1 = E_{pfc}$ = modulus of elasticity of PFC material [MPa]
$E_2 = E_{frc}$ = modulus of elasticity of FRC material [MPa]

Moment of inertia of an ideal cross section is given by equation:

$$Ix_{ca} = \left(Ix_{FRC} + A_{FRC} \bullet c_{FRC}^2\right) + \left(Ix_{redPFC} + A_{redPFC} \bullet c_{PFC}^2\right) \tag{56}$$

where
Ix_{FRC} = moment of inertia of FRC part [mm^4]
A_{FRC} = area of FRC part [mm^2]
C_{FRC} = distance between centroids of FRC part and of the beam [mm]
Ix_{redPFC} = moment of inertia of reduced PFC part [mm^4]
A_{redPFC}= reduced area of PFC part [mm^2]
C_{PFC}= distance between centroids of PFC part and of the beam [mm]

The characteristic stresses were calculated according to the following steps:

1) Maximum internal moment (see Figure 22):

$$M = \frac{P \bullet L}{4} \tag{57}$$

where:
P = maximal load [N]
L = span of the beam [mm]

2) Moment of inertia of the cross - sectional area (rectangle)
for mono-layer cross section:

$$I = \frac{b \bullet d^3}{12} \tag{58}$$

where:
b = width of the beam [mm]
d = depth of the beam [mm]

for bi-layer cross section ("ideal" cross section) see equations (55), (56).

3) Normal stresses (parallel to longitudinal axis x) in the characteristic points of the cross section

Stress σ_T at point T - the farthest point away from neutral axis in the tension part of the cross section:

$$\sigma_T = \frac{M}{Ix_{ca}} \bullet \left(c_{FRC} + \frac{d_{FRC}}{2} \right) \tag{59}$$

where:
M = maximal internal bending moment [Nmm]
Ix_{ca} = moment of inertia of ideal cross section [mm^4]
c_{FRC} = distance between centroids of ideal cross section and FRC layer [mm]
d_{FRC} = thickness of the FRC layer [mm]

Stress σ_{BFRC} at point B_{frc} - the point on the material borderline - FRC site:

$$\sigma_{BFRC} = \frac{M}{Ix_{ca}} \bullet \left(c_{FRC} - \frac{d_{FRC}}{2} \right) \qquad (60)$$

where:
M = maximal internal bending moment [Nmm]
Ix_{ca} = moment of inertia of ideal cross section [mm^4]
c_{FRC} = distance between centroids of ideal cross section and FRC layer [mm]
d_{FRC} = thickness of the FRC layer [mm]

Stress σ_C at point C - the farthest point away from neutral axis in the compression part of the cross section:

$$\sigma_C = -n \bullet \frac{M}{Ix_{ca}} \bullet \left(c_{PFC} + \frac{d_{PFC}}{2} \right) \qquad (61)$$

where:
M = maximal internal bending moment [Nmm]
Ix_{ca} = moment of inertia of ideal cross section [mm^4]
c_{PFC} = distance between centroids of ideal cross section and PFC layer [mm]
D_{PFC} = thickness of the PFC layer [mm]

Stress σ_{BPFC} at point B_{pfc} - the point on the material borderline - PFC site :

$$\sigma_{BPFC} = n \bullet \sigma_{BFRC} \qquad (62)$$

where:
n = transfomation factor
σ_{BFRC} = normal stress at point B_{frc}

4) Drawing stress distribution charts

For mono-layer beams see Figure 43, for bi-layer beams see Figure 44.

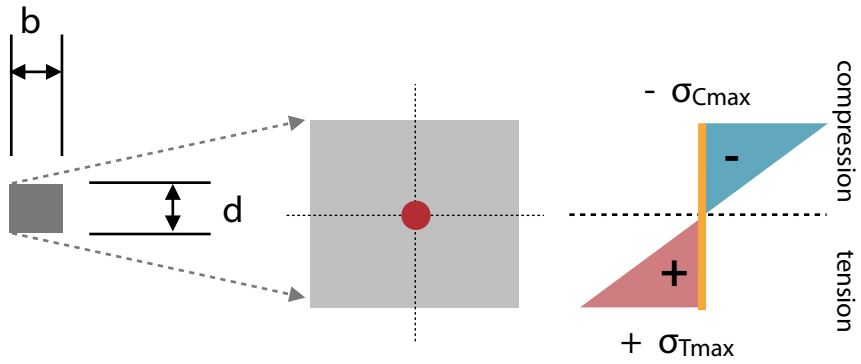

***FIGURE 43**: Normal stress distribution in a mono-layer beam*

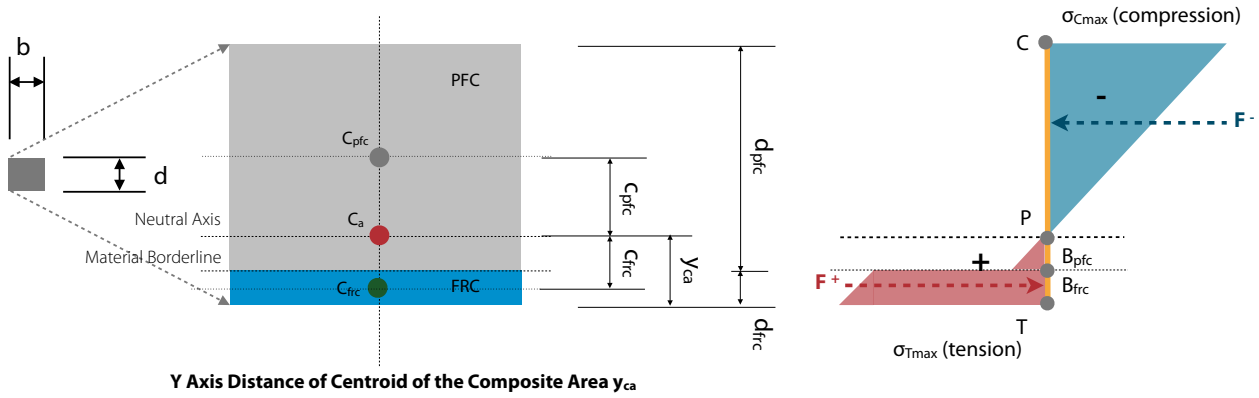

***FIGURE 44**: Normal stress distribution in a bi-layer beam*

Based on this procedure characteristic stresses were calculated for all types of the test specimens. Following features were of our interest:

- The maximum value of tension and compression which indicates the limit strength of the specimen
- The difference between the maximum tension and compression which indicates the complexity of the response of the specimen to flexural load
- The difference between stresses on the border of layers which plays an important role in possible delamination during failure. This difference is demonstrated as longitudinal shear between layer and it tends to slide layers in the direction of longitudinal axis x. Longitudinal shear stress is signed as τ_B ($\tau_B = \sigma_{FRC} - \sigma_{PFC}$).
- The position of the neutral axis and its relation to the geometry of layered specimen as well as to distribution of normal stresses.

5.2.4.1. Influence of the filler content of PFC on normal stress

As shown in Table 15 and Figures 45 and 46, there is an influence of filler content of PFC on the longitudinal shear stress τ_B. Larger longitudinal shear between layers exhibits the beam with higher filler content of PFC.

Based on the concept of homogeneization the effective strength of the PFC is a function of the content of a component with higher strength i.e. the filler. It is then apparent that the PFC with higher filler content should have higher strength compared to the PFC with lower filler content. This assumption is in accordance with our experimental results.

***TABLE 15**: Influence of the filler content of PFC on normal stress distribution*

Type of the specimen	σ_{Tmax} [MPa]	σ_{BFRC} [MPa]	σ_{BPFC} [MPa]	σ_{Cmax} [MPa]	τ_B [MPa]
F1P	367 ± 54	188 ± 36	70 ± 14	-228 ± 34	118 ± 23
C1P	362 ± 132	202 ± 79	115 ± 21	-334 ± 122	87 ± 34

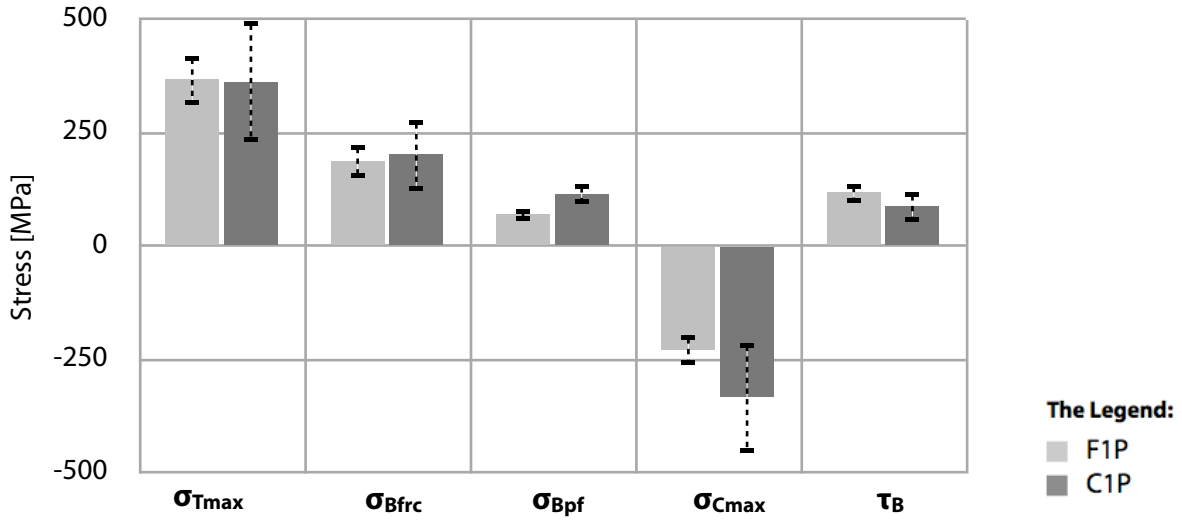

***FIGURE 45**: Influence of the filler content of PFC on normal stress distribution*

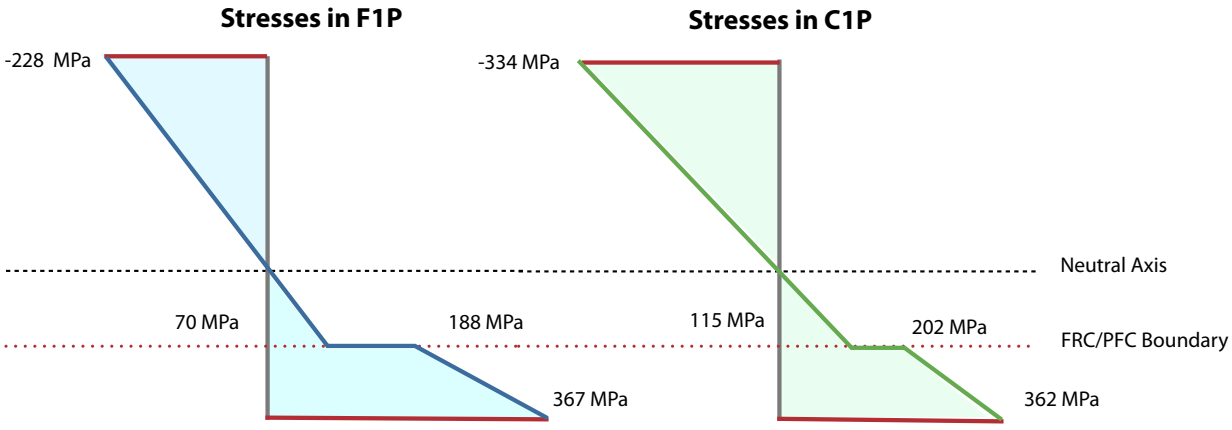

***FIGURE 46**: Stress distribution chart for specimens with different filler content in PFC*

The difference between the stresses on the borders of the layer indicates the difference of individual PFCs to carry the load. The normal stresses on the border on the site of the FRC are very close in both specimen (188 ± 36 MPa for F1P and 202 ± 79 for C1P) the respective stresses on the site of PFC are very different (70 ± 14 for F1P and 115 ± 21). This conclusion correlates with different values of maximum compression for both specimen. Larger difference between the strength of adjacent layers creates larger longitudinal shear stress. The relative position of the border of the layer and the neutral axis is the second factor which influences the value of longitudinal shear on the layers border.

5.2.4.2. Influence of the FRC reinforcement on normal stress

When analysing the influence of the reinforcement on normal stress and its distribution we use the same approach as for stiffness. It is based on the concept of multi-scale modeling where the properties on micro-scale are homogenized and used as an input on meso-scale. Due to the homogenization of FRC layer it is possible to treat FRC as a homogenous layer. In this respect the measure of the reinforcement is the volume content of FRC layer in the specimen measured by the portion of FRC layer on the cross section area of the beam.

The rate of reinforcement has a key impact on the way the stress is distributed across the beam cross section. Table 16 summarizes data used in analysing influence of the FRC reinforcement, Figure 47 compares values of respective stresses in individual types of layered beams, Figure 48 depicts the relation between maximum normal tension and compression and Figure 49 illustrates stress distribution in individual types of layered beams.

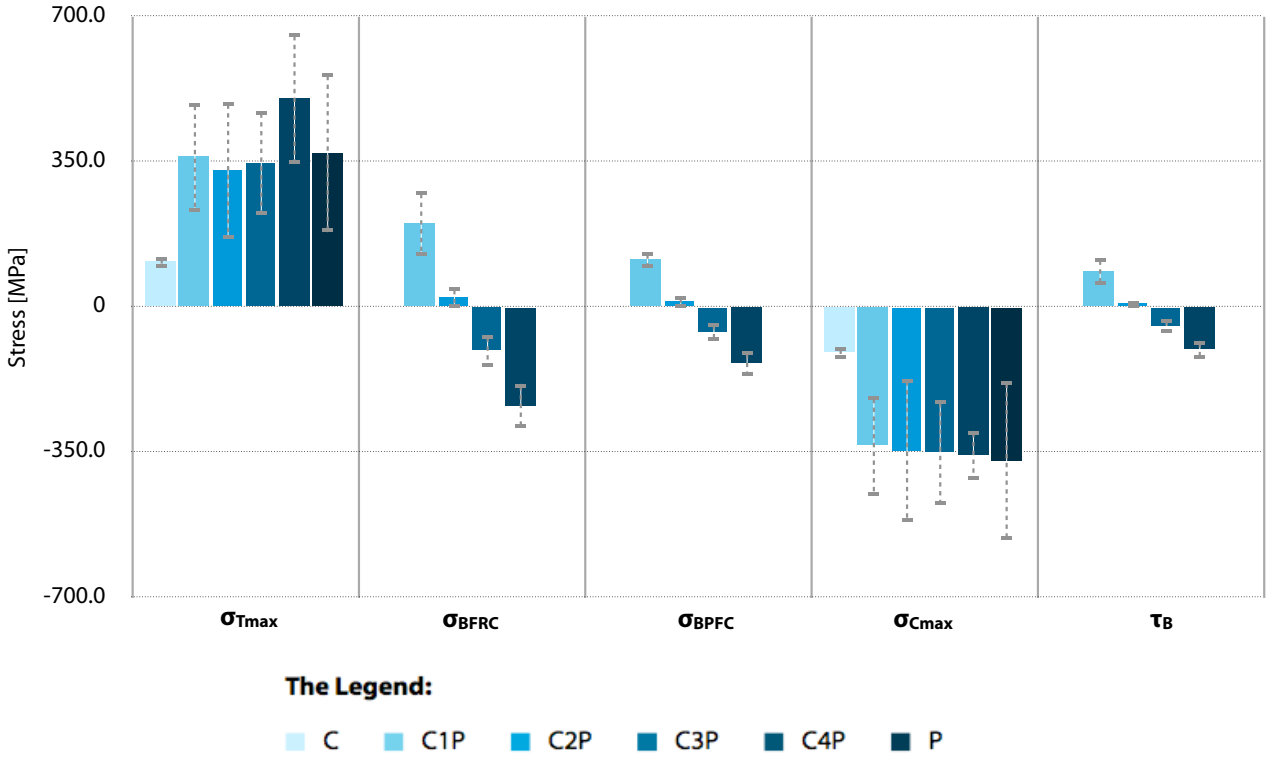

***FIGURE 47**: Comparison of the characteristic normal stresses in beams with a different rate of the reinforcement*

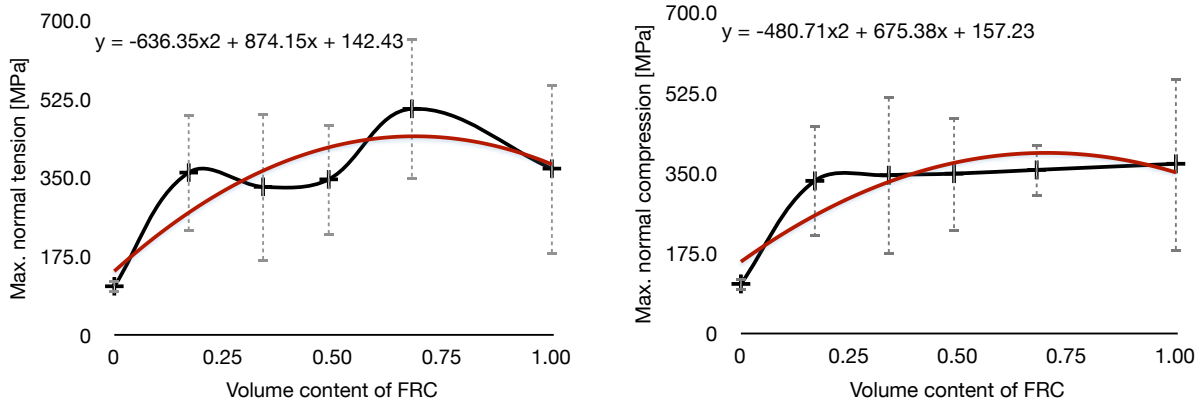

***FIGURE 48**: Maximum normal tensions and compressions as a function of the rate of the reinforcement*

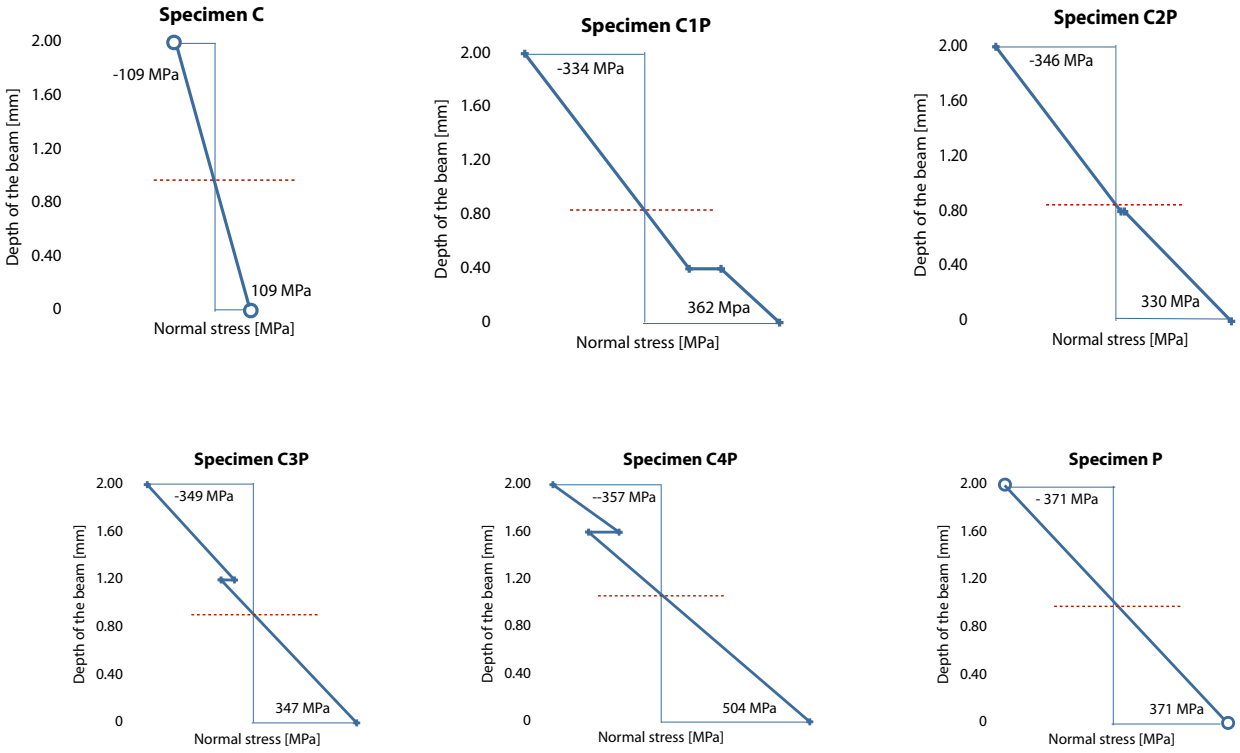

***FIGURE 49**: Normal stress distribution chart for specimens with a different rate of the reinforcement*

***TABLE 16**: Normal stresses for specimens with a different rate of the reinforcement*

Type of the specimen	σ_{Tmax} [MPa]	σ_{BFRC} [MPa]	σ_{BPFC} [MPa]	σ_{Cmax} [MPa]	τ_B [MPa]
C	109 ± 16			-109 ± 16	
C1P	362 ± 132	202 ± 79	115 ± 21	-334 ± 122	87 ± 34
C2P	330 ± 166	23 ± 25	13 ±15	-346 ± 173	8 ± 10
C3P	347 ± 125	-104 ± 39	-59 ± 22	-349 ± 127	-45 ± 17
C4P	504 ± 159	-238 ± 54	-136 ± 31	-357 ± 59	-102 ± 23
P	371 ± 191			-371 ± 191	

Based on the calculated data, it is suggested that the volume content of the FRC layer influences normal stress and its distribution in several ways:

- FRC layer increases the maximum stresses compared to PFC mono-layer specimen. It is because FRC has larger strength in tension compared to PFC as indicated in the failure behavior of mono-layer specimen during three point bending tests.
- There was no relation between the volume content of FRC and maximum stresses observed. It is suggested that there is a certain range of effective volume content and out of this range the reinforcing effect of FRC drops down (see Figure 48). This feature is well known in reinforced concrete.
- The presence of FRC layer and its area in the beam cross section shifts the position of the neutral axis according to the equations of ideal cross section.
- The volume content of FRC layer influences the relative position of the border of the layers and the neutral axis as well. Larger volume content means larger area of cross-section occupied by the layer. Providing the FRC layer is placed from the very bottom of the specimen with raising volume content of the FRC, the layer's border goes closer to the neutral axis. With a certain volume content the neutral axis may lay in the area of the cross section occupied by FRC layer (refer to C3P and C4P on the Figure 49). The relative position of the layer's border and the neutral axis determines the value of longitudinal shear between the layers which influence delamination of the layers. It should be noted here that in case the layer's border is very close to the neutral axis, the longitudinal shear is very low (refer to C2P on Figure 49). However, in the position of neutral axis the transversal shear reaches its maximum and this may cause delamination especially in a short beam.

5.2.4.3. Influence of the interlayer on normal stress

Table 17 and Figure 50 provides data and comparison of stresses in layered beams with and without interlayer. It is evident that there is no influence of interlayer on stresses displayed.

This statement does not exclude the hypothesis that the interlayer increases the adhesion between layers. But this eventual increase does not apply to the strength or to stress distribution during the test of given protocol and specimen's geometry. It is in a good agreement with the proposed failure mechanism where delamination of the layer does not activate the final failure in layer beams.

***TABLE 17**: Influence of interlayer on normal stress*

Type of the specimen	σ_{Tmax} [MPa]	σ_{BFRC} [MPa]	σ_{BPFC} [MPa]	σ_{Cmax} [MPa]	τ_B [MPa]
C1P	367 ± 54	188 ± 36	70 ± 14	-228 ± 34	118 ± 23
C1PI	362 ± 132	202 ± 79	115 ± 21	-334 ± 122	87 ± 34

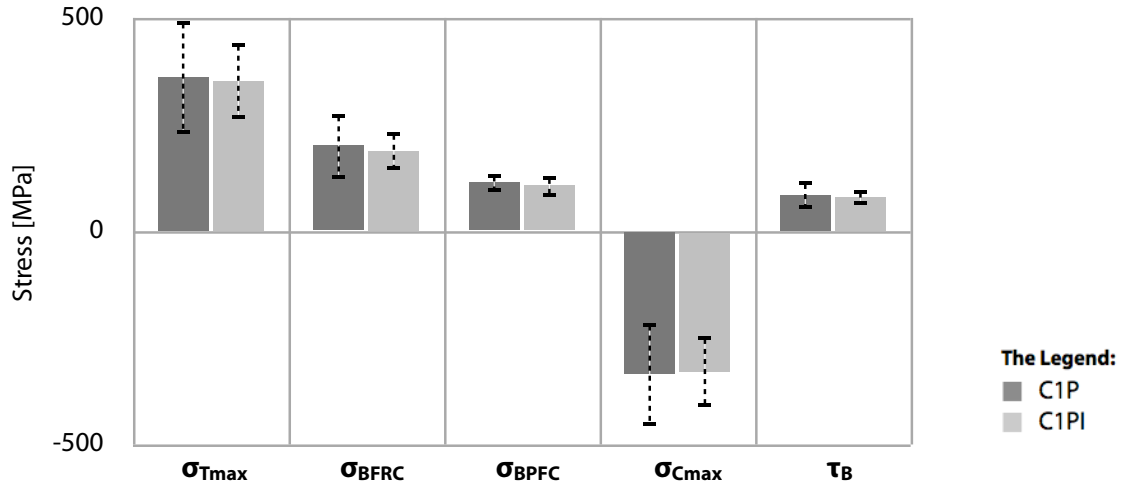

***FIGURE 50**: Influence of interlayer on normal stress*

5.2.4.4. Influence of different architecture of FRC on normal stress

Two types of the beams were chosen in order to study the influence of architecture of FRC on normal stress. Both have neutral axis in about the same position so the influence of different geometry of layers can be neglected. Based on the data in Table 18, Figures 51 and 52 it is evident that the fiber architecture in the layers strongly influences normal stresses in the beam. Unidirectional FRC layer is capable to carry larger tensile stresses as well as longitudinal shear at the border interface between the layers.

***TABLE 18**: Influence of interlayer on normal stress*

Type of the specimen	σ_{Tmax} [MPa]	σ_{BFRC} [MPa]	σ_{BPFC} [MPa]	σ_{Cmax} [MPa]	τ_B [MPa]
C1P	362 ± 132	202 ± 79	115 ± 21	-334 ± 122	87 ± 34
C1S	67 ± 23	43 ± 15	50 ± 17	-111 ± 39	-6 ± 2

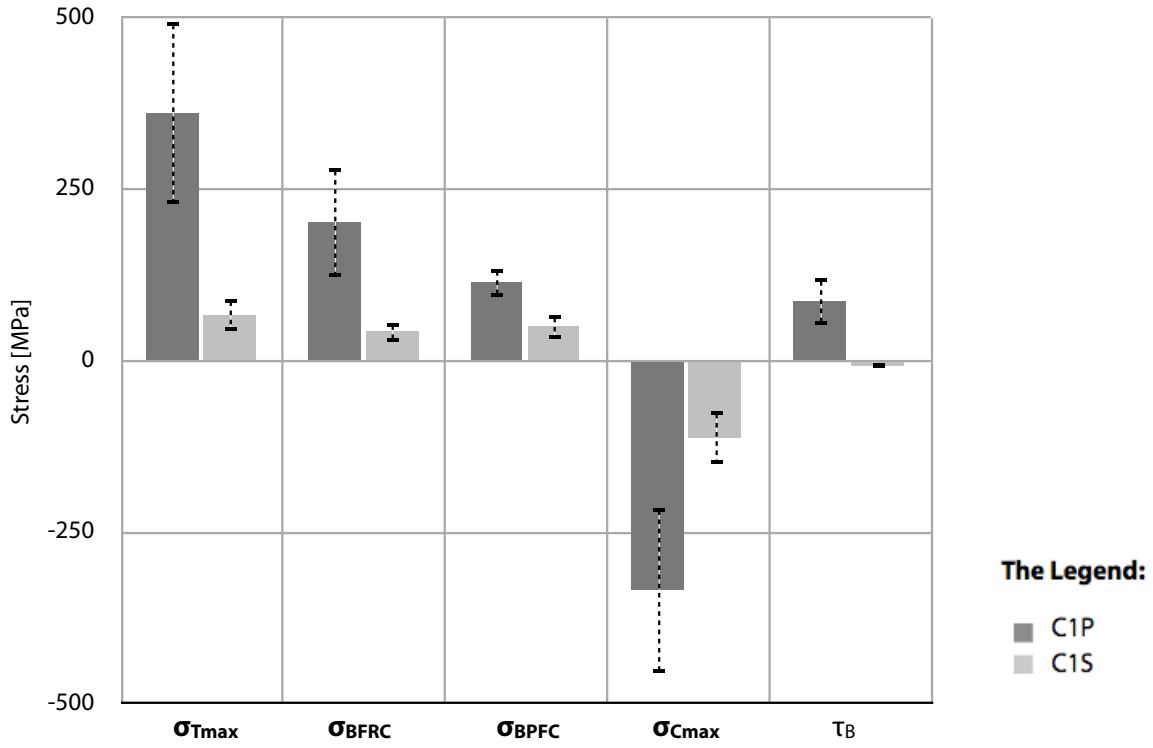

***FIGURE 51**: : Influence of interlayer on normal stress*

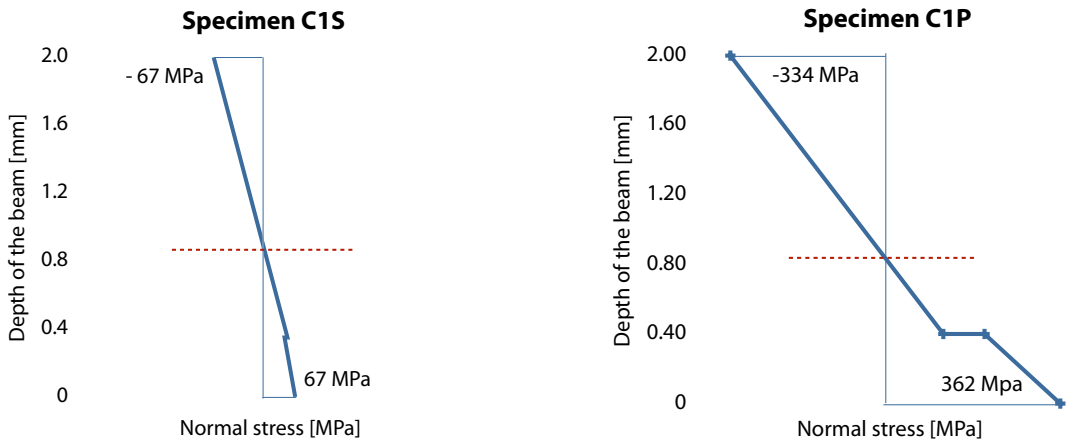

***FIGURE 52**: : Distribution of the normal stress in specimen with different FRC architecture*

From multi-scale modeling point of view the architecture – layout of fibers (micro-scale feature) - influences the effective strength of FRC lamina (meso-scale feature) according to the well-known rules of lamina. On the macro-scale of the layered beam the architecture of fibers is reflected indirectly as one of the factors contributing to the effective strength of the FRC layer.

6 CONCLUSIONS

The concept of using advanced layered composites as a load bearing substructures for various dental applications was investigated. The main focus was to study how the resistance of layered composites to deformation and stress distribution is influenced by structural parameters of the constituents and their spatial arrangement. These parameters included:

- filler content of particulate filled composite,
- volume content of FRC layer (rate of the reinforcement),
- interlayer between two different layers,
- internal architecture of FRC.

Two types of FRC pre-impregnated layers, two types of dental PFC and two types of interlayer were examined.

FRC prepregs included:

- PFU laminae where fibres are oriented uni-directionally and are made of S2 glass
- SFM laminae where fibres are oriented multi-directionally (in three dimensions) and are made of E glass

Particulate filled composites used in this work included:

- Particulate filled composite with lower filler content (66 wt.% of silica) - FLOW
- Particulate filled composite with higher filler content (76 wt.% of silica) - CB

Concerning interlayer two designs were used:

- Immediate connection of two adjacent layers
- A thin interlayer made of light curing methacrylate based resin (50% BIS-GMA, 50% TEGMA)

The analysis consists of different types of tests and observation techniques.

Thermogravimetric analysis was used in order to determine the content of inorganic phase in constituent of layered composite (filler in PFC and fibres in FRC). Differential scanning photo-calorimetry was carried out to testify if there were transitions present during irradiation of the specimens.

Three point bending was the loading modus used in mechanical testing. Dynamic mechanical thermal analysis in this modus was employed to evaluate viscoelastic properties of individual types of layered composites and a comparative values for stiffness of such composites. Static three point bending test were carried out in order to obtain basic set of material response data. These data were used for calculating stiffnesses and stresses of layered composites.

Scanning electron microscopy served as a technique for description of the microstructure features of loaded specimens and high speed camera records enabled us to assign deformation events to characteristic points on the load - deformation curve.

All types of specimens were bi-layered (one layer of FRC, one layer of PFC). As a reference specimens mono-layer beams made of PFU, SFM, FLOW and CB constituents were also prepared.

Rule of mixture (Voigt) as an analytical model for prediction of effective stiffness was evaluated and stiffness gained from static three-point test was used as a comparative criterion.

The conclusions can be summarised in the following items:

The contents of fibres in FRC ascertained by TGA were in a good agreement with the data supplied by their manufacturers. The content of particles in PFC were in a good agreement with the values typical for low and high viscous dental PFCs. The data from the manufacturer were not available.

The filler content of the PFC layer influences the stiffness and the maximum stresses of layered composites according to the principles of homogeneization of effective properties. The growing difference between the stiffnes of an individual layer causes growing longitudinal stress between layers providing the neutral axis is in the same position.

The volume content of the FRC layer (the rate of the reinforcement) influences the stiffness of layered composites. Voigt version of Rule of mixture is in a good agreement with experimental data. Normal stress is influenced by volume content of FRC too. It influences the position of the neutral axis as well as the relative position of the layer's border and the neutral axis. The maximum stress growth with the volume content of the FRC layer in the certain range, out of this range the reinforcing becomes non effective.

There was no influence of interlayer on overall stiffness nor normal stress and its distribution shown because in the test protocol applied the delamination of the layers does not activate the final failure.

The internal architecture of the FRC layer influences the mechanical response of the layered beams both in stiffness and normal stress. Both effects are in accordance with the concept of effective homogeneization.

Multi-scale modeling is found as a usefull approach to predict and calculate modulus of elasticity and normal stresses of layered composites. Micro-scale is in this respect represented by constituents of PFCs and FRCs, FRC a PFC layer is treated as a meso-scale feature while the whole beam is a macro-scale superstructure.

Following clinical recommendation results from this study:

There is a preferable combination of uni-directional FRC with PFC with higher filler content (CB) and multi-directional FRC and PFC with lower filler content (FLOW).

In this study we focused on how structural features on micro- and meso-scale of constituents influence mechanical response of layered composites used in dentistry. The results confirmed that the internal structure of constituents has a predictable impact on mechanical response.

Layered composites represents a concept in which by using several layouts on different scales new required properties of final superstructure may be obtained.

However further work is required in order to bring predictable results to dental practice. Clinical testing of different treatment protocols using layered composites would be beneficial in this respect.

7 REFERENCES

[1] Callister Jr., W.D.: Materials Science and Engineering: an introduction. 5th edition, John Wiley and Sons, Inc., 1999

[2] Meyers M., Chawla K.: Mechanical Behavior of Materials, 2nd edition, Cambridge University Press, 2009

[3] Berthelot J.M.: Composite Materials: mechanical behavior and structural analysis, Springer - Verlag, New York, 1999

[4] Kaw A. K.: Mechanics of Composite Materials

[5] Beer R., Baumann M.A., Kielbassa A.M.: Pocket atlas of endodontics, Georg Thieme Verlag, Stuttgart - New York, 2006

[6] Powers J.M., Sakaguchi R.L.: Craig's Restorative Dental Materials. 12th edition, Mosby Elsevier, 2006

[7] Van Noort R.: Introduction to Dental Materials, 3rd edition, Mosby Elsevier, 2007

[8] Kenneth J. Anusavice: Phillip's Science of Dental Materials, W. B. Saunders Company, Philadelphia, 1996

[9] Fouassier J.P., Rabek J.F.: Radiation curing in polymer science and technology, Vol.1: Fundamentals and methods, Eslevier, New York, 1993

[10] Gunduz N.: Synthesis and photopolymerization of novel dimethacrylates, Master of Science Thesis, Virginia Polytechnic Institute and State University, Blacksburg, 1998

[11] Pappas S.P.: Radiation curing, Science and Technology, Plenum Press, New York, 1992

[12] Curtis A.R.: The influence of 'nanocluster' reinforcement on mechanical properties of resin-based composite material, PhD Thesis, University of Birmingham, 2008

[13] Trautmann R.: Morphogenesis of tetrafunctional light cured polymer networks, MSc Thesis, VUT Brno 2002

[14] Cook W.D.: Photopolymerization kinetics of dimethacrylates using the camphorquinone/amine initiation system. Polymer, 1992; 33: 600-609

[15] Venhoven B.A.M.: Dental resin composites - Curing and coherence, PhD. Thesis, University of Amsterdam, 1996

[16] Decker C., Jeckins A.D.: Macromolecules, 18, 1241, 1985

[17] Lanczos C.: The variational principles of mechanics, 4th edition, Dover publications Inc., New York, 1986

[18] Antonucci J.M., et al: Chemistry of silanes: Interfaces in dental polymers and composites, Journal of research of the National institute of standards and technology, vol. 110, Nr.5, 2005

[19] Christensen R.M.: Mechanics of composite materials, Dover Publications Inc., Mineola, New York, 2005

[20] Rösler J., Harders H., Bäker M.: Mechanical behavior of engineering materials: Metals, Ceramics, Polymers and Composites, Springer-Verlag, Berlin, Heidelberg, 2007

[21] de With, G.: Structure, deformation and integrity of materials, Wiley-VCH Verlag GmbH, Weinheim, 2006

[22] Ashby M., Shercliff H., Cebon D.: Materials: Engineering, science, processing and design, Elsevier, 2007

[23] Janssen M., Zuidema J., Wanhill R.J.H.: Fracture mechanics, 2nd edition, Spon Press, 2009

[24]Mishnaevsky L.: Computational mesomechanics of composites, Wiley 2007

[25] Zeman J.: Analysis of composite materials with random microstructure, PhD Thesis, Klokner Institute, Czech Technical University in Prague, 2003

[26] Al Kassem G.: Micromechanical material models for polymer composites through advanced numerical simulation techniques, PhD Thesis, Fakultät für Maschinenwesen der Reinisch-WestfälischenTechnischen Hochshule Aachen, 2009

[27] Weinberger C., Cai W.: Elasticity of microscopic structures - Lecture note, Stanford University, Winter 2004, http://micro.stanford.edu/~caiwei/me340b/content/me340b-lecture02-v03.pdf

[28] Bardella L.: Mechanical behavior of glass-filled epoxy resins: experiments, homogenization methods for syntactic foams, and applications, PhD Thesis, Universita deli Studi di Brescia, Dipartimento di Ingeneria Civile, 2000

[29] Mishnaevsky L., Brøndsted P.: Micromechanical modeling of strength and damage of fiber reinforced composites, Annual report on EU FP6 Project, Risø National Laboratory, Technical University of Denmark, Roskilde, 2007

[30] Suresh S.: Fatigue of materials, Cambridge University Press, 1998

[31] Wong K.J., Yousif B.F., Low K.O., Ng Y., Tan S.L.: Effects of fillers on the fracture behavior of particulate polyester composites, Journal of Strain Analysis, Vol. 45, pp.67 - 78

[32] Cox B., Flanagan G.: Handbook of analytical methods for textile composites, NASA, Langley Research Center, 1997

[33] ISO-Standards. ISO 4049 Polymer-based filling, restorative and luting materials Technical Committee 106 – Dentistry Geneve: International Organization for Standardization. 2000. p. 1-27.

[34] Cowie J.M.G, Arrighi V.: Polymers: Chemistry and physics of modern materials, 3rd. edition, CRC Press, Taylor and Francis, 2008

[35] Chiang Y.: Polymerization Shrinkage with light initiated dental composites, PhD Thesis, Medizinische Fakultät, Ludwig-Maxmilians-Universität, München, 2009

[36] Braga R.R., Ballester R.Y., Ferracane J.L.: Factors involved in the development of polymerization shrinkage stress in resin composites: A systematic review, Dental Materials (2005) 21, 962-970

[37] Van Landuyt K.L. et al., Systematic review of the chemical composition of contemporary dental adhesives, Biomaterials 28 (2007), 3757 - 3785

[38] Ghivari S., Chandak M., Narendra M.: Role of oxygen inhibited layer on shear bond strength of composites, Journal of Conservative Dentistry 2010, Jan - Mar; 13(1): 39-41

[39] Slopek R.,P.: In-situ monitoring of the mechanical properties during the photopolymerization of acrylate resins using particle tracking microrheology, PhD thesis, School of Chemical and Biomolecular Engineering, Georgia Institute of Technology, May 2008

[40] Gauthier M.A., Stangel I., Ellis T.H., Zhu X.X.: Oxygen inhibition in dental resins, Journal of dental research 2005, 84(8), 725 - 729

[41] Rueggeberg F.A., Margeson D.H.: The effect of oxygen inhibition on an unfilled/filled composite system, Journal of dental research 1990, 69, 1652 - 1658

[42] Kučera M.: Vznik makromolekul, VUTIUM Brno, 2003

[43] Decolon C.: Analysis of composite structures, Kogan Page Science, London, 2004

[44] Jančář J.: Mechanics and failure of plastics, VUT Brno, 2005

[45] Kucherov L.: Delamination In Periodically Layered Bi-material Composites, PhD Thesis, Tel Aviv University, 2003

[46] Ding W.: Delamination Anaylsis of composite Laminates, PhD Thesis, University Toronto, 1999

[47] Patton Chan Y.M.: Laminated beam theory based on homogenization, Master Thesis, University of Toronto, 2000

[48] Reddy J.N.: Canonical relationship between bending solutions of classical and shear deformation beam and plate theories, Ann. Solid Structure Mechanics (2010) 1, 9-27, Springer Verlag

[49] Roos R.: Model for interlaminar normal stresses in doubly curved laminates, Dr.sc. Thesis, ETH Zurich, 2008

[50] Tessler A., Di Sciuva M.: Refined zigzag theory for homogenous, laminated composites, and sandwich plates: A homogenous Limit methodology for zigzag function selection, NASA/TP-2010-216214, Langley research center, Hampton, Virginia, 2010

[51] Wanji Ch., Zhen W.: A selective review on recent development of displacement-based laminated plate theories, Recent Patents on Mechanical Engineering, 2008,1, 29-44

[52] Degrieck J, Van Paepegem W.: Fatigue damage modelling of fibre-reinforced composite materials: Review, Applied Mechanics Reviews, 54(4), 2001, 279 – 300

[53] Shah M.B., Ferracane J.L., Kruzic J.J.: R-curve behavior and micromechanisms of fracture in resin based dental restorative composites, Journal of the Mechanical Behavior of Biomedical Materials, Volume 2, Issue 5, October 2009, Pages 502–511

[54] Trautmann R.: Vliv složení na pevnost adheze mezi částicovými a vláknovými kompozity, Dizertační práce, VUT Brno, 2010

[55] Malick P. K.: Fiber reinforced composites, materials, manufacturing and design, 3rd Edition, CRC Press, 2008

[56] ASTM Standard D790 – 99: Standard test methods for flexural properties of unreinforced and reinforced plastics and electrical insulating materials, 2000

[57] Pardini L.C., Neto F.L., McEnaney B.: Modelling of mechanical properties of CRFC composite under flexure loading, Journal of the Brazilian Society of Mechanical Sciences, Volume 22, Number 2, Campinas 2000

[58] Beckwith S.W.: Composites reinforcement fibers: I – The Glass Family, SAMPE Journal, Volume 45, No. 5, 2009

[59] Mohite N., Kale V., Kumbhar S., Kengar V.: Stress and load-displacemement analysis of fiber composite laminates under different loading conditions, International Journal of Engineering Science & Advanced Technology, Volume 2, Issue 6, 1663-1669, 2012

[60] Pupurs A.: Micro-crack initiation and propagation in fiber reinforced composites, Doctoral thesis, Department of Engineering Sciences and Mathematics, Luleå University of Technology, Luleå, Sweden, 2012

[61] Ferreira R.T.L., Rodrigues H.C., Guedes J.M, Hernandes J.A: Hierarchical optimization of laminated fiber reinforced composites, 10th World Congress on Structural and Multidisciplinary Optimization, May 19-24, 2013, Orlando, FL, USA, *Submitted paper,* 2013

[62] Würkner M., Berger H., Gabbert U.: Numerical study of effective elastic properties of fiber reinforced composites with rhombic cell arrangements and imperfect interface, International Journal of Engineering Science 63, 1-9, Elsevier 2013

[63] Rathnakar G., Shivanan H.K.: Experimental evaluation of strength and stiffness of fibre reinforced composite under flexural loading, International Journal of Engineering and Innovative Technology, Volume 2, Issue 7, 219-222, 2013

[64] Šmilauer V., Hoover Ch., Bažant Z.P., Caner F., Waas A.M., Shahwan K.: Multiscale simulation of fracture of braided composite via repetitive unit cells, Engineering Fracture mechanics, 78 (2011), 901-918

[65] Chen F.: Interface mechanics of layered composite beam-type structures, PhD Thesis, Department of Civil and Environmental Engineering, Washington State University, 2011

[66] Leprince J.G., Palin W.M., Hadis M.A., Devaux J., Leloup G.: Progress in dimethacrylate- based dental composite technology and curing efficiency, Dental Materials, Volume 29, Issue 2, 139-156, 2013

[67] Graciani E.: Numerical Analysis of the single fiber fragmentation test including the effect of interfacial friction, PhD Thesis, Department of Applied Physics and Mechanical Engineering, Luleå University of Technology, Luleå, Sweden, 2010

[68] Pěnčík J.: Dřevěné prefabrikované schodišťové sestavy, Habilitační práce, VUT Brno, *DRAFT*, 2013